The Abdus Salam International Centre for Theoretical Physics

United Nations Educational, Scientific and Cultural Organization

IAEA International Atomic Energy Agency

Strongly Correlated Matter: from Quantum Criticality to Flat Bands | (SMR 3732)

22 Aug 2022 - 02 Sep 2022
ICTP, Trieste, Italy

P01 - ABOUIE Jahanfar

Frustrated spin chains: three-site interactions and flat-band magnons

P02 - ADAM Mukhtar Lawan

Fermi surface tuning in MoTe2 using doped Chalcogenide

P03 - ALEMAYEHU Getahun Kumela Getahun

Design and Simulation Analysis of An Efficient Optoplasmonic Biosensor for Lung Cancer Telediagnosis

P04 - ALILOUTE Soumia

Bidirectional teleportation through entangled coherent quantum network

P05 - ARIAN ZAD Hamid

Intermediate magnetization plateaus in the spin-1/2 Ising-Heisenberg and Heisenberg models on two-dimensional martini lattice

P06 - ARREDONDO LEON Yesenia

Standarization of the synthesis of double perovskites Sr2XWO6, X=Co, Ni, Cu, via sol-gel and solid state reactions

P07 - AVELLA Giovanni Richard

Density probabilities and quantum critical phenomena of a Bose-Fermi Mixture in 1D Double well potential

P08 - AWOGA A. Oladunjoye

Superconductivity in graphene systems

P09 - BAGGA Sonika

Planar Hall effect in Cu intercalated PdTe2

P10 - BALDO MESA CASA Lucas

Defects in twisted bilayer graphene

P11 - BANDYOPADHYAY Soumik

Universal dynamics of Sachdev-Ye-Kitaev model and Engineering long-range interacting disorded models

P12 - BARBOSA RODRIGUES Joao Nuno

Identifying materials with charge-spin physics from first principles calculations

P13 - BASAK Surajit

Yu-Shiba-Rusinov bound states in systems with density of states singularities

P14 - BEIRANVAND Razieh

Anisotropic conductance in spin-orbit coupled and superconductor graphene junctions

P15 - BELAID Walid

Low-Dimensional and Frustrated Quantum Magnets

P16 - BONDYOPADHAYA Nilanjan

Nonequilibrium Thermal and Spin Transport in Open Quantum Systems of Topological Superconductors and semiconductors

P17 - BRIGHI Pietro

Recursive quantum Hilbert space fragmentation and slow transport in U(1) conserving generalised East model

P18 - CHAFAI Ahmed

An ab initio perspectives on the electronic and optical characteristics of ML-MoSe2: Role of electric field

P19 - CHANG Yung-Yeh

Topological Kondo superconductor

P20 - CHAN Si Min

Superconductivity on the Quasi One-Dimensional Flat Band

P21 - CHERNOV Evgeniy

Metal-insulator Transition in Strongly Correlated Binary Manganese Chalcogenides

P22 - CHIKA Khouloud

Quantum injection model for hot and cold charge transfer states in organic solar cells

P23 - CHUDNOVSKIY Alexander

Superconductor -- insulator transition in a non-Fermi-liquid

P24 - COSTA PRAUCHNER Leonardo

Interplay between the correlations responsible for the pseudogap and the charge density wave phase

P25 - DAS Anirban

Effect of interface hybridization on proximity induced superconductivity in quantum spin Hall insulator 1T'-WTe2

P26 - DEBNATH Debika

Magneto-transport Properties of the Double Quantum Dot Transistor in the Strongly Correlated Regime

P27 - DE PODESTA Kelvin Christian

High pressure structural instability in CeSb2

P28 - DERZHKO Oleh

Flat-band physics in the spin-1/2 Heisenberg frustrated bilayers

P29 - DE Suman Jyoti

Low energy excitation between two Quantum Hall Ferromagnet

P30 - DJERMOUNI Mostefa

Pressure effect on strongly correlated iron-chalcogenides : DFT study

P31 - DO ESPIRITO SANTO Santiago Tiago

Exact diagonalization of Rydberg atoms Hamiltonian in fractal lattices

P32 - DORA Kumar P Rakesh

Nature of the anomalous 4 / 13 fractional quantum Hall effect in graphene

P33 - ESSALAH Kaouther

Flat bands in alternating Hubbard ladder

P34 - FAMUTIMI Femi Olalekan

Thermal Properties of Soil Samples from Different Landforms in Three Local Government Areas of Ondo State, Nigeria.

P35 - FEIJOO Sebastian Javier

Topological Shiba states in a 1D superconductor with a local magnetic impurity

P36 - FIORE Jacopo

Contributions of Collective Excitations to Third Harmonic Generation in Superconducting MgB2

P37 - FRANCHINI Fabio

The frustration of being odd

P38 - GANIEV Orifjon

Influence of pairing symmetry and multiple energy gaps on the behaviour of critical current through the Josephson junction

P39 - GHOHROODI GHAMSARI Farnood

Viscoelasticity of an anisotropic electron liquid

P40 - GHORAI Unmesh

Excitonic metal and non-Fermi liquid behaviour in twisted double bilayer graphene

P41 - GHORASHI Sayed Ali Akbar

Topological and stacked flat bands in bilayer graphene with a superlattice potential

P42 - GINDIKIN Iakov

Spin-dependent electron-electron interaction in Rashba materials

P43 - GIRI Debasmita

Skyrme crystal in twisted double bilayer graphene

P44 - GLEZER MOSHE Aviv

Tunneling study in granular aluminum near the Mott metal-to-insulator transition

P45 - GUTMAN Dmitri

Thermal and electric conductivity in Weyl-semimetals.

P46 - HADDAD Sonia

Twistronics versus straintronics in twisted bilayers of graphene and transition metal dichalcogenides

P47 - HAZRA Tamaghna

Triplet pairing mechanisms from Hund's-Kondo models: applications to UTe2 and CeRh2As2

P48 - HERRERA MENDOZA Ariel Jhony

Vortex structure deformation of rotating Holographic Superconductors

P49 - IMARA Ziyad

measure entanglement

P50 - IROULART Esteban Andrés

Majorana bound states study and characterization in an antiferromagnetic skyrmion background

P51 - IŞKIN Menderes

Effective-mass tensor of the two-body bound states and the quantum-metric tensor of the underlying Bloch states in multiband lattices

P52 - JASTRZEBSKI Jakub

Electric Field Induced Spin-orbit Coupling in Graphene-based Moiré Heterostructures

P53 - JOY Sandeep

Spontaneous orbital magnetization of the Wigner Crystal phase in Bernal bilayer graphene

P54 - KABATAŞ Murat

Tuning the Oxygen Vacancies, Strain Engineering, and Tungsten Doping Synergistic Interactions to Control the Metal-Insulator Transition Properties of VO2 Thin Films

P55 - KARNAUKHOV Nikolaevich Igor

Electron liquid state in the spin-1/2 anisotropic Kondo lattice

P56 - KAUR Navdeep

An integrated probe for the transport properties of Fe-based quaternary Heusler Compound

P57 - KHAN Mayur

Biaxial strain-induced band gap engineering in monolayer MoS2 using DFT

P58 - KHUDAYBERDIEV Sagdullaevich Zafar

METAL-INSULATOR TRANSITIONS IN DOPED La-BASED SUPERCONDUCTORS WITH SMALL-RADIUS DOPANTS

P59 - KUMARI Preeti

Ab initio investigation of the structural, optical, mechanical, elastic, and thermophysical performance of Ce-based oxide Perovskite for energy applications

P60 - KUMBHAKAR Shreya

Glassy electron kinetics across first order Mott metal-insulator transition

P61 - KUNDU Sarbajaya

Theory of phonon instabilities in Weyl semimetals at high magnetic fields

P62 - KURBANOV Ulugbek

METAL-INSULATOR TRANSITIONS IN DOPED La-BASED SUPER CONDUCTORS WITH SMALL-RADIUS DOPANTS

P63 - LUNTS Peter

Non-Hertz-Millis scaling of the antiferromagnetic quantum critical metal via scalable Hybrid Monte Carlo

P64 - MARCIANI Marco

Multiorbital Boltzmann transport and the resistivity anisotropy of nematic FeSe

P65 - MASHKOORI Mahdi

Detrimental effect of disorder on two dimensional time-reversal invariant topological superconductor

P66 - MASROUR Rachid

Photovoltaic, Electronic and Optical properties of Cesium bromate oxygen perovskite: First-principles investigation

P67 - MATVEEVA Polina

One-dimensional topological insulators and superconductors with chiral symmetry

P68 - MESSICA Haim Yonatan

Thermal conductivity in TRS-breaking Weyl-semimetals in the hydrodynamic regime

P69 - METAYER Simon

Two-loop mass anomalous dimension in reduced quantum electrodynamics and application to dynamical fermion mass generation

P70 - MOELLER Gunnar

Exotic criticality of interaction-driven plateau transition between integer and fractional Chern Insulators

P71 - MOHAMMADIZADEH Mohammadreza

Electron-phonon interaction in TixOy using first-principles calculations

P72 - MOHAMMED-KRARROUBI Chaimaa

The electronic structure of the conventional hydride superconductors

P73 - MUKHACHEV Roman

Study of magnetic properties of GdTMSi (TM = Mn, Ru) intermetallic compounds accounting for strong electron correlations

P74 - MUKHERJEE Shantonu

Electron-vortex interaction and fermion pairing

P75 - MURTHY Chaitanya

A stability bound on the T-linear resistivity of conventional metals

P76 - NAQVI Sayed Faheem

A Comparative Study on thermodynamics properties of Se-Te- Zn and Se-Te-Ag Ternary Chalcogenide Glasses

P77 - NGANFO YIFOUE Willy Aniset

Dynamics of exciton polaron in microtubule

P78 - NOSOV Pavel

Superconductivity and localization near a two-dimensional ferromagnetic quantum critical point

P79 - OBAIDURRAHMAN Mohd

Resistivity due to acoustic phonons scattering with chiral carriers in impure Bilayer Graphene

P80 - OHANESJAN Vladimir

Quantum thermodynmics of strongly correlated systems

P81 - OHLRICH Frances Miriam

Intrinsic, robust, and isolated flat bands present at half-filling in the minimal model of the superconducting metal-organic framework, Cu-BHT

P82 - PARAMEKANTI Arun Sampathkumar

Multiorbital SYK model: Nematicity, non-Fermi liquid, and Elastotransport

P83 - PIMENOV Dimitri

Twists and Turns of pairing from repulsive dynamical interactions

P84 - RAHMAN Ur Saeed

Transverse flow velocity and differntial Temperature in high energy nucleus nucleus collision

P85 - RANJBAR NAEINI Omid Reza

The Reduction of the Thermal Decoherence using Hybrid Structure Toroidal Whispering Gallery Modes Resonator

P86 - RAWAT Divya

Crystalline Anharmonicity in 2D Ferroelectric α-In2Se3 Single Crystal

P87 - RODRIGUEZ P Jose

High-Tc Superconductivity in FeSe by Exchange of Hidden Spin Fluctuations

P88 - ROHIT Mukherjee

Schwinger Boson mean field Study of spin 1/2 J_{1}-J_{2}-J_{\chi} model in Honeycomb lattice : Thermal Hall signature

P89 - ROY Roumita

Spin Orbit Coupling driven Novel Quantum Magnetism in Iridate Double Perovskites.

P90 - SADECKA Katarzyna

Fine structure of excitons in TMD type-II heterostructures

P91 - SAHU Chandra Krushna

Quantum spin liquids in dipolar-octupolar pyrochlore magnets

P92 - SAKHEL Raji Asaad

Unpredictable Condensate-Depletion Dynamics in one-dimensional Power-Law Traps

P93 - SAKHEL Raji Roger

Unpredictable Condensate Depletion Dynamics in one-dimensional Power-Law Traps

P94 - SALAZAR Ignacio

Engineering holographic flat bands

P95 - SALEEM Yasser

Broken Sublattice Symmetry Effects and Phase Transitions in Triangular Artificial Graphene Quantum Dots

P96 - SALEHI Morteza

Andreev Transfer Torque on the Surface of three dimensional Topological Insulators

P97 - SARKAR Madhumita

Quantum order-by-disorder induced phase transition in Rydberg ladders with staggered detuning

P98 - SEYED YAZDI Jamileh

Degenerate versus non-degenerate Josephson parametric amplifiers' gains and application in quantum two-mode squeezed radar

Tunneling conductance in surface states of a topological insulator and Single Weyl node

P99 - SHAHBAZI DASTJERDEH Farhad

Theory of spin-lattice interaction in Tb2Ti2O7

P100 - SHAH Muzamil

Photo-induced quantum phase transitions in moiré superlattices

P101 - SHALABY Mustafa Saeed Ahmed

Significant improvement of critical current density in (Bi1.6Pb0.4)Sr2Ca2Cu3-yCoyO10 superconductors

P102 - SHANKAR Aravindh Swaminathan

Kondo effect in Twisted Bilayer Graphene

P103 - SHAPIRO Dmitriy

Microwave response of a chiral Majorana interferometer

P104 - SHARMA Shailja

Electronic studies of transition metal doped Bi2Se3 and Bi2Te3 topological insulators

P105 - SOUS John

Bipolaronic high-temperature superconductivity

P106 - SOUZA Gabriel Moreira Huan

Effective Field Theory for Fractons

P107 - SOW Malick

Correlation Factor Taking into Account Spherical Harmonics Through Hypergeometric Functions to Calculate Energies of Lithium-Like Ions

P108 - SQUIRE Oliver

Quantum critical point in the high-pressure structure of CeSb2

P109 - SUR Samudra

Driven Hubbard model on a triangular lattice: tunable Heisenberg antiferromagnet with chiral three-spin term

P110 - SWAMI Shaileshkumar Jeel

Microscopic origin of Strongly Correlated ACrO3

P111 - TAMERSIT Khalil

Carbon Nanotube Tunneling Field-Effect Transistor as a Radiation Sensor: A quantum Simulation Study

P112 - TIRRITO Emanuele

Topological chiral currents in the Gross-Neveu model extension

P113 - VELA WAC Atilio

Emerging exotic phases in magnetic spin systems due to RKKY interaction

P114 - WEI Chenan

Quantum Chaos, Superconductivity, and Information Scrambling in Disordered Magic-Angle Twisted Bilayer Graphene

P115 - YERIN Yuriy

Magneto-topological-induced transitions in multi-component superconductors

P116 - ZAMPRONIO PEDROSO Vinicius

Triangular lattice Hubbard Model

P117 - ZEGGAI Nadjet

New diluted magnetic semiconductors : DFT prediction

P118 - ZIANE Mustapha

Quantifying entanglement in non-Gaussian systems using the Wigner function

P119 - ZYUZIN A. Alexander

Superconductivity in flat-band semimetals

P01

Frustrated spin chains: three-site interactions and flat-band magnons

The ground state phase diagram of frustrated spin chains with three-site interactions is investigated by means of spin wave theory, cluster mean field theory and cluster variational method. The interplay of next-nearest-neighbor and three-site interactions leads to the emergence of a plethora of quantum phases in the ground state phase diagram. We show that aside from the ferromagnetic and Neel orders, the ground state possesses different non-magnetic orders such as antiferro-quadrupole order and quantum spin-liquid phase. We demonstrate that the ground state also shows a magnetic phase with up-up-down-down (uudd) order in which magnon excitations are flat-band.

P02

Fermi surface tuning in MoTe2 using doped Chalcogenide

Herein, we utilized doping mechanism to tune the surface states in the Weyl semimetal MoTe2.

P03

Design and Simulation Analysis of An Efficient Optoplasmonic Biosensor for Lung Cancer Telediagnosis

Alemayehu Getahun[1], Abebe Belay[1], Tamirat Abebe[1] and Alemu Kebede[1]

[1] *Department of applied physics, School of Applied Sciences, Adama Science and Technology University, Adama, P.O.Box 1888, Ethiopia.*

The quantum technology applications to dispatch face-to-face medical activities in an accurate and secure fashion has gained substantial interest. Unfortunately, the work on remote medical treatment applying quantum medication and information processing techniques is notoriously hard to observe. In this research, we have proposed the novel numerical model of fiber optics-based optoplasmonic biosensor for remote lung cancer detection, soliciting quantum mechanical principles. A proposed biosensor was constituted of a multi-mode silica core and cladding. The cladding part at the starting gate contains a sensor region layout sequentially as; GGG-prism, Ag, Fe_2O_3 and bio-molecules with TP53 genes that are found only in lung cells. A biosignals generated following irradiation of fiber cable with powerful laser, in addition the biosensor performance was determined by the Fresnel and transfer matrix equations in line with EP17-CLSI guidelines. The result reveals, adding layers of sensor medium and DNA concentration significantly affects the sensitivity of the sensor's . Moreover, applying quantum teleportation, the resulted highly sensitive biosignals were teleported to assure the best possible remote-based lung cancer diagnosis. It will be expected that in the near future, the quantum and classical investigation of light matter interaction at nanoscale will be a valuable tool for personalized remote based medical diagnoais and treatment.

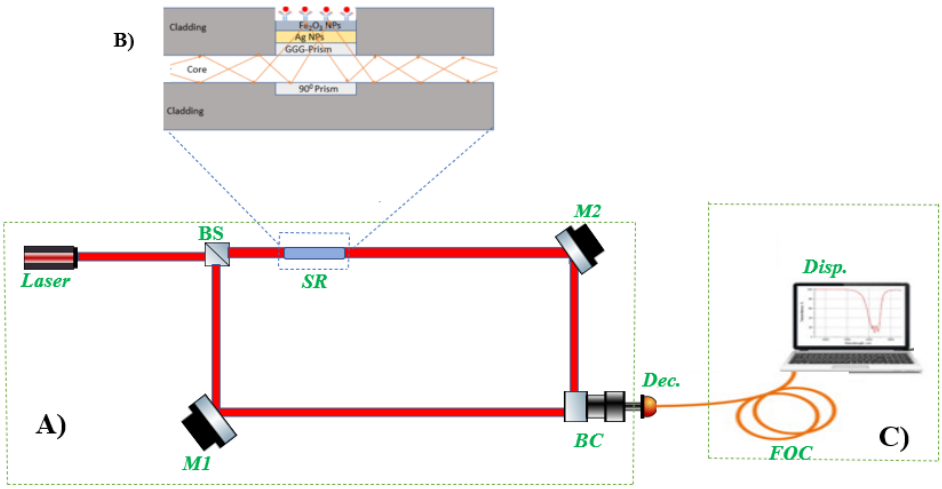

Figure 1: Schematic of experimental setup of proposed OPB. Laser, light amplification by stimulated emission of radiation; Bs, Beam splatter; SR, Sensor region; M1, First mirror; M2, Second mirror; BC, Beam combiner; Dec., Detector; Disp., Display; FOC, fiber optics cable. A) shows laser light path and interaction with sensor region inside fiber cable. B) Shows arrangement of fiber optics-based sensor region, with the multi-mode silica core ($d_{fc} = 40\mu m$) and plastic cladding ($d_c = 48\mu m$) detached at the center to insert a sensor region of $12mm$ length. That composed of four layers arranged as GGG-prism (12 μm), Ag (7 μm), Fe_2O_3 (13 μm) and biomolecules (16 μm). C) Shows how the output biosignals were interpreted to show the result (either effected or non effect cell).

P04

Bidirectional teleportation through entangled coherent quantum network

A bidirectional quantum teleportation protocol is introduced over a quantum network consists of more than four members sharing a coherent entangled state, where it is implemented in a perfect or noisy environment. The results show that the amplitude of the coherent state and the decoherence parameter play an important role on maximizing or minimizing this probability. At fixed values of the amplitude and the decoherence parameters, the success of probability increases as the number of users increases. The fidelity of the teleported coherent state depends on the type of the encoded information, whether entangled/partial or classical information, namely depends on the weight parameter. The stable behavior of the fidelity is displayed when the users teleport classical information.

P05

Intermediate magnetization plateaus in the spin-1/2 Ising-Heisenberg and Heisenberg models on 2D frustrated martini lattice

Hamid Arian Zad[1,2], **Jozef Strečka**[1]

[1]*(Hamid Arian Zad) A.I. Alikhanyan National Science Laboratory, 0036, Yerevan, Armenia*
[2]*Department of Theoretical Physics and Astrophysics, Faculty of Science, P. J. Šafárik University, Park Angelinum 9, 041 54 Košice, Slovak Republic*

In this work, we consider the spin-1/2 Ising-Heisenberg [1] and quantum Heisenberg models on frustrated martini lattice in the presence of an external magnetic field. The former is exactly solved by the combination of generalized star-triangle transformation, the transfer-matrix technique and Monte Carlo method. The generalized star-triangle transformation establishes an exact mapping correspondence with the effective spin-1/2 Ising model on a pure Ising triangular lattice with a temperature-dependent field, two- and three-body interactions, which are numerically calculated using MC simulations. Full Heisenberg XXX model on martini lattice is investigated by utilizing the infinite projected entangled-pair state (iPEPS) [2, 3] within the tensor-network framework. The Ising-Heisenberg spin model reveals in its ground-state phase diagram two unconventional dimerized and one trimerized quantum ground states together with two classical ground states. It is demonstrated that the spin frustration is responsible for a variety of magnetization scenarios with up to two or three intermediate magnetization plateaus. The total magnetization m_{T} of the Ising-Heisenberg model on martini lattice shows fractional plateaus at 1/12, 1/6 and 1/4 of the saturation magnetization. It is demonstrated that the total magnetization exhibits a smooth increase between intermediate plateaus, denoting the existence of a gapless phase. The exact results for the total magnetization of the Ising-Heisenberg model are confronted with the corresponding results for the Heisenberg model which were derived by the tensor-network method. Although the exact ground states for the Ising-Heisenberg model does not capture the actual ground states for the pure Heisenberg model [4], the zero-temperature magnetization process of both models is quite reminiscent, such that some insight into the ground states of the Heisenberg model can be obtained from combining of the star-triangle transformation, the transfer-matrix formalism and MC simulations of the quantum-classical Ising-Heisenberg analogous.

[1] H. Arian Zad, J. Strečka, Phys. Rev. E **105**, 044115 (2022).
[2] N. Schuch, M. M. Wolf, F. Verstraete and J. I. Cirac, Phys. Rev. Lett. **98**, 140506 (2007).
[3] R. Haghshenas, S. S. Gong, and D. N. Sheng, Phys. Rev. B **99**, 174423 (2019).
[4] J. Cisarova, F. Michaud, F. Mila, J. Strecka, Phys. Rev. B **87**, 054419 (2013).

P06

Standarization of the synthesis of double perovskites Sr2XWO6, X=Co, Ni, Cu, via sol-gel and solid state reactions

The half-metallic aspect of double perovskites Sr2XWO6, X=Co, Ni and Cu has potential applications in the field of spintronics due to the single valued spin channel of conductivity. To generate some prototypes, we propose a standarization in the synthesis of such materials via sol-gel and solid-state reactions.

P07

Density probabilities and quantum critical phenomena of a Bose-Fermi Mixture in 1D Double well potential

R. Avella[1], **J. Nisperuza** [1], **and JP Rubio**[1]

[1]*Fundación Universitaria los Libertadores, Faculty of Engineering and Basic Sciences, Department of Aeronautical Engineering, A. A. 75087 Bogotá, Colombia.*

This document is the template for contributed abstracts (posters and/or talks) and gives the guidelines for preparing and submitting abstracts for the *Strongly Correlated Matter: from Quantum Criticality to Flat Bands — (smr 3732)* to be held online from *22 Aug 2022* to *2 Sep 2022*.

The time evolution of probability density, the ground-state fidelity and the entanglement of a Bose-Fermi mixture in a 1D double well potential, are studied through the two mode approximation [1, 2, 3]. We found that the behaviour of the quantum return probability present three distinct regions. The first region is characterized by a complete miscibility [7, 8], and correlated tunneling of bosons [4] and fermion [5, 6]. The second region is characterized by correlated sequential tunneling and in the last region we find an increase in the tunneling frequency of the two species.

We found through the Von Neumann entropy, that the boson-fermion coupling allows a maximum entanglement of quantum correlations of bosons and fermions in the same value. Finally we calculated the fidelity in the $\lambda_{FF} - \lambda_{BF}$ and $\lambda_{BB} - \lambda_{BF}$ planes and we found that the drop of the two fidelities becomes deeper and deeper as the boson-fermion interaction decreases.

[1] Ananikian, David and Bergeman, Thomas, Physical Review A **73**, (2005).
[2] Ostrovskaya, Elena A. and Kivshar, Yuri S. and Lisak, Mietek and Hall, Bjorn and Cattani, Federica and Anderson, Dan, American Physical Society. **61**, 031601 (2000).
[3] Rey, A.-M. and Blakie, P. B. and Clark, Charles W., American Physical Society. **67**, 053610 (2003).
[4] Dutta, Sunayana and Barman, Apurba and Siddharth, Anat and Khan, Ayan and Basu, Saurabh, The European Physical Journal B. **88**, (2015).
[5] Thorwart, M. and Egger, R. and Grifoni, M., American Physical Society. **72**, 035330 (2005).
[6] Yang, Yong, 10.48550/arXiv.2206.04243 (2022).
[7] jiang, xunda and wu, shuyuan and Ye, Qinzhou and Lee, Chaohong, New Journal of Physics. **21**, (2019).
[8] Siegl, P. and Mistakidis, S. I. and Schmelcher, P., American Physical Society. **97**, 053626 (2018).

P08

Superconductivity in graphene systems

We show how to identify superconducting paring symmetry in graphene systems.

P09

Planar Hall effect in Cu intercalated $PdTe_2$

Sonika[1], M. K. Hooda[1, 2], Shailja Sharma[1] and C. S. Yadav[1, *]

[1](Sonika)*School of Basic Sciences, Indian Institute of Technology Mandi, Kamand, Mandi 175075, India*

[2]*Department of Physics, Indian Institute of Technology Kanpur, Kanpur 208016, India*

The planar Hall effect (PHE) in topological semimetals have gained tremendous research interest lately. However, there is no clear picture about the origin of PHE in these systems due to the coexistence of chiral anomaly and orbital magnetoresistance (MR). $PdTe_2$ is a type-II Dirac semimetal with positive longitudinal MR, which makes it a good candidate to host topological superconducting states [1, 2]. It shows superconductivity below 1.7 K and exhibit topologically non-trivial surface states [3]. The intercalation of 5% Cu enhances the superconducting transition temperature to 2.6 K [4]. Recently there have been reports of PHE in $PdTe_2$ [5, 6]. This stimulated our interest in studying the PHE in the Cu intercalated compound; $Cu_{0.05}PdTe_2$. We observed positive longitudinal MR, linear field dependence of the amplitude of PHE, and the tilted prolate shaped orbits in parametric plot that point toward the importance of Fermi surface anisotropies in understanding the origin of PHE in a system like $PdTe_2$. The existence of positive MR and PHE raises a doubt over the notion of chiral anomaly as an origin of PHE in the systems [7].

References:

1) H. J. Noh *et al.*, Phys. Rev. Lett. **119**, 016401 (2017).
2) F. Fei *et al.*, Phys. Rev. B **96**, 041201 (2017).
3) Amit and Yogesh Singh, Physical Review B **97**, 054515 (2018).
4) Ryu G., J. Supercond. Nov. Magn., 28 3275 (2015).
5) S. Xu *et al.*, arXiv:1811.06767 (2018).
6) J. Meng *et al.*, J. Phys.: Condens. Matter **32**, 015702 (2020).
7) Sonika *et al.*, Appl. Phys. Lett. **119**, 261904 (2021).

P10

Defects in twisted bilayer graphene

Lucas Baldo Mesa Casa [1], Tomas Löthman [1], Patric Holmvall[1] and Annica M. Black-Schaffer[1]

[1]Department of Physics and Astronomy, Uppsala University, Box 516, S-751 20 Uppsala, Sweden

Twisted Bilayer Graphene (TBG) is a very tunable platform which at low twisting angles presents extremely large moiré unit cells and low-energy flat bands. We investigate the effects of defects on the low-energy spectrum of normal-state TBG thorough an atomistic tight-binding model. It has recently been shown that the introduction of a single Dirac impurity per moiré unit cell leads to the lifting of the Dirac cones degeneracy and the emergence of triple point fermions (TPF) [1]. We show that the emergent TPFs is actually not as robust as previously thought and that they can be simply destroyed by the introduction of either extended or multiple defects in the moiré unit cell. We also investigate how the local density of states (LDOS), integrated over the energy range of the four low-energy flat moiré bands, changes for different defect locations. We find that on the atomic length scale a localized defect state emerges, situated at the Dirac point in the case of vacancies, while on the moiré length scale we find a depletion of the LDOS in all the neighboring lattice AA regions. We also find a surprising band exchange, where one of the moiré bands is fully replaced by a valence or conduction band.

[1] A. Ramires, J. Lado, PRB 99, 245118 (2019).

P11

Universal dynamics of Sachdev-Ye-Kitaev model and Engineering long-range interacting disorded models

Long-range interacting, disordered quantum many-body models have a wide range of applications across disciplines, from spin glasses in condensed-matter physics, over holographic duality in high-energy physics, to annealing algorithms in quantum computing. In the first part of the presentation, we shall discuss an universal equilibration dynamics of an all-to-all connected, disordered fermionic system described by the Sachdev-Ye-Kitaev (SYK) model, which is a quantum theory holographically dual to extremal charged black holes with two-dimensional anti-de Sitter horizon. By devising an equivalent open quantum system description of the disorder averaged Hamiltonian dynamics of a generic disordered model, we explain the key features of a super-exponential universal equilibration process obtained in our state-of-the-art exact numerical evolution of the SYK model. And, we infer the universality from the spectral analysis of the corresponding Lindbladian. In the later part of the presentation, we shall discuss our recent experimental and theoretical work which realizes an all-to-all interacting, disordered spin system by subjecting a fermionic atomic cloud inside a cavity to a controllable light shift. In the experiment, the system is tuned between disordered versions of a central-mode and the Lipkin-Meshkov-Glick (LMG) [an instance of a Richardson–Gaudin model] models by adjusting the detuning between the atomic resonance and the cavity mode. In particular, we explore the competition of interactions with disorder across a broad range of parameters by spectroscopically probing the low-energy excitations. Our study shows how disorder in the central-mode model breaks the strong collective coupling, making the dark state manifold cross over to a random distribution of weakly-mixed light-matter “grey” states. And, the ferromagnetic ground state of the finite size LMG system evolves towards a paramagnet as disorder is increased. We expect our investigations shed light on understanding the novel physics arising from the competition between disorder and long-range interactions, and challenging questions for systems far from equilibrium, such as, thermalization of closed and disordered quantum systems.

P12

Identifying materials with charge-spin physics from first principles calculations

We present a quantity termed charge-spin susceptibility, which measures the charge response to spin degrees of freedom in strongly correlated materials. This quantity is simple to evaluate using both standard density functional theory and many-body electronic structure techniques, enabling comparison between different levels of theory. A benchmark on 28 layered magnetic materials shows that large values of charge-spin susceptibility correlate with unconventional ground states such as disordered magnets and unconventional superconductivity.

P13

Yu-Shiba-Rusinov bound states in systems with density of states singularities

Surajit Basak[1], **and Andrzej Ptok**[1]

[1]*Institute of Nuclear Physics, Polish Academy of Sciences, W. E. Radzikowskiego 152, PL-31342 Kraków, Poland*

Magnetic impurity placed in a superconductor can lead to the emergence of a pair of bound states, symmetric in energy with respect to the Fermi level, known as the Yu–Shiba–Rusinov (YSR) [1, 2, 3] states. The properties of the YSR bound states depends strongly on the density of states (DOS) at the Fermi level. Here I will present our recent study of the properties of YSR bounds states in systems with DOS singularities (Dirac point, van Hove singularity, and flat band singularity), more specifically we considered honeycomb, kagome, and Lieb lattices [4]. The position of the singularities were tuned to both at the Fermi level and away from the Fermi level to uncover the properties of YSR states in those systems. It was observed that although all the properties are generic regardless of the type of lattices, the properties can change drastically if the system contains more than one non-equivalent sublattices (e.g. Lieb lattice). The value of critical magnetic coupling (J_c) was found to enhance or reduce depending on the sublattice it resides in. To explain the scenario more clearly, I will also present the differences in the local DOS and coherence lengths for different sublattices for Lieb lattice.

[1] L. Yu, Acta Phys. Sin. **21**, 75 (1965).
[2] H. Shiba, Prog. Theor. Exp. Phys **40**, 435 (1968).
[3] A. I. Rusinov, Zh. Eksp. Theor. Fiz. **57**, 2047 (1969).
[4] S. Basak, A. Ptok, Phys. Rev. B **105**, 094204 (2022).

P14

Anisotropic conductance in spin-orbit coupled and superconductor graphene junctions

We theoretically study spin-transfer torque (STT) in a graphene system with spin-orbit coupling (SOC). We consider a graphene-based junction where the spin-orbit coupled region is sandwiched between two ferromagnetic (F) and superconducting (S)segments. The magnetization in each ferromagnetic segment can possess arbitrary orientations. Our results show that the presence of SOC results in anisotropically modified STT, magnetoresistance, and charge conductance as a function of relative magnetization misalignment in the F regions. Our findings can be exploited for experimentally examining proximity-induced SOC in a graphene system

P15

Low-Dimensional and Frustrated Quantum Magnets

Over the last three decades, significant breakthroughs in experimentally detecting high-field entropy have advanced our understanding of magnetic materials. This article discusses high-field entropy measurement methods and their applicability to low-dimensional and/or frustrated magnets. The three-dimensional long-range ordering in these magnets may be repressed or revealed by applying magnetic fields, which create specific physical features with an exotic magnetic ground state. Entropy measurements have aided in the characterization of novel ground states as well as a better understanding of the physical process underpinning field-induced events. The effective calorimetric investigations in the literature are reviewed, with a special emphasis on the link between the exotic ground state and its thermodynamic features.

P16

Nonequilibrium Thermal and Spin Transport in Open Quantum Systems of Topological Superconductors and semiconductors

We study nonequilibrium transport in various open quantum systems whose systems and leads/baths are made of topological superconductors (TSs), semiconductors, and metals. We show ballistic thermal transport in an open TS wire in the topological phase under temperature or voltage bias. The thermal current values grow significantly near the topologi- cal phase transition, where thermal conductance displays a sharp quantized peak as predicted earlier. We relate the quantized thermal conductance to the zero-frequency thermoelectric transmission coefficient of the open TS wire. We also observe a large thermoelectric current near the topological transition of the TS wires. We introduce a differential spin conductance which displays a quantized zero-bias peak at zero temperature for a spinful TS wire in the topological phase. The role of superconducting baths in transport is demonstrated by thor- oughly examining the features of zero-temperature differential electrical conductance and thermal conductance in open systems with TS baths. Our new thermoelectric and spin trans- port findings in various two-terminal geometries are beneficial to the present challenges in probing the emergence of Majorana quasi-particles in experiments.

P17

Recursive quantum Hilbert space fragmentation and slow transport in U(1) conserving generalised East model

Kinetically constrained models have lately been subject of thorough investigation due to the interesting phenomena arising in this framework, such as Hilbert space fragmentation, disorder-free localization and in general anomalous dynamics. In this work, we study a family of kinetically constrained models featuring a conserved U(1) charge and inversion-symmetry breaking. Our analysis shows that these two ingredients lead to Hilbert space fragmentation in the eigenstates, in addition to the "classical" one in the computational basis. Due to this emergent fragmentation, the system has a growing number of eigenstates with exactly zero entanglement entropy across several bipartite cuts, and product states initialized in small subsectors of the Hilbert space present long-lived revivals. Furthermore, we investigate uncommon characteristics in the dynamics, including an extremely slow thermalization whose qualitative nature can be understood by studying the adjacency graph related to the Hamiltonian. Studying a classical circuit implementing the same constraint we manage to investigate large systems, and retrieve similar features. Finally, we propose a possible experimental realization of this model using Rydberg atoms in a tilted field.

P18

An ab initio perspectives on the electronic and optical characteristics of ML-MoSe2: Role of electric field

The presence of an external electric field has a large influence on the properties of low-dimensional materials. Here, we examine the change of the band gap (Eg), the optical absorption coefficient (OAC), the refractive index (RI), and the optical conductivity of a monolayer MoSe2 (ML) with respect to the variation in the external electric field strength. Our results, based on a DFT calculation, exhibit an increase in the band gap when the electric field is turned on. However, we are witnessing a remarkable decrease in Eg for electric field strengths exceeding 0:7 V A˚–1. Further, we obtained a great correlation between the external electric field and the OAC. On the other hand, we have established that the light polarization perpendicular to the plane of the ML MoSe2 shifts the position of the OAC peak to shorter wavelengths, and leads to split the OAC peak located at 110 nm. We have also achieved that the external electric field reduces the optical conductivity of the ML MoSe2, this effect is found to be more pronounced for negative field strengths. Lastly, we found that the RI shrinks when the electric field is turned on.

P19

Topological Kondo superconductor

Yung-Yeh Chang[1] **, Khoe Van Nguyen**[2] **, Kuang-Lung Chen**[2] **and Chung-Hou Chung**[1,2]

[1]*Physics Division, National Center for Theoretical Sciences, Hsinchu 30013, Taiwan, R.O.C.*
[2]*Department of Electrophysics, National Yang Ming Chiao Tung University, Hsinchu 30010, Taiwan, R.O.C.*

We theoretically propose a topological Kondo superconducting phase in a two-dimensional Kondo lattice. Due to the odd parity of the localized f-orbitals, the Kondo hybridization between f-electrons and conduction electrons shows an odd-parity momentum dependent form factor. Consequently, this effectively features the spin-orbit interaction. This unconventional type of Kondo hybridization gives rise to an effective ferromagnetic Ruderman-Kittel-Kasuya-Yosida (RKKY) interaction among the localized f-orbitals via perturbation theory, leading to spin-triplet resonating-valence-bond (RVB) pairing between f-electrons with $p+ip$-wave gap symmetry. There exists competition and collaboration between the Kondo hybridization and the ferromagnetic RKKY coupling. Via a static mean-field approach, we explore the phase diagram of this model. Apart from a Kondo-dominating and a RVB-dominating phase, we find a Kondo triplet RVB coexisting phase in the intermediate range of the Kondo to RKKY coupling ratio. This is a superconducting phase with spin-triplet $p+ip$-wave pairing gap. We further show that this co-existing phase is a time-reversal invariant topological superconducting state which supports helical Majorana zero modes at the edges of a nano-strip system. Our results provide an unique example of topological superconductivity arising from Kondo correlations, and are relevant for the possible topological Kondo superconducting state in heavy-fermion compounds.

P20

Superconductivity on the Quasi One-Dimensional Flat Band

Si Min Chan[1,2], **B. Grémaud**[3], **and G. G. Batrouni**[4,1,2,5]

[1]*Centre for Quantum Technologies, National University of Singapore*
[2]*Department of Physics, National University of Singapore*
[3]*Aix Marseille Univ, Université de Toulon, CNRS, CPT, Marseille, France*
[4] *Université Côte d'Azur, CNRS, Institut de Physique de Nice (INPHYNI), 06103 Nice, France*
[5] *Beijing Computational Science Research Center, Beijing 100193, China*

Flat band systems offer the possibility of revealing exotic quantum phases with the highly degenerate states that they support. We study theoretically and analytically the validity of the BCS approach in studying superconductivity on topological flat bands and compare the results with exact density matrix renormalisation group (DMRG) computation. We show with the full multiband mean-field decomposition of the Hubbard interaction term, that the superfluid density, D_s, on the flat band is not necessarily proportional to the quantum metric. This is evident for systems with inequivalent sublattice sites, where the pairing order parameter and sublattice fillings are distinct. Additionally, with several examples, we establish that the full mean-field can qualitatively and quantitatively describe the superconductivity across the entire range of interaction, U.

[1] S. M. Chan, B. Grémaud, G. G. Batrouni, Physical Review B **105**, 024502 (2022)

P21

Metal-insulator Transition in Strongly Correlated Binary Manganese Chalcogenides

E. Chernov[1], **A. Lukoyanov** [1,2]

[1]*M.N. Mikheev Institute of Metal Physics of the Ural Branch of the Russian Academy of Sciences, Yekaterinburg*
[2]*Ural Federal University, Yekaterinburg*

Manganese chalcogenides are being actively studied both experimentally and theoretically because of metal-to-insulator transition under pressure and possible catalytic, optical and magnetic applications [1, 2, 3]. In particular, binary manganese sulphide MnS was found in several crystal phases: α–γ-MnS. The α-MnS phase crystallizes in cubic structure (Space Group $Fm\bar{3}m$), γ-MnS — in hexagonal structure (SG $P6_3mc$). It is known that γ-MnS is metastable when heated to 200-300° C, it becomes the α-MnS phase [1]. We carried our theoretical studies of this compound taking into account antiferromagnetic ordering of the manganese ions at the ambient conditions and in compressed unit cells. To study the electronic structure of MnS, our calculations were done in the Quantum ESPRESSO software package [4] using the DFT+U method [5] for the Pedew-Burke-Ernsenhof (PBE) form of exchange-correlation functional [6]. MnS is a wide-gap insulator at the ambient condition, but in order to reproduce the wide gap, strong electronic correlations should be taken into account. To obtain the experimental value of the band gap, the values of the Coulomb interaction parameter U = 6.9 eV and the exchange interaction J = 0.86 eV were taken. For the compressed volumes of the unit cell it is found that the band gap is decreased and finally closed for the volume of the cell about 50% of the ambient volume. Thus the closure of the energy gap and increase of the metallic states at the Fermi energy demonstrate a transition from an insulator to a metal in MnS observed experimentally. The work was supported by RFBR grant (project 20-02-00234).

[1] X. Yang, et al., J. Phys. Chem. C, **116**, 3292 (2012).
[2] A.A. Dyachenko, et al., Phys. Rev. **98**, 085139 (2018).
[3] P. Wang, et al., Chem. Mater. **34**, 3931 (2022).
[4] P. Giannozzi, et al., J. Phys. Condens. Matter. **21**, 395502 (2009).
[5] V. Anisimov, O. Gunnarsson, Phys. Rev. **43**, 7570 (1991).
[6] J. Perdew, et al., Phys. Rev. Lett. **9**, 767 (1996).

P22

Quantum injection model for hot and cold charge transfer states in organic solar cells

Khouloud Chika[1], Jouda Jemaa Khabthani[1], and Didier Mayou[2]

[1] *Laboratoire de Physique de la Matière Condensée,Département de Physique,Faculté des Sciences de Tunis, Université Tunis El Manar, Campus Universitaire,1060 Tunis,Tunisia*

[2] *CNRS, Institut NEEL, F-38042 Grenoble, France. Université Grenoble Alpes,Institut NEEL, F-38042 Grenoble, France*

Theoretical models describing organic solar cells (OSCs) are developed in a semi-classical way and do not provide a good understanding of what is going on. The complexity of the charge separation mechanism at the interface of organic solar cells requires the use of a quantum model which can take into account all the parameters that play a very important role in this mechanism. We use a fully quantum modeling of electronic transport in organic solar cells. The advantage of this approach is that it is an efficient numerical tool with a very low numerical cost compared to other quantum approaches. We use quantum modeling to understand the physical phenomena that occur as a result of electron-hole dissociation and we also want to understand the effect of phonon modes on charge injection. We present the effect of recombination at the donor-acceptor interface in the charge transfer mechanism and the hot and cold transfer criteria.

P23

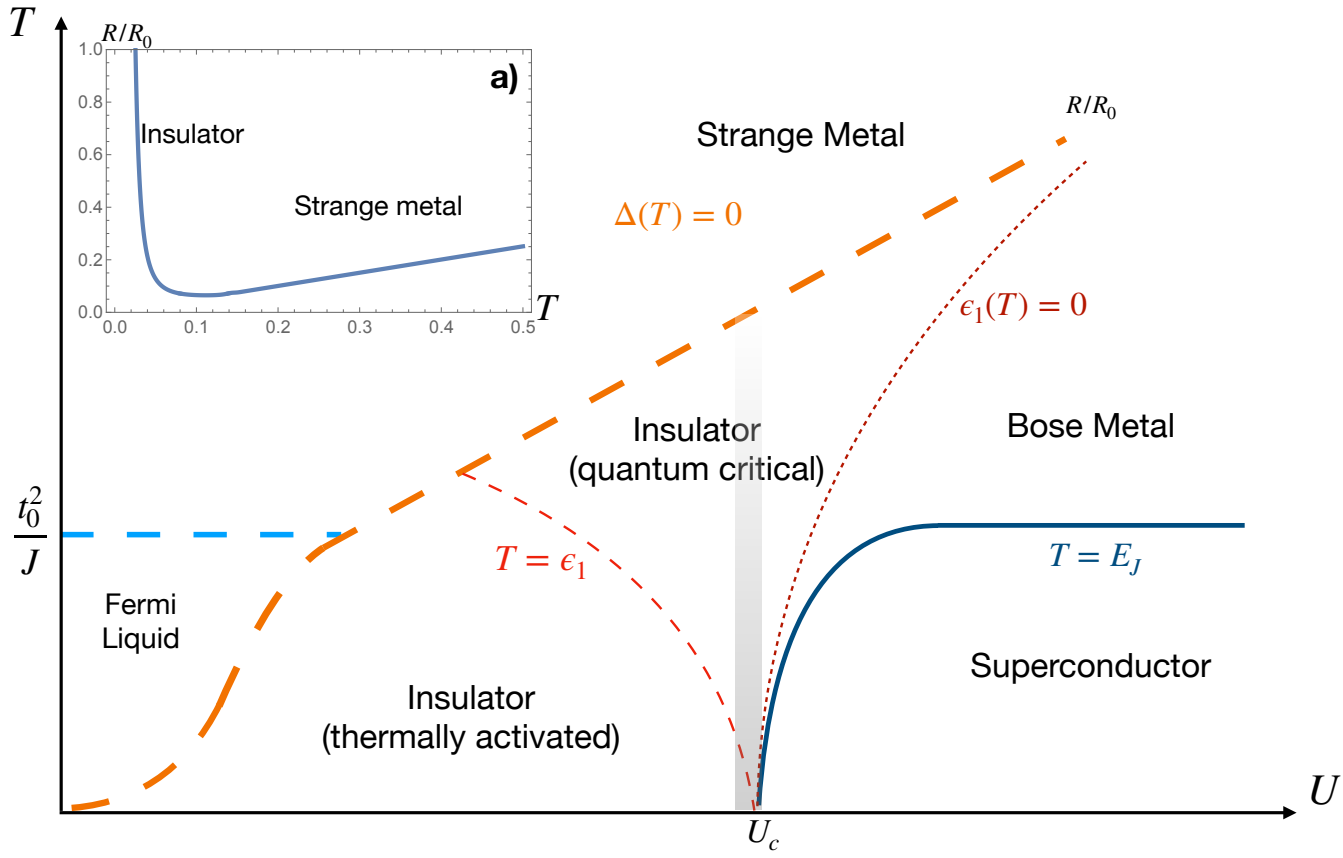
T
R/R0
a)
Insulator
Strange metal
T
Strange Metal
R/R0
Δ(T) = 0
ϵ1(T) = 0
Insulator
(quantum critical)
Bose Metal
t0²/J
T = ϵ1
T = EJ
Fermi
Liquid
Superconductor
Insulator
(thermally activated)
U
Uc

P24

Interplay between the correlations responsible for the pseudogap and the charge density wave phase

Prauchner, L. C[1], **Magalhães S.G**[1], **and Calegari, E.J**[2]

[1]*Instituto de Física, Universidade Federal do Rio Grande do Sul, 91501-970, Porto Alegre, RS, Brazil*

[2]*Departamento de Física - Universidade Federal de Santa Maria, 97105-900, Santa Maria, RS, Brazil*

Strongly correlated electron systems present a wide array of phenomena that are still not fully explained, such as the pseudogap, observed in the cuprate superconductors[1]. Characterized by a partial gap on the Fermi surface, as well as a suppression of the number of states around the Fermi level, the pseudogap is a focus of discussion between different scopes of research, both theoretical and experimental. One of the main points of this high interest is the interplay between the pseudogap and unconventional superconductivity, as well as with pair-density waves[2, 8]. It is believed that understanding other phases and phenomena which are associated with instabilities caused by the same correlations, can be the key to better understand the pseudogap phenomena and superconductivity in these systems. Recent experimental [3, 4] results suggest that the pseudogap is caused by the short-range antiferromagnetic correlations, present in the underdoped strongly correlated regime of cuprates. Therefore, the main focus of this work is to investigate how the antiferromagnetic correlations, which can be responsible for a pseudogap, may affect the charge density wave (CDW) phase. In this work, we consider the Green's functions within the Matsubara's finite temperature formalism , alongside a n-pole approximation [6], to take into account both the correlations due to the repulsive Coulomb interaction U, and the antiferromagnetic correlations. The CDW order parameter comes from a BCS-like model[5], while the Coulomb interaction is included through a two-dimensional Hubbard model[7]. A careful analysis demonstrated that an increase in U favors antiferromagnetic fluctuations and, from those fluctuations, it is shown that the re-normalized band becomes flat around the anti-nodal points $(0, \pm\pi)$ and $(\pm\pi, 0)$. The pseudogap manifests itself through the band structure and the density of states, therefore, we investigated both these quantities for different values of U and occupation number $(n_T = n_\sigma + n_{-\sigma})$. In order to analyze the effects of the antiferromagnetic correlations on the CDW state, we evaluated the CDW order parameter for the same set of parameters considered in the re-normalized band structure and density of states study.

[1] Keimer B, Kivelson S A, Norman M R, Uchida S and Zaanen J, Nature **518** (2015)
[2] W. A. Atkinson, S. Ufkes, and A. P. Kampf, Phys. Rev. B **97** (2018)
[3] M.K. Chan, C. Dorow, L. Mangin-Thro, Y. Tang, Y. Ge, M.J. Veit, G. Yu, X. Zhao, A.D. Christianson, J.T. Park, Y. Sidis, P. Steffens, D.L. Abernathy, P. Bourges and M. Greven, Nat. Commun. **7** (2016)
[4] K.H.A. Villegas, V.M. Kovalev, F.V. Kusmartsev and I.G. Savenko, Phys. Rev. B **98** (2018)
[5] Balseiro C A and Falicov L M, Phys. Rev. B **20** (1979)
[6] Laura M. Roth, Phys. Rev. **184** (1969)
[7] J. Hubbard, Proceedings of the Royal Society of London. Series A, Mathematical and Physical Sciences, **277** (1964).
[8] S. V. Borisenko, A. A. Kordyuk, A. N. Yaresko, V. B. Zabolotnyy, D. S. Inosov, R. Schuster, B. Büchner, R. Weber, R. Follath, L. Patthey, and H. Berger, Phys. Rev. Lett. **100** (2008)

P25

Effect of interface hybridization on proximity induced superconductivity in quantum spin Hall insulator 1T'-WTe_2

Anirban Das[1,2], **Bent Weber**[3,4], **and Shantanu Mukherjee**[1,2,5]

[1]*Department Of Physics, Indian Institute Of Technology Madras, Chennai, 600036, India*
[2]*Computational Materials Science Group IIT Madras, Chennai, Tamil Nadu 600036, India*
[3] *Division of Physics and Applied Physics, School of Physical and Mathematical Sciences, Nanyang Technological University, Singapore 637371, Singapore*
[4]*ARC Centre of Excellence for Future Low-Energy Electronics Technologies (FLEET), School of Physics, Monash University, Clayton VIC 3800, Australia*
[5] *Quantum Centres in Diamond and Emergent Materials (QCenDiem)-Group IIT Madras Chennai, Tamil Nadu 600036, India*

The interplay of topology and superconductivity has become a subject of intense research in condensed matter physics for the pursuit of topologically nontrivial forms of superconducting pairing. An intrinsically normal-conducting material can inherit superconductivity via electrical contact to a parent superconductor via the proximity effect. However, at high interface transparency, strong coupling inevitably leads to changes in the band structure owing to hybridization of electronic states. Here, we investigate such strongly proximity-coupled heterostructures of monolayer 1T' WTe_2 , grown on 2H-$NbSe_2$ by van der Waals epitaxy. We argue that the quantum spin Hall gap in 1T'-WTe_2 and the corresponding helical conducting edge states are renormalized when placed in proximity to an s-wave superconductor like 2H-$NbSe_2$. Our material-specific tight-binding model captures the hybridized heterostructure quantitatively and confirms that strong interlayer hopping gives rise to a semi metallic density of states in the two-dimensional WTe_2 bulk, even for nominally band-insulating crystals. The model accurately reproduces the measured superconducting gap of 0.6 meV induced in the WTe_2 monolayer bulk. We further show how both the surface and edge properties are anisotropic between the orthogonal edges of this orthorhombic monolayer QSHI.

[1] W Tao, Z J Tong, A Das, D Q Ho, Y Sato, M Haze, J Jia, Y Que, F Bussolotti, K. E. J Goh, B Wang, H Lin, A Bansil, S Mukherjee, Y Hasegawa, and B Weber, Physical Review B, **105**, 094512 (2022).

P26

Abstract template for Strongly Correlated Matter: from Quantum Criticality to Flat bands

Magneto-transport Properties of the Double Quantum Dot Transistor in the Strongly Correlated Regime

Debika Debnath [1], **Ashok Chatterjee** [2]

School of Physics, University of Hyderabad, Gachibowli, Hyderabad, Telangana, India, 500046

Quantum magneto-transport in a dissipative double quantum dot transistor is investigated at finite temperature in the presence of electronic correlation and electron-phonon interaction within the framework of the Anderson-Holstein-Caldeira-Leggett Hamiltonian [1]. The electron-phonon interaction and the phonon dissipation are dealt with by the canonical transformation. The phonons are first removed from the theory by averaging the Hamiltonian with respect to a coherent phonon state and the resultant electronic Hamiltonian is finally solved with the help of the Green function technique by Keldysh [2]. The variations of the transport properties such as spectral function, tunnelling current, differential conductance and spin polarization are determined with respect to the Coulomb correlation and the polaronic interaction.

[1] Narasimha, R. C., Ashok, C., Scientifc Reports **6**, 18511 (2016).
[2] Keldysh, L. V., Sov. Phys. JETP **20**, 1018–1026 (1965).

P27

High pressure structural instability in $CeSb_2$

C. K. de Podesta[1], T. I. Weinberger[1], J. Chen[1], G. I. Lampronti[2], C. M. Beavers[3], Z. Feng[1], P. Nikowitz[4], T. Giles[4], and F. M. Grosche[1]

[1]*Cavendish Laboratory, University of Cambridge, Cambridge CB3 0HE, UK.*

[2]*Department of Earth Sciences, University of Cambridge, Cambridge CB2 3EQ, UK*

[3]*Diamond Light Source Ltd., Harwell Campus, Didcot OX11 0DE, UK*

[4] *Department of Physics, Royal Holloway University of London, Egham TW20 0EX, UK*

Ambient pressure $CeSb_2$ is a rare instance of a Ce-based Kondo lattice material with a ferromagnetic ground state [1], as well as at least two further magnetic states in a complex field-temperature phase diagram. This invites closer examination under applied hydrostatic pressure, which can often be used as a tuning parameter to explore quantum phase transitions where magnetism is suppressed. Previous studies showed that the magnetic phase diagram is initially robust under the application of moderate pressure but changes abruptly above ~15 kbar [2].

Extensive high-pressure transport measurements reveal that this abrupt change coincides with a pronounced hysteretic anomaly in the resistivity of the material, which suggests a first-order structural transition. We investigate the structural origin of this anomaly in diamond anvil cell powder X-ray diffraction measurements, up to 80 kbar at 300 K. Our findings indicate that above ~10 kbar, $CeSb_2$ undergoes a first-order structural transition from the "$SmSb_2$-type" *Cmca* low-pressure structure [3], to the "$EuSb_2$-type" $P2_1/m$ structure. This new symmetry corresponds to a translation between the now offset neighboring Ce-Sb planes, and a compression in the perpendicular c-axis.

In the high-pressure state, the Ce atoms lie closer together in zig-zag chains, producing a profoundly different electronic structure to that of ambient pressure $CeSb_2$. A detailed investigation of transport and thermodynamic properties within the "$EuSb_2$-type" high pressure state of $CeSb_2$ reveals a very low-lying maximum in the electrical resistivity at < 4 K, indicating a low coherence temperature, high carrier effective mass, and two new transition anomalies, which are continuously suppressed by further increased pressure [4].

[1] S. L. Bud'ko, P. C. Canfield, C.H. Mielke, A. H. Lacerda, Phys. Rev. B **57,** 13624 (1998).
[2] T. Kagayama, G. Oomi, S. L. Bud'ko, P. C. Canfield, Physica B **281–282,** 90 (2000).
[3] R. Wang, H. Steinfink, Inorg. Chem. **6,** 1685 (1967).
[4] O. P. Squire *et al.* , this conference (2022).

P28

Flat-band physics in the spin-1/2 Heisenberg frustrated bilayers

Oleg Derzhko

Institute for Condensed Matter Physics, National Academy of Sciences of Ukraine, Svientsitskii Street 1, 79011 L'viv, Ukraine

We consider several bilayer lattices consisting of two square, honeycomb, or triangular planes and the $S{=}1/2$ Heisenberg model with the antiferromagnetic exchange couplings J, $J_\perp$, and $J_\times$ corresponding to the nearest-neighbor intra-, interplane, and next-nearest-neighbor interplane interactions, respectively. In the fully frustrated case $J{=}J_\times$, a dispersionless (flat) one-magnon band emerges and it becomes the lowest one if $J_\perp/J$ is sufficiently large. Flat-band states (localized magnons) are the singlet located on the strongest bonds $J_\perp$. Flat-band physics emerges at low temperatures in the presence of a magnetic field [1, 2, 3, 4, 5]. Since many-magnon ground states can be constructed from the localized magnons placed on the $J_\perp$ bonds and obeying certain hard-core rules concerning the occupation of the neighboring $J_\perp$ bonds, the low-temperature thermodynamics of the frustrated bilayer in a field is related to the well-known two-dimensional Ising or Potts models. The emergent discrete symmetry associated with the occupation of the $J_\perp$ bonds by localized magnon can be spontaneously broken at finite temperature: The spin-1/2 Heisenberg frustrated bilayers exhibits an order-disorder phase transition falling into the two-dimensional Ising [1, 2, 3, 4] or three-state Potts [5] model universality class.

The recently synthesized magnetic compound $Ba_2CoSi_2O_6Cl_2$ [6] seems to be an almost perfect candidate to observe the described flat-band physics in experiments. We develop a theory for $Ba_2CoSi_2O_6Cl_2$ [4] and propose new experimental studies to detect a field-driven phase transition related to a Wigner-crystal-like ordering of localized magnons at low temperatures. This phase transition occurs in high magnetic fields $\mathsf{H}{>}32.16$ T and can be driven either by temperature or by magnetic field. To detect this transition in experiment we propose low-temperature measurements of the specific heat c at $\mathsf{H}{>}32.16$ T to find the characteristic singularity in c at $T{<}3.17$ K.

[1] J. Richter, O. Derzhko, T. Krokhmalskii, Phys. Rev. B **74**, 144430 (2006).
[2] O. Derzhko, T. Krokhmalskii, J. Richter, Phys. Rev. B **82**, 214412 (2010).
[3] T. Krokhmalskii, V. Baliha, O. Derzhko, J. Schulenburg, J. Richter, Phys. Rev. B **95**, 094419 (2017).
[4] J. Richter, O. Krupnitska, V. Baliha, T. Krokhmalskii, O. Derzhko, Phys. Rev. B **97**, 024405 (2018).
[5] J. Strecka, K. Karlova, V. Baliha, O. Derzhko, Phys. Rev. B **98**, 174426 (2018).
[6] H. Tanaka, N. Kurita, M. Okada, E. Kunihiro, Y. Shirata, K. Fujii, H. Uekusa, A. Matsuo, K. Kindo, H. Nojiri, J. Phys. Soc. Jpn. **83**, 103701 (2014).

P29

Low energy excitation between two Quantum Hall Ferromagnet

Suman Jyoti De[1], **Sumathi Rao**[2], **and Ganpathy Murthy**[3]

[1] *Harish-Chandra Research Institute, A CI of Homi Bhabha National Institute, Chhatnag Road, Jhunsi, Prayagraj 211019, India*

[2] *International Centre for Theoretical Sciences (ICTS—TIFR), Shivakote, Hesaraghatta Hobli, Bangalore 560089, India*

[3] *Department of Physics and Astronomy, University of Kentucky, Lexington KY 40506-0055, USA*

We study the interface between two regions of monolayer graphene in a perpendicular magnetic field, (the quantum Hall setup) with filling fractions $\nu = -1$ and $\nu = 1$, in the presence of long-range Coulomb and short-range valley anisotropic interaction terms. By tuning the width of the interface(W), we find two distinct interface phases characterised by different low energy excitations. For small W, the interface prefers to be a spin ferromagnet(FM) with an excitation gap equal to the Zeeman energy. For larger W, the interface prefers to be in a canted anti-ferromagnet(CAF) phase, which spontaneously breaks the $U(1)$ spin symmetry about the Zeeman field in the Hartree-Fock calculation. However, by going beyond Hartree-Fock theory, we find that the CAF phase has two counter propagating bulk gapless Goldstone modes, apart from the two chiral edge modes. These modes restore the $U(1)$ symmetry. The phase transition between the FM and the CAF phases can be detected in a two terminal conductance measurement across the junction. In the FM phase, the two chiral edge modes have opposite spins and hence the static-disorder induced current across the junction is small, whereas in the CAF phase, the chiral edge modes can and will have non-zero spin overlap giving rise to a much larger current across the junction.

P30

Pressure effect on strongly correlated iron-chalcogenides : DFT study

Mott metal-insulator transition (MIT) is one of the major questions of condensed matter, where the interactions between the electrons of a conductor become strongly correlated and localized to the atoms of the crystal. As this transition corresponds to the emergence of antiferromagnetism, Mott insulators are considered important not only from a fundamental point of view but also for the new technology of electronic devices. We will use the theory of density function (DFT) with a particular exchange-correlation treatment to study MIT under the effect of hydrostatic pressure. Indeed, the objective is on the one hand to consolidate our fundamental knowledge on this MIT and on the other hand, to predict new Mott insulator materials with specific properties.

P31

Exact diagonalization of Rydberg atoms Hamiltonian in fractal lattices

The experimental control of Rydberg atoms with lasers reached a level in which the atoms can bepositioned in 2D lattices with the desired geometry. The van der Waals interaction between atoms goes beyond a nearest-neighbor model. The system can be described theoretically as a transverse field Ising model. We use exact diagonalization as a first approach to obtain the phase diagram to systems up to 24 atoms in the fractal Sierpinski triangle. We compute observables such as the entanglement entropy, and susceptibility to try to understand the phases and phases transition. The aim is to propose experiments to dynamically prepare quantum phases with the system.

P32

Nature of the anomalous 4 / 13 fractional quantum Hall effect in graphene

Extensive fractional quantum Hall effect (FQHE) has been observed in graphene-based materials. Some of the observed fractions are anomalous in that FQHE has not been established at these fractions in conventional GaAs systems. One such fraction is 4/13, where incompressibility has recently been reported in graphene [Kumar et al., Nat. Commun. 9, 2776 (2018)]. We propose a partonic wave function at 4/13 and show it to be a viable candidate to describe the Coulomb ground state. Using the effective edge theory, we make predictions for experimentally measurable properties of the state.

P33

Flat bands in alternating Hubbard ladder

Kaouther Essalah, Ali Benali[1], Anas Abdelwahab, Eric Jeckelmann[2], and Richard Scalettar[3]

[1] *University of Tunis El-Manar, Tunis, Tunisia*
[2]*Leibniz University, Hannover, Germany ,*
[3] *University of California, Davis, USA*

We investigate the Hubbard Hamiltonian on alternating ladders, these geometries are bipartite with non-equal or equal number of sites on the two sublattices. Thus they share a key feature of the Hubbard model in a class of lattices which Lieb has shown analytically to exhibit long-range ferrimagnetic order, while being amenable to powerful numeric approaches developed for quasi-one-dimensional geometries. The Density Matrix Renormalization Group (DMRG) method is used to obtain the ground state properties, e.g. excitation gaps, charge and spin densities as well as their correlation functions at half-filling. We show the presence of flat bands as well as the existence of long-range ferrimagnetic order in the one-dimensional ladder geometries.

[1] Kaouther Essalah et al. Magnetic properties of alternating Hubbard ladders. Physical Review B **103**, 1357 (2021).

P34

Thermal Properties of Soil Samples from Different Landforms in Three Local Government Areas of Ondo State, Nigeria.

ABSTRACT The study examines the thermal properties of some selected soil samples from different landforms, namely Sand Hill (SH), Sand Ridges (SR) and Coastal Sand (CS) in three local government area of Ondo State, Nigeria. The soil samples were sieved into different particle sizes such as 300 µm, 425 µm, 600 µm, 850 µm, and 1180 µm with appropriate mesh and moulded in form of a Lee's disc. The result shows that, increase in the moisture content results to increase in thermal conductivity of the samples. It also shows that, the thermal conductivity decreases with increase in the particle sizes of the soil materials. The thermal conductivity and diffusivity of the sample falls within the range 0.2493 W/mK-1.8894 W/mK and 0.29x10-7m2s-1- 3.23x10-7m2s-1 respectively. Study of the elemental composition revealed that the soil samples contain manganese (Mn), zinc (Zn), iron (Fe) and copper (Cu) which are essential for plant growth. Based on this experimental result and comparison with previous researches, it was observed that the thermal conductivity obtained are good for agricultural, building and construction purposes.

P35

Topological Shiba states in a 1D superconductor with a local magnetic impurity

In this work we study the physical properties in a superconducting 1D system with a local magnetic impurity. The Bogolivob de Gennes Hamiltonian shows an energy gap around the Fermi levels, the presence of a magnetic field has shown to introduce energy levels inside the gap, called Shiba states. The position of the Shiba states depends on the strenght of the local magnetic field and the width of the peak around a site in the chain. This state is a coherent superposition of particles and holes with energy +-E, due to the particle-hole symmetry of the Hamiltonian, these quasiparticles have a definite Parity and can determinate a topological invariant of the system. The topological charge described by the Pfaffian of the Hamiltonian describes the parity of the ground state, when the state crosses the zero energy level the parity change and we have a different topological charge.

P36

Contributions of Collective Excitations to Third Harmonic Generation in Superconducting MgB_2

J. Fiore[1], M. Udina[1], M. Marciani[1], G. Seibold[2] and L. Benfatto[1]

[1] Department of Physics, Sapienza University of Rome, and ISC-CNR, Rome, Italy
[2] Institut für Physik, BTU Cottbus-Softenberg, Cottbus, Germany

Recent experimental findings from non-linear THz spectroscopies in superconducting (SC) systems stimulated a long debate on the role of collective excitations in determining for instance the Third Harmonic Generation (THG) intensity. In this case an increase of THG signal is observed when the frequency of the incident field matches the SC gap value, where both amplitude or Higgs fluctuations and the BCS response can be activated. While in clean samples it is now clear that the latter dominates, in disordered systems the situation is more debated, since light couples with the possible excitations with different strengths and the level of disorder is fundamental to determine their hierarchy [1,2]. In two-bands systems the situation is even more complicated, since 1) there are two order parameters with the two bands being at different disorder levels and 2) the same spectra of the Higgs excitations vary with the degree of interband coupling. In addition, in this case a third massive mode is present, the so-called Leggett mode, connected to the fluctuations of the relative phase of the two SC order parameters. Recent experimental results on thin films of MgB_2 showed an enhancement of THG only when the incident field resonates either with the Leggett [3] or with the smaller gap [4], making it necessary to address the interplay of the various phenomena to understand the reason of the observed selectiveness. Here we first address the nature of the amplitude fluctuations in a two-bands superconductor, showing that the spectral weight of the Higgs fluctuations rapidly shifts towards the larger gap as the interband coupling is turned on. Second, we provide a quantitative estimate of the contribution of various processes to THG in MgB_2, by estimating the disorder level from a fit of the experimental optical conductivity. By using exact numerical simulations [5] to estimate the relative contribution of the Higgs mode and BCS response we find that the observed resonance with the small gap must be attributed to the BCS response. Indeed, from one side in MgB_2 the spectral weight of the Higgs fluctuations at the smaller gap is very small. From the other side the paramagnetic coupling of light with the Higgs fluctuations is still smaller than the quasiparticle one at the disorder level derived from the fit of the experimental optical conductivity. Finally, we discuss [5] how paramagnetic processes can also trigger a stronger visibility of the Leggett mode as compared to diamagnetic processes considered so far [3].

References

[1] M. Silaev, Phys. Rev. B **99**, 224511 (2019)
[2] G. Seibold, M. Udina, C. Castellani and L. Benfatto, Phys. Rev. B **103**, 014512 (2021)
[3] F. Giorgianni, T. Cea, C. Vicario, C. P. Hauri, W. K. Withanage, X. Xi and L. Benfatto, Nat. Phys. **15**, 341 (2019)
[4] S. Kovalev et al., Phys. Rev. B **104**, L140505 (2021)
[5] J. Fiore, M. Udina, M. Marciani, G. Seibold and L. Benfatto, preprint 2022

P37

The frustration of being odd

We consider the effects of so-called Frustrated Boundary Conditions (FBC) on quantum spin chains, namely periodic BC with an odd number of sites. First, we show that, in absence of external fields, FBC allow for the direct determination of correlation functions that signal a spontaneous symmetry breaking, such as the spontaneous magnetization. When paired with anti-ferromagnetic interactions, FBC introduce geometrical frustration into the system and the ground state develops properties which differ from those present with other boundary conditions, thus brining striking, yet puzzling, evidence that certain boundary conditions can affect the bulk properties of a 1D system. Finally, we argue that FBC introduce long-range order in the system, similar to that enjoyed by SPT phases. Our results prove that even the weakest form of geometrical frustration can deeply affect a system's properties and pave a way for a bottom-up approach to better understand the effects of frustration and their exploitations also for technological purposes.

P38

Influence of pairing symmetry and multiple energy gaps on the behaviour of critical current through the Josephson junction

The extended Ambegaokar–Baratoff model was applied to calculate the critical current (Ic) of a superconductor/insulator/superconductor (S/I/S) Josephson junction with multiple tunnelling channels. We analysed the sensitivity of the critical current, multiplied by normal-state resistance (i.e., IcRn product), to the symmetries of the order parameter in the Bardeen–Cooper–Schrieffer (BCS)-type gap formula. In addition, we showed that the temperature dependence of the product IcRn(T), which corresponds to multigap symmetry, exhibits a shoulder-like feature and has a pronounced kink at T=10 K for the SmFeAsO0.9F0.1 superconductor.

P39

Viscoelasticity of an anisotropic electron liquid

It is well-known that in long-wavelength limit and finite frequency of external perturbation, the current density within linear response regime is equivalent to a viscoelastic model of electron liquid. A question is that what this elasticity/hydrodynamics correspondence would be in the case of an anisotropic liquid like that of phosphorene. This talk is about an attempt to answer this question, by means of some extensions and generalizations of the existed and verified model. One interesting aspect of this generalization is that it may be considered as an example of a holographic correspondence.

P40

Excitonic metal and non-Fermi liquid behaviour in twisted double bilayer graphene

We show that twisted double bilayer graphene, whose band structure shows low energy electron and hole pockets, forms an excitonic metal near the charge neutrality point at very low temperatures ~ a few K. This leads to interesting implications for low-temperature transport in the system as a function of carrier density. Above the transition temperature, the density fluctuations in this critical metal lead to non-Fermi liquid features, which can also be seen in the temperature dependence of transport in the system. Similar features are also observed in recent experiments on these systems.

P41

Topological and stacked flat bands in bilayer graphene with a superlattice potential

We show that bilayer graphene in the presence of a 2D superlattice potential provides a highly tunable setup that can realize a variety of flat band phenomena. We focus on two regimes: (i) topological flat bands with non-zero Chern numbers, C, including bands with higher Chern numbers $|C| > 1$; and (ii) an unprecedented phase consisting of a stack of nearly flat bands with $C = 0$. For realistic values of the potential and superlattice periodicity, this stack can span nearly 100 meV, encompassing nearly all of the low-energy spectrum. Our results provide a realistic guide for future experiments to realize a new platform for flat band phenomena.

P42

Spin-dependent electron-electron interaction in Rashba materials

Yasha Gindikin[1] **and Vladimir A. Sablikov**[2]

[1] *W.I. Fine Theoretical Physics Institute, University of Minnesota, Minneapolis, MN 55455, USA*

[2] *Kotelnikov Institute of Radio Engineering and Electronics, Russian Academy of Sciences, Fryazino, 141190, Russia*

The work is devoted to the effects of the pair spin-orbit interaction (PSOI) [1]. The PSOI is the electron-electron interaction component that depends on the spin and momentum of the electrons. It is produced by the Coulomb fields of interacting electrons in materials with the giant Rashba effect. The main nontrivial feature of the PSOI is that it is attractive for electrons in certain spin configurations tied to their momentum and competes with the Coulomb repulsion of the electrons. In many-electron systems the PSOI results in the instabilities of the uniform ground state with respect to the density fluctuations, which develop on different spatial scales depending on the electron concentration, density of states and the geometry of the electric fields that produce the PSOI [2, 3]. If the PSOI is not too strong the electronic system is stable, but its collective excitations reveal the highly unusual spin-charge structure and spectrum, which manifest themselves in the frequency dependence of the dynamic conductivity [4].

[1] Yasha Gindikin and Vladimir A. Sablikov, *Pair spin-orbit interaction in low-dimensional electron systems*, The European Physical Journal Special Topics, **229**, 503 (2020).

[2] Yasha Gindikin and Vladimir A. Sablikov, *Electron correlations due to pair spin-orbit interaction in 2D electron systems*, Physica E, **143**, 115328 (2022).

[3] Yasha Gindikin and Vladimir A. Sablikov, *Image-potential-induced spin-orbit interaction in one-dimensional electron systems*, Physical Review B **95**, 045138 (2017).

[4] Yasha Gindikin and Vladimir A. Sablikov, *Dynamics of one-dimensional electrons with broken spin-charge separation*, Phys. Status Solidi RRL, **12**, 1700313 (2018).

P43

SKYRME CRYSTAL IN TWISTED DOUBLE BILAYER GRAPHENE

Debasmita Giri [1] , **Dibya Kanti Mukherjee** [2,3] , **H.A. Fertig**[2,3], **Arijit Kundu** [1]

[1]*Department of Physics, Indian Institute of Technology Kanpur, Kanpur 208016, India*
[2] *Department of Physics, Indiana University, Bloomington, IN 47405*
[3]*Quantum Science and Engineering Center, Indiana University, Bloomington, IN, 47408*

The discovery of correlated insulating (CI) states and superconductivity in twisted bilayer graphene (TBG) has prompted a new window for intense theoretical and experimental studies in the 2D \moire system.
The ground state of the half-filled first moire conduction band in twisted double bilayer graphene(TDBG) is spin-polarised. Our primary interest is to find the solution for the charged excitation of the ferromagnetic ground state just away from half-filling(>0.5). The simplest excitation would be one particle exciation, when one electron is removed from (or added to) the ground state. Instead we will show that under certain condition the spin texture or the skyrmions are the lowest energy charge exciation. There is experimental evidence that in quantum hall ferromagnets(QHF), the topological spin texture or skyrmion is the lowest energy charge excitation. So far, most of the theoretical studies of skyrmions rely upon analysing the effective non-linear sigma model(NLSM). While such studies provide qualitative insight, it does not give accurate description of charge spin texture. In this paper we study the nature of charged spin-texture excitation within self-consistent Hartree-Fock calculation(HF). We also show that compared to twisted bilayer graphene(TBG), a vertical electric field can change the topology of bands in TDBG, which also account for skyrmions with different quantised charges.

[1] L. Brey, H. A. Fertig, R. Cote, and A. H. MacDonald, PRL, 75(13):2562-2565(1995).

P44

Abstract for Strongly Correlated Matter: from Quantum Criticality to Flat Bands I (smr 3732), 22.08.22-02.09.22

Tunneling study in granular aluminum near the Mott metal-to-insulator transition

Aviv Glezer Moshe [1,2,3] , **Gal Tuvia** [1] , **Shilo Avraham**[1,2], **Eli Farber**[2], **and Guy Deutscher** [1]

[1] *Raymond and Beverly Sackler School of Physics and Astronomy, Tel Aviv University, Tel Aviv 6997801, Israel*

[2] *Department of Physics and Department of Electrical and Electronic Engineering, Ariel University, Ariel 40700*

[3] *National Institute of Chemical Physics and Biophysics, Akadeemia tee 23, 12618 Tallinn, Estonia*

We find that in superconducting granular aluminum films, consisting of nano-scale metallic grains weakly coupled together, the optical gap and the tunneling gap are in excellent agreement up to the Metal to Insulator transition [1,2]. This is in sharp contrast to atomically disordered superconductors such as NbN_x, for which the optical gap becomes smaller than the tunneling gap [3]. This difference is being attributed to the respective natures of the Metal to Insulator transition in these materials, being of the Mott type in the former and of the Anderson type in the latter. The large increase seen in the strong-coupling ratio and a finite value of the gap at T_c near the metal-to-insulator transition are consistent with a BCS-to-BEC crossover [4,5], induced by the narrow band being formed near the Fermi level in the vicinity of a Mott transition [6].

[1] A. Glezer Moshe, G. Tuvia, S. Avraham, E. Farber, and G. Deutscher, Phys. Rev. B 104, 054508 (2021).
[2] A. Glezer Moshe, E. Farber, and G. Deutscher, Phys. Rev. B 99, 224503 (2019).
[3] D. Sherman, U. S. Pracht, B. Gorshunov, S. Poran, J. Jesudasan, M. Chand, P. Raychaudhuri, M. Swanson, N. Trivedi, A. Auerbach, M. Scheffler, A. Frydman, and M. Dressel, Nature Physics 11, 188 (2015).
[4] L. Pisani, P. Pieri, and G. C. Strinati, Phys. Rev. B 98, 104507 (2018).
[5] L. Pisani, A. Perali, P. Pieri, and G. C. Strinati, Phys. Rev. B 97, 014528 (2018).
[6] A. Georges, G. Kotliar, W. Krauth, and M. J. Rozenberg, Rev. Mod. Phys. 68, 13 (1996).

P45

Thermal and electric conductivity in Weyl-semimetals.

We compute the conductivity tensor of a TRS-breaking Weyl-semimetal. The problem is solved in two regimes: non-interacting electron and viscous electronic fluid. In the non-interacting case, we find an analytic expression for electric and thermal conductivities in terms of scattering phases. The effect is dominated by skew scattering in the limit of dilute and strong disorder. The limit of viscous hydrodynamic is qualitatively different from the non-interacting one. We start by constructing an effective hydrodynamic description of the problem in the vicinity of the Weyl points. The conductivity tensor (with all components, including electric, electrothermal, and thermal) is governed by the combined effect of zero and finite energy modes. This results in the non-monotonous behavior of various components of conductivity tensor (both longitudinal and Hall) on the disorder strength, temperature, and chemical potential. Surprisingly, some of them respect Wiedemann-Franz law, and some of them do not.

P46

Twistronics versus straintronics in twisted bilayers of graphene and transition metal dichalcogenides

Since de discovery of an intrinsic superconductivity in twisted bilayer graphene (TBLG) rotated at the so-called magic angle (MA) [1], the heterostructure of bilayer two-dimensional (2D) systems continue to be one of the hottest subjects in Condensed Matter Physics [1]. They are considered as an excellent playground to investigate the interplay between correlations, strain, twist angle, disorder, and topology. Several numerical studies have shown that the electronic properties of twisted bilayers of graphene (TBLG) and transition metal dichalcogenides (TMDs) are tunable by strain engineering of the stacking layers. In particular, the flatness of the low-energy moiré bands of the rigid and the relaxed TBLG was found to be, substantially, sensitive to the strain. However, to the best of our knowledge, there are no full analytical calculations of the strain dependence of these bands. We derive, based on the continuum model proposed by Bistritzer and MacDonald [3], the low-energy Hamiltonians of twisted homobilayers of graphene and TMDs under strain at small twist angles. We discuss how strain could correct the twist angles and bring them closer to the magic angle θm=1^0.05 of TBLG and how it may reduce the widths of the lowest-energy bands at charge neutrality of the twisted homobilayer of TMDs [4]. [1] Y. Cao, V. Fatemi, S. Fang, K. Watanabe, T. Taniguchi, E. Kaxiras, and P. Jarillo-Herrero, Nature, 556, 43 (2018). Y. Cao, V. Fatemi, A. Demir, S. Fang, S. L. Tomarken, J. Y. Luo, J. D. Sanchez-Yamagishi, K. Watanabe, T. Taniguchi, E. Kaxiras, R. C. Ashoori, and P. JarilloHerrero, Nature, 556, 80 (2018) [2] E. Y. Andrei and A. H. Macdonald, Nature Materials, 19, 1265 (2020). [3] R. Bistritzer and A. H. MacDonald, Proc. Natl. Acad. Sci. U.S.A., 108, 12233 (2011). [4] M. Mannaï and S. Haddad, Phys. Rev. B 103, L201112 (2021).

P47

Triplet pairing mechanisms from Hund's-Kondo models: applications to heavy fermion superconductors

Tamaghna Hazra[1], **and Piers Coleman**[1,2]

[1] *Center for Materials Theory, Rutgers University, Piscataway, New Jersey 08854, USA*
[2]*Department of Physics, Royal Holloway, University of London, Egham, Surrey TW20 0EX, United Kingdom*

A number of heavy-fermion candidate-triplet superconductors share the common structural motif of two or more U/Ce sublattices in the unit-cell separated by an inversion center. We present a pairing mechanism for triplet superconductivity that is enabled by such a locally non-centrosymmetric structure. Extremely high upper critical fields in these materials suggest the importance of local pairing scenarios with coherence lengths comparable to the lattice spacing. For instance, UTe_2 remains superconducting at fields above 60T, suggesting a coherence length shorter than 2nm. A legitimate driver of these local triplet pairing correlations is atomic Hund's coupling, which leads to pre-formed triplet pairs between the electrons trapped inside local moments. The sublattice degree of freedom allows these onsite spin-triplet pairs to acquire odd-parity form factors as they Kondo-hybridize with the dispersive electrons, leading to a pairing instability in a triplet channel. We show how the Hund's coupling modifies the Kondo hybridization leading to an anisotropic "triplet" Kondo coupling. Using a simple two-channel Kondo model, derived from a minimal mixed-valent construction with Hund's coupling, we demonstrate the emergence of odd-parity spin-triplet superconductivity in a mean-field calculation. This unifies the emergence of triplet superconductivity with the Kondo hybridization in a coherent framework, and we present support for this hypothesis from existing experiments.

*This work is supported by the National Science Foundation Grant No. DMR-1830707 and US Department of Energy, Basic Energy Sciences grant DE-FG02-99ER45790.

[1] T. Hazra, P. Coleman, arXiv:2205.13529 [cond-mat] (2022).

P48

Abstract template for poster: Vortex structure deformation of rotating Holographic Superconductors

Jhony A. Herrera-Mendoza[1], **Daniel F. Higuita Borja**[2], **Julio A. Méndez-Zavaleta**[2], **Alfredo Herrera-Aguilar, Felipe Pérez-Rodríguez**[1]

[1]*(Presenting author underlined) Instituto de Física, Benemérita Universidad Autónoma de Puebla, Puebla, México.*

[2]*Facultad de Física, Universidad Veracruzana, Xalapa-Enríquez, México.*

We study the effects of the magnetic field on the vortex structure, including continuous deformations both from triangular to square lattices or vice versa. Our holographic model reproduces known experimental vortex lattice deformations driven by changes in the external magnetic field.

[1] J. A. Herrera-Mendoza, D. F. Higuita-Borja, J. A. Méndez-Zavaleta, A. Herrera-Aguilar, F. Pérez Rodríguez, e-Print: 2208.05988 [hep-th], 2022.

P49

Royaime du Maroc
Université Abdelmalek Essaadi
Faculté des Sciences et Thechniques
Al Houceima

المملكة المغربية
جامعة عبد المالك السعدي
كلية العلوم والتقنيات الحسيمة

Master science et technique
Information quantique modélisation et applications

Mémoire du mini projet

La Mesure De L'Intrication

Réalisé par

JAD ANASS IMARA ZIYAD AZOUZ YOUNEES

Sous la direction du Pr : KADIJA El ANOUZ

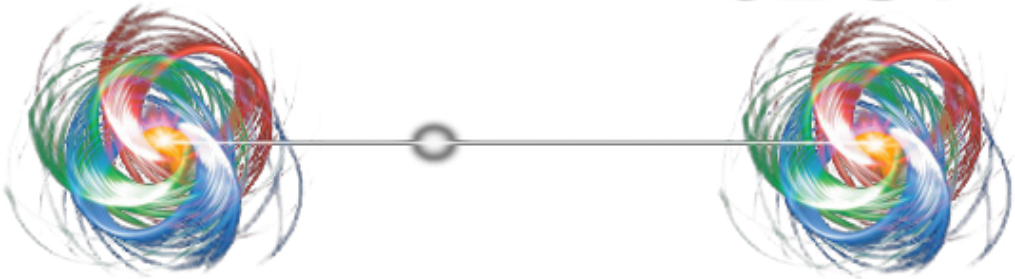

Année Universitaire : 2021-2022

Remerciements

Nous remercient avant tout Dieu de sa grâce. De nombreuses pages ne suffiront sûrement pas pour exprimer la richesse des liens tissés au cours de ces derniers semaines. Cependant, ces quelques lignesne manqueront point de sincérité et de dévouement envers les personnes auxquelles nous'adressemeents remerciements. Au terme de ce travail, nous tiens à exprimer notre gratitude à tous ceux qui ont participé à notre formation à la faculté des sciences et technique d'al hoceima et en particulier ceux du l'equipe pédagogie du master IQMA. Avant d'entamer ce rapport, nous profitent de l'occasion pour remercier tout d'abord noter en-cadrante ***Dr KHADIJA EL ANOUZ*** n'a pas cessée de nous'encourager pendant la durée du projet. nous la remercie également pour l'aide et les conseils concernant les missions évoquées dans ce rapport, qu'elle nous avons apporter lors des différents suivis, etla confiance qu'il nous avons témoignent. notre vifs remerciements et mes reconnaissances aux professeurs de m'avoir incité à travailler en mettant à ma disposition leurs expériences et leurs compétences.nous remercient toutes les personnes que nous avons contacter durant notre muni projet , auprès desquelles nous avons trouver l'accueil chaleureux.

Table des matières

1 Introduction a la théorie de l'information quantique **3**

1.1 Entropie de Shannon 3

1.2 Entropie conjointe 4

1.3 l'entropie conditionnelle 4

1.4 Information mutuelle 4

2 Intrication Quantique **6**

2.1 Theoréme de schmidt 7

2.1.1 énoncé 7

2.2 les Conséquences du théorème de schmidt 8

3 Mesure De L'Intrecation : **9**

3.1 La Concurrence : 9

3.1.1 Pour les états pures 9

3.1.2 pour les état mixtes 10

3.2 L'entropie de Von Neumann 10

3.3 Intrication de formation 11

3.4 Application 11

3.4.1 Application 1 11

3.4.2 Application 2 12

4 Discord Quantique : **15**

4.1 Discord entropique 15

4.2 Discorde géométrique 17

4.3 Discord Quantique pour les états X a deux q-bite (discord de Mazhar Ali) 18

4.4 la relation entre discord et l'intrication quantique : 20

Chapitre 1

Introduction a la théorie de l'information quantique

1.1 Entropie de Shannon

Clausius a introduit " Entropie de Shannon" d'appré le concept de l'entropie de la thermodynamique. dans la physique classique et la physique statistique l'entropie il était considéré comme une mesure du désordre d'un système. et dont le domaine de l'information n'a pas de sens.

L'entropie d'une variable aléatoire est une mesure quantitative de l'incertitude associée aux valeurs prises par la variable aléatoire[7].et la quantité des informations dépend plus de la distribution de probabilité d'un événement x particulier[7].

Soit X une variable aléatoire, prenant les valeurs $\{x_1, x_2.....x_n\}$ correspondant respectivement a les probabilité $\{P_1, P_2.....P_n\}$, Entropie de Shannon est définie par :

$$H(x) = H(P_1, P_2.....P_n) = -\sum_{0}^{n} P_i \log(P_i) \tag{1.1}$$

On prend par convention $0log_2(0) = 0$ le cas ou pas d'information. on a la probabilité $0 \leq \rho \leq 1$ dans le cas d'un système a bipartie, pour l'entropie de shannon binaire la probabilité on trace $H(p)$ lorsque la probabilité de trouvé système dans l'etat $|1\rangle$ égale P, la probabilité de trouvé systéme dans l'etat $|0\rangle$ égale (1-P) alors $H(p) = -p\log_2(p) - (1-p)\log_2(1-p)$

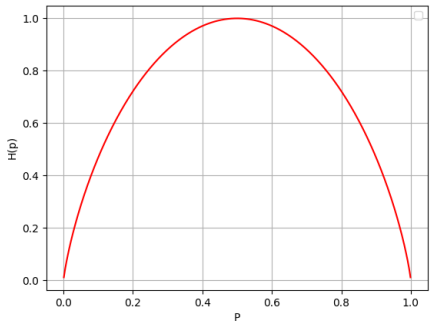

FIGURE 1.1 – Entropie de Shannon binaire en fonction de p.

1.2 Entropie conjointe

Soient A et B deux variables aléatoires, l'entropie conjointe H(A,B) est l'entropie pour (A,B) donnée par :

$$H(A,B) = -\sum_{x,y} p(x,y)\log_2(p(x,y)) \tag{1.2}$$

l'entropie conjointe est symétrique

$$H(A,B) = H(B,A) \tag{1.3}$$

Elle verifié l'inégalité suivent.

$$H(A,B) \leq H(A) + H(B) \tag{1.4}$$

si A sont B non-corrélé (séparable) alors $H(A,B) = H(A) + H(B)$

1.3 l'entropie conditionnelle

Entropie conditionnelle est une quantité un très importante dans en théorie de l'information. En effet, on s'intéresse souvent à l'incertitude sur A compte tenu de l'information représentée par B Alors l'entropie conditionnelle est définie par :

$$H(A|B) = -\sum_{x,y} p(A,B)\log_2(p(A|B)) \tag{1.5}$$

ELLe satisfait la propriété suivante :

$$H(A,B) = H(A) + H(B|A) = H(B) + H(A|B) \tag{1.6}$$

1.4 Information mutuelle

L'information mutuelle est une grandeur qui mesure un rapport entre deux système aléatoires échantillonnées simultanément. eprésente leur degré de dépendance au sens probabiliste. La distribution conjointe entre A et B est définie par

$$\sum_{AB} \log_2 \frac{P(A,B)}{P(A)P(B)} \tag{1.7}$$

Information mutuelle est définie par :

$$\begin{aligned} H(A:B) &= H(X) + H(Y) - H(X,Y) \\ &= H(X) - H(X|Y) = H(Y) - H(Y|X) \end{aligned} \tag{1.8}$$

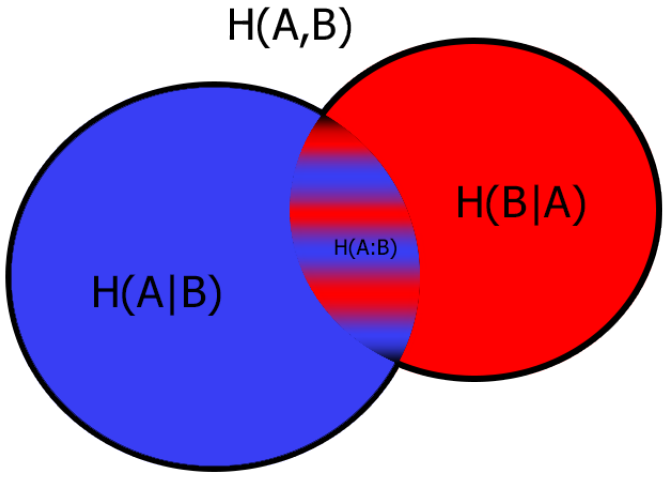

FIGURE 1.2 – Diagramme de Venn à deux système A et B

Chapitre 2

Intrication Quantique

Définition

- soit $|\psi\rangle$ est non intriqué s'il existe deux état $|\psi_1\rangle$ et $|\psi_2\rangle$ tels que :

$$|\psi\rangle = |\psi_1\rangle \otimes |\psi_2\rangle \tag{2.1}$$

- S'il n'existe aucun $|\psi_1\rangle$ et$|\psi_2\rangle$ tels que $|\psi\rangle = |\psi_1\rangle \otimes |\psi_2\rangle$, alors le qubit ψ est dit intriqué .

Exemples 1
exemple 1 : état non intriqué

soit

$$|\psi\rangle = |0.0\rangle - |0.1\rangle + |1.0\rangle - |1.1\rangle$$

alors

$$|\psi\rangle = |0\rangle (|0\rangle - |1\rangle) + |1\rangle (|0\rangle - |1\rangle)$$

$$= (|0\rangle + |1\rangle) \otimes (|0\rangle - |1\rangle)$$

on pose $|\psi_1\rangle = |0\rangle + |1\rangle$ *et* $|\psi_2\rangle = |0\rangle - |1\rangle$ *alors :*

$$|\psi\rangle = |\psi_1\rangle \otimes |\psi_2\rangle$$

alors $|\psi\rangle$ *est non intriqué.*

exemple 2 : état intriqué

L'état de Bel $|\phi^+\rangle$ *s'ectire sous la forme :*

$$|\phi^+\rangle = \frac{1}{\sqrt{2}}|0.0\rangle + \frac{1}{\sqrt{2}}|1.1\rangle$$

Preuve :

Supposons par l'absurde que $|\phi^+\rangle$ *ne soit pas intriqué, alors il existerait* $|\psi_1\rangle = \alpha|0\rangle + \beta|1\rangle$ *et* $|\psi_2\rangle = \alpha'|0\rangle + \beta'|1\rangle$*, telle que* $|\phi^+\rangle = |\psi_1\rangle \otimes |\psi_2\rangle$ *avec* $\alpha, \beta, \alpha', \beta'$ *,sont des nombres complexes. D'une part, on aurait :*

$$|\phi^+\rangle = |\psi_1\rangle \otimes |\psi_2\rangle = \alpha\alpha'|0.0\rangle + \alpha\beta'|0.1\rangle + \beta\alpha'|1.0\rangle + \beta\beta'|1.1\rangle$$

avec :

$$|\phi^+\rangle = \frac{1}{\sqrt{2}}|0.0\rangle + \frac{1}{\sqrt{2}}|1.1\rangle$$

alors :

$$\begin{array}{ll} \alpha\alpha' = \frac{1}{\sqrt{2}} & \alpha\beta' = 0 \\ \beta\beta' = \frac{1}{\sqrt{2}} & \beta\alpha' = 0 \end{array}$$

Les équations de gauche impliquent que $\alpha, \alpha', \beta,$ *et* β' *ce qui contredit les équations de droite. Ainsi notre hypothèse de départ est nécessairement fausse, alors L'état de Bel* $|\phi^+\rangle$ *est intriqué*

2.1 Theoréme de schmidt

2.1.1 énoncé

Soit $|\psi_{AB}\rangle$ est un état pure (définition des états pure dans le référence [1]) composé par deux sous-systèmes A + B, alors il existe $|i_A\rangle$ et $|i_B\rangle$ des état orthonormé des sous-systèmes A et B telle que :

$$|\psi_{AB}\rangle = \sum_i \lambda_i |i_A\rangle |i_B\rangle \tag{2.2}$$

* les λ_i sont des nombres réels, non-négatifs satisfaisant $\sum_i \lambda_i^2 = 1$, appelés coefficients de Schmidt.

Preuve :

La décomposition de Schmidt est essentiellement une reformulation de la décomposition de la valeur singulière dans un contexte différent.
Premier-ment Soit la base orthonormé $|j^A\rangle \subset H^A$ et $|k^B\rangle \subset H^B$.
Alors

$$|\psi_{AB}\rangle = \sum_{jk} \alpha_{jk} |j^A\rangle |k^B\rangle \quad ; \alpha_{jk} = \langle j^A| \langle k^b|\psi_{AB}\rangle \tag{2.3}$$

Avec :

$$\alpha = UDV \tag{2.4}$$

ou D est une matrice diagonale alors ;

$$|\psi_{AB}\rangle = \sum_{ijk} U_{ji} D_{ii} V_{ik} \, |j^A\rangle \, |k^B\rangle \tag{2.5}$$

soit :

$$\sum_{ijk} U_{ji} \, |j^A\rangle = |i_A\rangle \qquad \sum_{ijk} V_{ik} \, |k^B\rangle = |i_B\rangle \tag{2.6}$$

$$|\psi_{AB}\rangle = \sum_{i} \lambda_i \, |i_A\rangle \, |i_B\rangle \tag{2.7}$$

2.2 les Conséquences du théorème de schmidt

- le nombre de coefficients λ_i de Shmidt non nuls est appelé le nombre de Shmidt.
- un état quantique pur est dit séparable si le nombre de schmidt est unitaire, c'est-à-dire que le vecteur d'état du système composite peut être représenté comme un produit tensoriel des vecteurs de chaque état.
- un état pur est dit intriqué si le nombre de schmidt est supérieur à un.
- Le nombre shmidt est utilisé comme critère de séparabilité de l'état

Chapitre 3

Mesure De L'Intrecation :

3.1 La Concurrence :

3.1.1 Pour les états pures

La concurrence est une la quantité pour mesuré l'intrication bipartite. Au debut elle est considérée comme une quantique auxiliaire utilisée pour calculer l'intrication de la formation des systèmes quantiques bipartites. Cependant la concurrence est considérée comme une quantité de mesure indépendante .
soit $|\psi\rangle$ un état intrique bipartie d'éfinie par :

$$|\psi\rangle = \mu\,|\alpha\rangle \otimes |\beta\rangle + \nu\,|\gamma\rangle \otimes |\sigma\rangle \tag{3.1}$$

telle que μ et ν sont des nombres complexes, $|\gamma\rangle$ et $|\beta\rangle$ sont des état normalisé correspondant aux premier système et $|\beta\rangle$,$|\sigma\rangle$ du deuxième système. En général on vas travailler dans le cas non orthogonal C-á-d $\langle\alpha|\gamma\rangle \neq 0$ et $\langle\beta|\sigma\rangle \neq 0$

sachant que la norme de l'état $|\psi\rangle$:

$$N = \sqrt{|\mu|^2 + |\nu|^2 + \mu\nu^*\,\langle\gamma|\alpha\rangle\,\langle\sigma|\beta\rangle + \mu^*\nu\,\langle\alpha|\gamma\rangle\,\langle\beta|\sigma\rangle} \tag{3.2}$$

Supposons que :

$$a = \tfrac{\mu}{N} \qquad b = \tfrac{\nu}{N}$$

La renormalisation de l'état (Eq. 2.1) nous donne la formule suivante :

$$|\psi\rangle = a\,|\alpha\rangle \otimes |\beta\rangle + b\,|\gamma\rangle \otimes |\sigma\rangle \tag{3.3}$$

$|\alpha\rangle$ et $|\gamma\rangle$ sont des état non orthogonaux et linéairement indépendants, alors on défini une base $\{|0\rangle\,, |1\rangle\}$ orthogonale :
soit : $|0\rangle = |\alpha\rangle$ alors :

$$|\gamma\rangle = \langle\gamma|1\rangle\,|1\rangle + \langle\gamma|0\rangle\,|0\rangle \tag{3.4}$$

On a $|0\rangle = |\alpha\rangle$ alors $\langle\gamma|0\rangle\,|0\rangle = \langle\gamma|\alpha\rangle\,|0\rangle = P_1\,|0\rangle$

et soit $N_1 = \langle\gamma|1\rangle$

$$|\gamma\rangle = N_1\,|1\rangle + P_1\,|0\rangle \tag{3.5}$$

D ou

$$|1\rangle = \frac{1}{N_1}(|\gamma\rangle - P_1\,|\alpha\rangle) \tag{3.6}$$

de même pour le deuxième soit $|0\rangle = |\beta\rangle$

$$|1\rangle = \frac{1}{N_2}(|\gamma\rangle - P_2\,|\beta\rangle) \tag{3.7}$$

la concurrence C pour mesuré l'intrécation de l'état $|\psi\rangle$ est donné par la relation suivante :

$$C = |\,\langle\psi|\tilde{\psi}\rangle\,| \tag{3.8}$$

avec :

$$|\tilde{\psi}\rangle = (\sigma_y \otimes \sigma_y)\,|\psi^*\rangle \tag{3.9}$$

— $|\psi^*\rangle$ est le complexe conjuguée de $|\psi\rangle$ dans la base standard $|00\rangle, |01\rangle, |10\rangle, |11\rangle$

— σ_y est l'operateur de Pauli.

$$C = \frac{2|\mu\nu|\sqrt{(1-|P_1|^2)(1-|P_2|^2)}}{|\mu|^2 + |\nu|^2 + \mu\nu^* P_1^* P_2 + \mu^*\nu P_1 P_2^*} \tag{3.10}$$

— La concurrence varie entre 0 et 1.

— $C = 0$ si est seulement si état séparable

— $C = 1$ si est seulement si état est maximale-ment intriqué

3.1.2 pour les état mixtes

Pour un état mixte La définition de concurrence peut être généralisé pour les états mixtes. En particulier, la concurrence pour des un état mixte quelconque de $2 \otimes 2$ dimension

$$C = max\{0, \lambda_0 - \lambda_1 - \lambda_2 - \lambda_3\} \tag{3.11}$$

avec : λ_i^2 les valeurs propres de la matrice suivante :

$$\rho\tilde{\rho} = \rho(\sigma_y \otimes \sigma_y)\rho^*(\sigma_y \otimes \sigma_y) \tag{3.12}$$

3.2 L'entropie de Von Neumann

L'entropie de Von Neumann on l'appelle aussi l'entropie quantique est le plus facile quantité pour mesuré intrication ou bien la Corrélation entre deux système quantique représenté par sa matrice de densité ρ donné par :

$$S = -Tr(\rho \log \rho) \tag{3.13}$$

s'écrit aussi en fonction des valeurs propres de 'ρ

$$S = -\sum_i \lambda_i \log \lambda_i \tag{3.14}$$

— λ_i des valeurs propres de la matrice dansoté ρ
— $0 \leq S(\rho) \leq 1$
— 1 est la valeur maximale de L'entropie de Von Neumann pour un état pur bipartite intrique d'une faucon maximale.
— L'entropie de Von Neumann est utiliser pour mesurer les corrélations quantiques des états purs bipartites, c'est a dire les états purs qui contient uniquement deux systèmes.

soit un espace d'Hilbert bipartite $\mathcal{H}_{\mathcal{AB}} = \mathcal{H}_{\mathcal{A}} \otimes \mathcal{H}_{\mathcal{B}}$ avec $dim\mathcal{H}_{\mathcal{A}} = n$, $dim\mathcal{H}_{\mathcal{B}} = m$ et $n \leq m$ Dans ce cas, on peut former dans les espaces d'Hilberts une base orthonormée $\{|\mu_i^A\rangle\}_{i=1}^n$ et $\{|\nu_j^B\rangle\}_{j=1}^m$

$$|\psi\rangle = \sum_{i=1}^{n} \lambda_i |\mu_i^A\rangle |\nu_i^B\rangle \tag{3.15}$$

avec λ_i sont les coefficients de Schmidt $\sum_{i=1}^n \lambda_i^2 = 1$ En utilisant la décomposition de Schmidt on peut trouver les matrice de densités réduites des sous-systèmes A et B qui sont de la forme :

$$\hat{\rho_A} = \sum_i^n \lambda_i^2 |\mu_i^A\rangle \langle\mu_i^A| \tag{3.16}$$

$$\hat{\rho_B} = \sum_i^n \lambda_i^2 |\nu_i^B\rangle \langle\mu_i^B| \tag{3.17}$$

3.3 Intrication de formation

Soit un état bipartite $\rho_{AB} \in H^A \otimes H^B$ Intrication de formation est donné par :

$$E_{AB} = H(\frac{1+\sqrt{1-c^2}}{2}) \tag{3.18}$$

avec :

$$H(x) = -x \log_2 -(1-x) \log_2(1-x) \tag{3.19}$$

3.4 Application

3.4.1 Application 1

on a choisie l'état suivant :

$$\rho = \frac{1}{\sqrt{3}}[(1-a)(|00\rangle \langle 00|) + 2 |\psi^+\rangle \langle\psi^+| + a |11\rangle \langle 11|] \tag{3.20}$$

avec $|\psi^+\rangle = \frac{1}{\sqrt{2}}(|01\rangle + |10\rangle)$ et $a \in [0,1]$

$$\rho = \frac{1}{3}\begin{pmatrix} (1-a) & 0 & 0 & 0 \\ 0 & 1 & 1 & 0 \\ 0 & 1 & 1 & 0 \\ 0 & 0 & 0 & a \end{pmatrix} \tilde{\rho} = \frac{1}{3}\begin{pmatrix} 0 & 0 & 0 & -(1-a) \\ 0 & 1 & 1 & 0 \\ 0 & 1 & 1 & 0 \\ -a & 0 & 0 & 0 \end{pmatrix} \tag{3.21}$$

$$\rho\tilde{\rho} = \frac{1}{9}\begin{pmatrix} 0 & 0 & 0 & -(1-a)^2 \\ 0 & 2 & 2 & 0 \\ 0 & 2 & 2 & 0 \\ -a^2 & 0 & 0 & 0 \end{pmatrix} \tag{3.22}$$

la concurrence donné par :

$$C = max\{0, \frac{2}{3}[1 - \sqrt{a(1-a)}]\} \tag{3.23}$$

on trace par rapport a la concurrence et l'intrication de formation

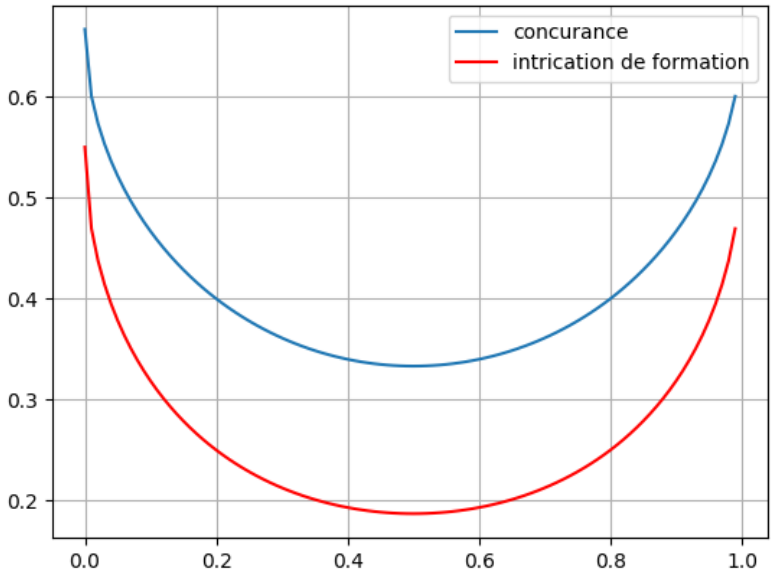

FIGURE 3.1 – la concurrence, l'intrication de formation

3.4.2 Application 2

Dans cette partie on va travailler sur l'état proposé par notre pr.KADIJA El ANOUZ $|\psi\rangle = \cos\phi\,|00\rangle + \sin\phi\,|11\rangle$ la concurrence de cette état est donné par équation (2.10) :

$$\rho = \begin{pmatrix} cos(\phi)^2 & 0 & 0 & cos(\phi)sin(\phi) \\ 0 & 0 & 0 & 0 \\ 0 & 0 & 0 & 0 \\ cos(\phi)sin(\phi) & 0 & 0 & sin(\phi)^2 \end{pmatrix} \tilde{\rho} = \begin{pmatrix} cos(\phi)^2 & 0 & 0 & cos(\phi)sin(\phi) \\ 0 & 0 & 0 & 0 \\ 0 & 0 & 0 & 0 \\ cos(\phi)sin(\phi) & 0 & 0 & sin(\phi)^2 \end{pmatrix} \tag{3.24}$$

$$\rho \otimes \tilde{\rho} = \begin{pmatrix} 2cos(\phi)^2 sin(\phi)^2 & 0 & 0 & 2cos(\phi)^3 sin(\phi) \\ 0 & 0 & 0 & 0 \\ 0 & 0 & 0 & 0 \\ 2cos(\phi)sin(\phi)^3 & 0 & 0 & 2cos(\phi)^2 sin(\phi)^2 \end{pmatrix} \tag{3.25}$$

$$C = |2cos(\phi)\sin(\phi)| = |\sin(2\phi)| \tag{3.26}$$

entropie de formation est donné par :

$$S = |\cos^2(\phi)\log\cos^2(\phi) + \sin^2(\phi)\log\sin^2(\phi)|| \tag{3.27}$$

On trace les deux on fonction de ϕ

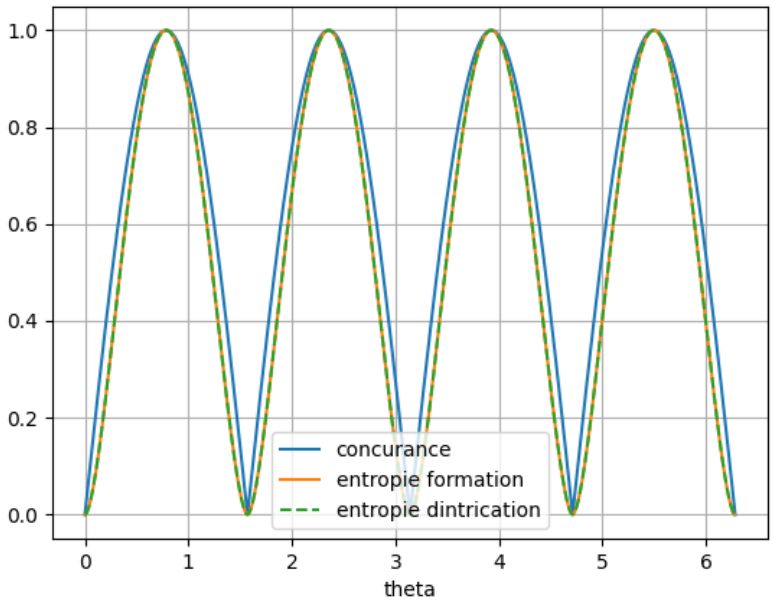

FIGURE 3.2 – la concurrence, entropie d'intrication et l'entropie de formation

Soit E_1 énergie de $|00\rangle$ et E_2 énergie de $|11\rangle$ par Hamiltonien H, opérateur d'evolution est donné par :

$$|\psi(t)\rangle = \sum_{i=0}^{1} e^{-iE_i t/\hbar} |\psi_i\rangle \tag{3.28}$$

D'ou

$$|\psi(t)\rangle = cos(\phi)e^{-iE_0 t/\hbar} |00\rangle + sin(\phi)e^{-iE_1 t/\hbar} |11\rangle \tag{3.29}$$

la concurrence est donné par :

$$C(t) = 2|cos(\phi)sin(\phi)cos(\omega_0 t)| \tag{3.30}$$

soit $E_1 - E_0 = \hbar\omega_0$

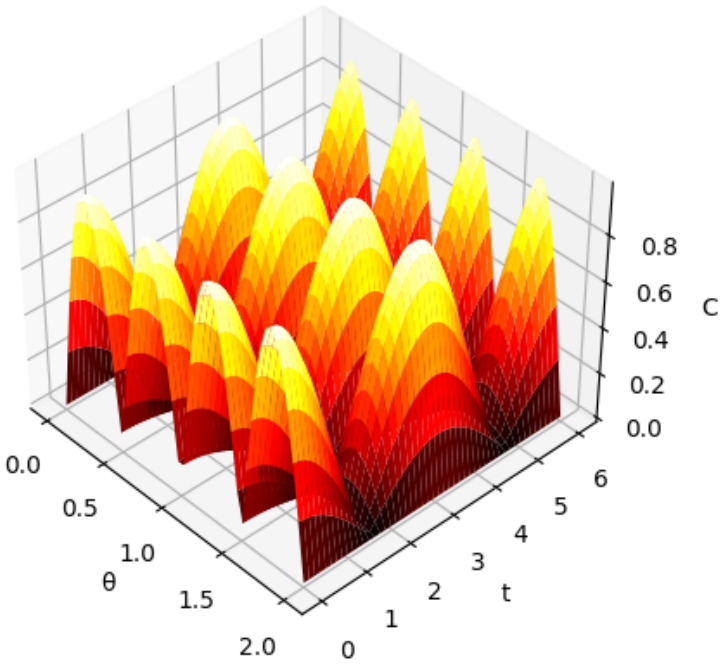

FIGURE 3.3 – la concurrence en fonction de ϕ et le temps

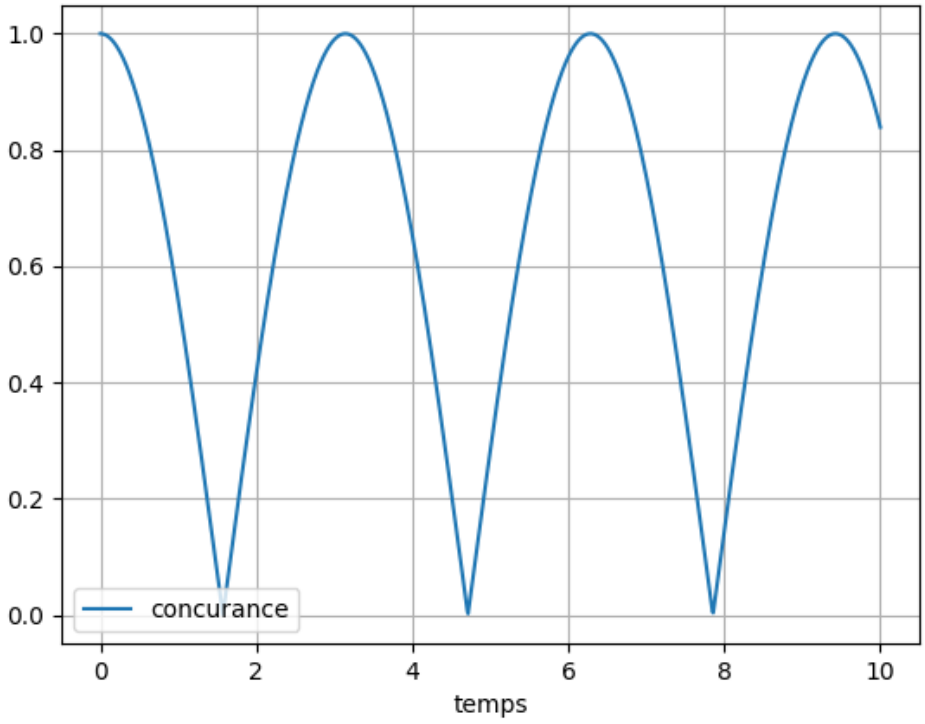

FIGURE 3.4 – la concurrence en fonction de ϕ et le temps

Chapitre 4

Discord Quantique :

Parmi les grands problèmes de la mécanique quantique est la perturbation de l'état après la mesure, mais on peut déduire que s' il ya une perturbation induite par une mesure sur un état alors il est intriqué. Cette perturbation modifie les propriétés de l'état global, alors il modifier les corrélations enter les sous-système. On ajoute que certains mélanges d'états non intriqués peuvent quand même présenter des corrélations supérieures aux corrélations classiques[7]. Alors on peut mesurer les corrélations quantiques plus qu'est détectées par l'entropie de formation. On va proposer deux types de mesure dans ce travail :

— discorde quantique

— discorde géométriques

EN définie La discorde quantique comme la différence entre les corrélations totale et les corrélations classique.

En utilisant la dissonance quantique, on peut voir que les états séparables mixtes contiennent Corrélation quantique. De ce point de vue, il s'agit d'une classe de corrélations quantiques sont plus générales que intrication .

4.1 Discord entropique

Dans la discord quantique on utilise la notion de l'information mutuelle. La définition de l'information mutuelle est donnée par la formulle suivante :

$$I(\rho_{AB}) = S(\rho_A) + S(\rho_B) - S(\rho_{AB}) \tag{4.1}$$

l'information mutuelle pour un état classique n'est pas perturbé par une mesure d'un des sous-systèmes :

$$J(\rho_{AB}) = S(\rho_A) - S(\rho_A|\rho_B) \tag{4.2}$$

avec

$$S(\rho_A|\rho_B) = S(\rho_{AB}) - S(\rho_B) \tag{4.3}$$

D'ou

$$J(\rho_{AB}) = S(\rho_A) + S(\rho_B) - S(\rho_{AB}) \tag{4.4}$$

Alors l'information mutuelle contient à la fois les corrélations classiques et quantiques entre les deux sous-systèmes.

— Corrélations classique $C(\rho_{AB})$
— Corrélations quantique $D(\rho_{AB})$

$$I(\rho_{AB}) = C(\rho_{AB}) + D(\rho_{AB}) \tag{4.5}$$

cherchon maintenant $C(\rho_{AB})$ soit :

$$\rho_k = \frac{(M_k \otimes I)\rho_{AB}(M_k \otimes I)}{P_{B,k}} \tag{4.6}$$

Avec

$$M_k = U\Pi_k U^\dagger \tag{4.7}$$

avec $\Pi_k = |k\rangle \langle k|$ ou $k = \{0, 1\}$
l'opérateur $U \in SU(2)$ est unitaire et la probabilité $P_{B,k}$ est donnée par :

$$P_{B,k} = Tr((M_k \otimes I)\rho_{AB}(M_k \otimes I)) \tag{4.8}$$

B est obtenue la quantité d'information suivent :

$$S_{\rho_B} - \sum P_{B,k} S(\rho_{B,k}) \tag{4.9}$$

La mesure des corrélations classiques résultantes est donnée par l'expression suivante :

$$c(\rho_{AB}) = Max[s(\rho_A) - \sum P_{Bk} S(\rho_{A,k})] \tag{4.10}$$

$$c(\rho_{AB}) = Max[s(\rho_A)] - S_{min} \tag{4.11}$$

par conséquence on définir les informations acquises sur le système A par :

$$c(\rho_{AB}) = Max[s(\rho_B) - \sum P_{Ak} S(\rho_{B,k})] \tag{4.12}$$

$$c(\rho_{AB}) = Max[s(\rho_B)] - S_{min} \tag{4.13}$$

La discorde quantique est obtenue par l'information mutuelle quantique :

$$D(\rho_{AB}) = I(\rho_{AB}) - C(\rho_{AB}) \tag{4.14}$$

— La discorde quantique correspond aux corrélations d'origine purement quantique .
— Elle est toujours positive $D(\rho_{AB}) \geq 0$.
— $D(\rho_{AB}) = 0$ pour les états classiquement corrélés .

4.2 Discorde géométrique

Discorde géométrique ou bien la Mesure géométrique de la discorde quantique, Elle est basée sur la norme de Hilbert-Schmidt,est définie comme la distance minimale séparant d'un état quantique de tous les états de discorde nulle. d'appré la définition on a :

$$D_g(\rho_{AB}) = min_{\chi\in\Omega_0}||\rho_{AB} - \chi||^2 \tag{4.15}$$

avec :$||A - B||^2 = Tr(A - B)^2$
pour un état à deux qubits arbitraire :

$$\rho = \frac{1}{4}\Big[\sigma_0 \otimes \sigma_0 + \sum_{i=1}^{3}(x_i\sigma_i \otimes \sigma_0 + x_y\sigma_i \otimes \sigma_0) + \sum_{i,j=1}^{3}(R_{ij}\sigma_i \otimes \sigma_j)\Big] \tag{4.16}$$

Avec :

- $x_i = Tr\rho(I \otimes \sigma_i)$, $y_i = Tr\rho(\sigma_i \otimes I)$ les les composantes des vecteurs locaux de Bloch.
- $R_{ij} = Tr\rho(\sigma_i \otimes \sigma_j)$ sont les composantes du tenseur de corrélation.
- σ_i $i = \{1, 2, 3\}$ Les matrices de Pauli.
- σ_i la matrice identité.

l'état de discorde nulle Pour un système de deux qubits est donné par :

$$\chi = p_1 \left|\psi_1\right\rangle \left\langle\psi_1\right| \otimes \rho_1 + p_2 \left|\psi_2\right\rangle \left\langle\psi_2\right| \otimes \rho_2 \tag{4.17}$$

avec $\{\left|\psi_1\right\rangle, \left|\psi_2\right\rangle\}$ une base orthonormée.
L'expression analytique de la mésure géométrique de la discorde quantique est donnée par [12] :

$$D_g(\rho) = (||X||^2 + ||R||^2 - K_{max}) \tag{4.18}$$

Avex $X = (x_1, x_2, x_3)^T$, K_{max} est la plus grande valeur propre de la matrice suivent :

$$K = XX^T + RR^T \tag{4.19}$$

Soient $\{\lambda_1, \lambda_1, \lambda_1\}$ les valeurs propres de la matrice K La mesure géométrique de la discorde quantique est donnée par la formule compacte suivante :

$$D_g(\rho) == \frac{1}{4}\min[\lambda_1 + \lambda_2, \lambda_1 + \lambda_3, \lambda_3 + \lambda_2] \tag{4.20}$$

Remarque : que pour obtenir la discorde géométrique pour un état à deux qubit, il suffit de diagonaliser la matrice K et comparer les valeur propres $\{\lambda_1, \lambda_2, \lambda_3\}$

4.3 Discord Quantique pour les états X a deux q-bite (discord de Mazhar Ali)

l'état du qubit X dans la représentation englobée par les états du produit de deux qubits $|1\rangle = |0\rangle_A \otimes |0\rangle_B$,$|2\rangle = |0\rangle_A \otimes |1\rangle_B$,$|3\rangle = |1\rangle_A \otimes |0\rangle_B$ et $|4\rangle = |1\rangle_A \otimes |1\rangle_B$

$$\rho = \begin{pmatrix} \rho_{11} & 0 & 0 & \rho_{14} \\ 0 & \rho_{22} & \rho_{23} & 0 \\ 0 & \rho_{32} & \rho_{33} & 0 \\ \rho_{41} & 0 & 0 & \rho_{44} \end{pmatrix} \tag{4.21}$$

L'équation (4.21) décrit un état quantique à condition que unitaire et les conditions de positivité :

— $\sum_{i=1}^{4} \rho_{ii} = 1$

— $\rho_{22}\rho_{33} \geq |\rho_{23}|^2$ et $\rho_{11}\rho_{44} \geq |\rho_{14}|^2$

les états sont intriqués si et seulement si :

— $\rho_{22}\rho_{33} < |\rho_{14}|^2$

— $\rho_{11}\rho_{44} < |\rho_{23}|^2$

les valeur propre de la matrice densité (4.21) :

— $\lambda_0 = \frac{1}{2}[(\rho_{11} + \rho_{44}) + \sqrt{(\rho_{11} - \rho_{44})^2 + 4|\rho_{14}|^2}\ ]$

— $\lambda_1 = \frac{1}{2}[(\rho_{11} + \rho_{44}) - \sqrt{(\rho_{11} - \rho_{44})^2 + 4|\rho_{14}|^2}\ ]$

— $\lambda_2 = \frac{1}{2}[(\rho_{22} + \rho_{33}) + \sqrt{(\rho_{22} - \rho_{33})^2 + 4|\rho_{23}|^2}\ ]$

— $\lambda_3 = \frac{1}{2}[(\rho_{22} + \rho_{33}) - \sqrt{(\rho_{22} - \rho_{33})^2 + 4|\rho_{23}|^2}\ ]$

Information mutual quantique est donné par :

$$I(\rho_x) = S(\rho_x^A) + S(\rho_x^B) + \sum_{j=0}^{3} \lambda_j log_2 \lambda_j \tag{4.22}$$

Avec :

$$S(\rho_X^A) = -[(\rho_{11} + \rho_{22}) \log_2(\rho_{11} + \rho_{22}) + (\rho_{33} + \rho_{44}) \log_2(\rho_{33} + \rho_{44})] \tag{4.23}$$

$$S(\rho_X^A) = -[(\rho_{11} + \rho_{33}) \log_2(\rho_{11} + \rho_{33}) + (\rho_{22} + \rho_{44}) \log_2(\rho_{33} + \rho_{44})] \tag{4.24}$$

Après avoir calculé l'information mutuelle quantique, nous devons ensuite de calculer la corrélation classique $C(\rho_x)$:

Nous considérons mesures projectives sur le sous-système B pour le sous-système A donnent les mêmes résultats si nous nous limitons à $\rho_{11} = \rho_{44}$ ou $\rho_{22} = \rho_{33}$.

D'appré l'equation (4.7) et (4.8) pour un système bipartie :

$$M_k = U\Pi_k U^\dagger$$

$$P_{B,k} = Tr((M_k \otimes I)\rho_{AB}(M_k \otimes I))$$

Nous pouvons écrire n'importe quel $U \in SU(2)$

$$U = tI + i\overrightarrow{y}\,\overrightarrow{\sigma} \tag{4.25}$$

avec :

— $t, y_1, y_2, y_3 \in \mathbb{R}$
— $t^2 + y_1^2 + y_2^2 + y_3^2 = 1$

Cela implique que ces paramètres, dont trois sont indépendants, prennent leurs valeurs dans l'intervalle [-1,1]
Les deux valeurs propres de ρ_0 et ρ_1 sont données comme suit :

$$\begin{aligned} v_+(\rho_0) &= \tfrac{1}{2}(1+\theta) \\ v_-(\rho_0) &= \tfrac{1}{2}(1-\theta) \\ u_+(\rho_0) &= \tfrac{1}{2}(1+\theta') \\ u_-(\rho_0) &= \tfrac{1}{2}(1-\theta') \end{aligned} \tag{4.26}$$

les probabilité corspondant donné par :

$$\begin{aligned} p_0 &= [(\rho_{11}+\rho_{33})k + (\rho_{22}+\rho_{44})l] \\ p_1 &= [(\rho_{11}+\rho_{33})l + (\rho_{22}+\rho_{44})k] \end{aligned} \tag{4.27}$$

Nous avons défini θ et θ' qui généralisent dans une seule expression Nous avons défini ? et ? qui généralisent une seule expression dans Ref[13]

$$\begin{aligned} \theta &= \sqrt{\frac{[(\rho_{11}-\rho_{33})k+(\rho_{22}-\rho_{44})l]^2+\Xi}{[(\rho_{11}+\rho_{33})l+(\rho_{22}+\rho_{44})k]^2}} \\ \theta' &= \sqrt{\frac{[(\rho_{11}-\rho_{33})l+(\rho_{22}-\rho_{44})k]^2+\Xi}{[(\rho_{11}+\rho_{33})l+(\rho_{22}+\rho_{44})k]^2}} \end{aligned} \tag{4.28}$$

avec $\Xi = 4kl[|\rho_{14}|^2 + |\rho_{23}|^2 + 2Re(\rho_{14}\rho_{23})] - 16mRe(\rho_{14}\rho_{23}) + 16nIm(\rho_{14}\rho_{23})$ avec Re(z) et Im(z) est le réel et l'imaginaire de z, et on a les paramétrés m,n,k et l est :

$$\begin{aligned} m &= (ty_1 + y_2y_3)^2 & k &= t^2 + y_3^2 \\ n &= (ty_2 - y_1y_3)(ty_1 + y_2y_3) & l &= y_1^2 + y_2^2 \end{aligned} \tag{4.29}$$

avec k+l=1 Le équation (4.28) donne une matrice de densité dépendent de trois paramètres réels, k, m et n. avec

— $k \in [0, 1]$
— $m \in [0, 1/4]$
— $n \in [-1/8, 1/8]$

les paramètres k, n, m dépendent de l'equation (4.25) et sont liés à l'ensemble $\{z_1, z_2, z_3\}$ tell que $4m = z_2^2$ $4n = -z_1z_2$ $k - l = z_3$ l'ensemble des entropies $\{\rho_i, p_i\}$ sont données comme suit :

$$S(\rho_0) = -\frac{1-\theta}{2}\log_2\frac{1-\theta}{2} - \frac{1+\theta}{2}\log_2\frac{1+\theta}{2} \tag{4.30}$$

$$S(\rho_1) = -\frac{1-\theta'}{2}\log_2\frac{1-\theta'}{2} - \frac{1+\theta'}{2}\log_2\frac{1+\theta'}{2} \tag{4.31}$$

Par conséquent, pour calculer la corrélation classique et la discorde quantique, nous devons $S(P_x|B_i|)$ [4.30] par rapport aux mesures de von Neumann. de von Neumann.
Pour le cas particulier des états X à deux qubits avec des restrictions $\rho_{11} = \rho_{44}$ et $\rho_{22} = \rho_{33}$, et avec des éléments hors-diagonale réels, nous définissons

$$\begin{aligned} \theta_1 = 2|\rho_{14} + \rho_{23}| \qquad\qquad \theta_2 = 2|\rho_{14} - \rho_{23}| \\ \theta_3 = \theta_4 = |(\rho_{11} + \rho_{44}) - (\rho_{22} + \rho_{33})| \end{aligned} \tag{4.32}$$

et l'entropie $S'(\rho_i)|_{\theta_i}$

$$S'(\rho_i) = -\frac{1-\theta_j}{2}\log_2\frac{1-\theta_j}{2} - \frac{1+\theta_j}{2}\log_2\frac{1+\theta_j}{2} \tag{4.33}$$

De plus, $S(\rho_0) = S(\rho_1)$, et la valeur minimale de $s(\rho|\{B_i\})$ est égale à la valeur minimale de $s(\rho_0)$, qui est donnée comme

$$min[s(\rho|\{B_i\})] = min[s(\rho_0)] = s'(\rho_0)|_{\theta_{sup}} \tag{4.34}$$

avec

$$\theta_{sup} = max\{\theta_1, \theta_2, \theta_3\} \tag{4.35}$$

4.4 la relation entre discord et l'intrication quantique :

Dans cette section, nous étudions la relation entre la corrélation classique , la discorde quantique et l'intrication pour divers états initiaux.

Example 1

Nous prenons la classe d'états définie comme :

$$\rho = a\,|\psi^+\rangle\langle\psi^+| + (1-a)\,|1,1\rangle\langle 1,1| \tag{4.36}$$

avec $|\psi^+\rangle = \frac{1}{\sqrt{2}}|0,1\rangle + |1,0\rangle$ est un état maximalement intriqué. En se basant Sur la base des résultats de la section précédente, nous sommes maintenant en mesure de calculer la corrélation classique et la discorde quantique.
on a : $\theta_1 = \theta_1 = \sqrt{a^2 + (1-a)^2}$, $\theta_3 = |2-3a|/(2-a)$ and $\theta_4 = 1$ comme $\theta_4 = 1$, on a $S'(\rho_1)|_{\theta_4} = 0$. on note $S'(\rho_0)|_{\theta_1} \leq S(\rho|B_i)|_{\theta_3\theta_4}$ c'est a dire , $min\{S'(\rho_0)|_{\theta_1}, S(\rho|B_i)|_{\theta_3\theta_4}\} = S'(\rho_0)|_{\theta_1}$ la corrélation quantique est :

$$C(\rho) = S(\rho^A) - S'(\rho_0)|_{\theta_0} \tag{4.37}$$

avec

$$S(\rho^A) = -\frac{a}{2}\log_2\frac{1}{2} - \frac{2-a}{2}\log_2\frac{2-a}{2} \tag{4.38}$$

information mutuelle :

$$I(\rho) = 2S(\rho^A) + S(\rho) \tag{4.39}$$

Et la discorde quantique donné par :

$$Q(\rho) = S(\rho^A) + S4(\rho_0)|_{\theta_1} - S(\rho) \tag{4.40}$$

avec :

$$S(\rho) = -a\log_2 a - (1-a)\log_2(1-a) \tag{4.41}$$

D'apres (Chapiter 3) on calcule la concurrence :

$$C'(\rho) = a \tag{4.42}$$

on trace la concurrence, discorde quantique et la corrélation classique

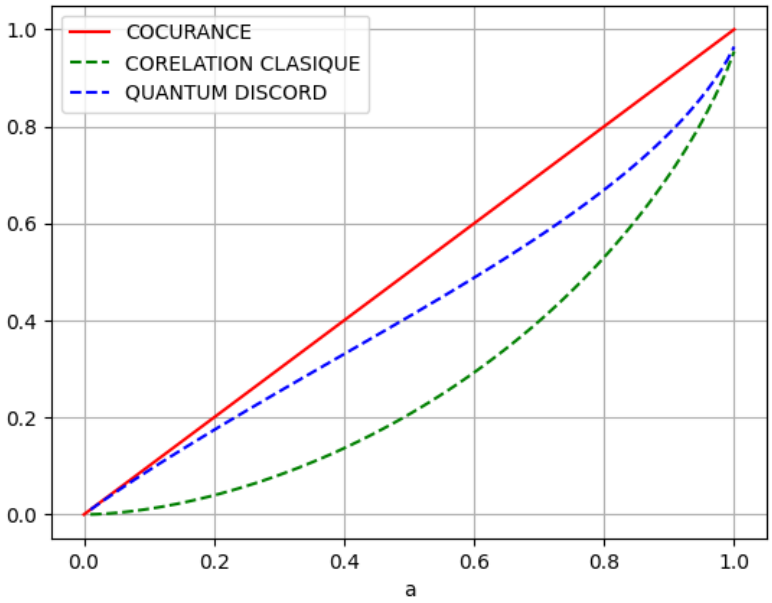

FIGURE 4.1 – la concurrence, LA discorde quantique et la corrélation classique

Example 2 :

Nous prenons la classe d'états définie comme :

$$\rho = a\,|\phi^+\rangle\langle\phi^+| + (1-a)\,|1,1\rangle\langle 1,1| \tag{4.43}$$

avec $|\psi^+\rangle = \frac{1}{\sqrt{2}}|0,0\rangle + |1,1\rangle$ est un état maximalement intriqué. En se basant Sur la base des résultats de la section précédente, nous sommes maintenant en mesure de calculer la corrélation classique et la discorde quantique.
on a : $\theta_1 = \theta_1 = \sqrt{a^2 + (1-a)^2}, \theta_3 = \theta_4 = 1$ comme $\theta_4 = 1$. on note $min\{S'(\rho_0)|_{\theta_1}, S(\rho|B_i)|_{\theta_3\theta_4}\} = 0$

la corrélation quantique est :

$$C(\rho) = S(\rho^A) \tag{4.44}$$

avec

$$S(\rho^A) = -\frac{a}{2}\log_2\frac{1}{2} - \frac{2-a}{2}\log_2\frac{2-a}{2} \tag{4.45}$$

information mutuelle :

$$I(\rho) = 2S(\rho^A) + S(\rho) \tag{4.46}$$

Et la discorde quantique donné par :

$$Q(\rho) = S(\rho^A) + -S(\rho) \tag{4.47}$$

D'apres (Chapiter 3) on calcule la concurrence :

$$C'(\rho) = a \tag{4.48}$$

on trace la concurrence, discorde quantique et la corrélation classique

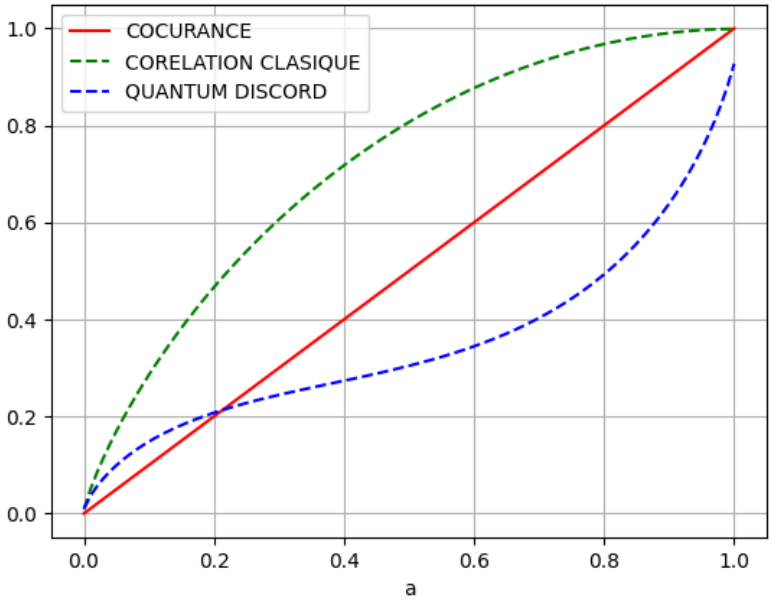

FIGURE 4.2 – la concurrence, LA discorde quantique et la corrélation classique

Example 3 :

Considérons l'état de Werner :

$$\rho = a\,|\psi^-\rangle\,\langle\psi^-| + \frac{1-a}{4}I \tag{4.49}$$

avec $|\psi^-\rangle = \frac{1}{\sqrt{2}}(|0,1\rangle - |1,0\rangle)$

— $\theta_1 = \theta_2 = \theta_3 = a$

$$C(\rho) = \frac{1-a}{2}\log_2(1-a) + \frac{1+a}{2}\log_2(1+a) \tag{4.50}$$

$$I(\rho) = \frac{3(1-a)}{4}\log_2(1-a) + \frac{1+3a}{4}\log_2(1+3a) \tag{4.51}$$

Discorde quantique :

$$Q(\rho) = I(\rho) - C(\rho) \tag{4.52}$$

concurrence :

$$C(\rho) = max\{0, \frac{3a-1}{2}\} \tag{4.53}$$

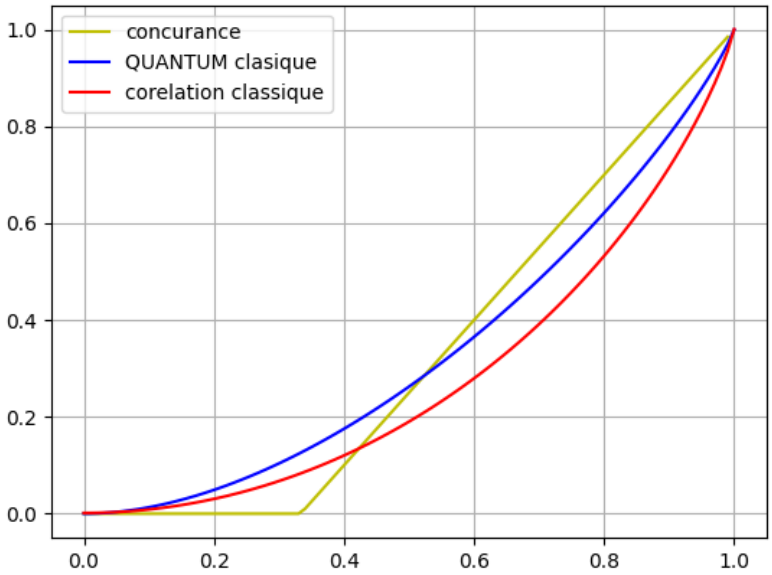

FIGURE 4.3 – la concurrence, LA discorde quantique et la corrélation classique

Bibliographie

[1] Dr Khadija El Anouz La théorie de l'information quantique Cours magistral (Faculté des Sciences et Techniques d'Al-Hoceima 2021/2022.)

[2] K. El Anouz,C. P. Onyenegecha, A.I. Opara, Ahmed Salah,AND A. El Allati,Dynamics of quantum Fisher information and quantum coherence of two interacting atoms under time–fractional analysis.Vol. 39, No. 3 / March 2022 / Journal of the Optical Society of America B.

[3] M. A. Nielsen and I. L. Chuang, Quantum Computation and Quantum Information (Cambridge University Press, Cambridge, England, 2000).

[4] F. F. Fanchini,T. Werlang, C. A. Brasil, L. G. E. Arruda, and A.O.Caldeira Non-Markovian Dynamics of Quantum Discord.

[5] A. Einstein, B. Podolsky et N. Rosen. Can Quantum - Mechanical Description of Physical Reality Be Considered Complete. Phys. Rev. 47, 1935.

[6] M. Scala, R. Migliore, and A. Messina, "Dissipation and entangle- ment dynamics for two interacting qubits coupled to independent reservoirs," J. Phys. A 14, 435304 (2008).

[7] KAYDI Wiam, THÈSE DE DOCTORAT(UNIVERSITE MOHAMMED V FACULTE DES SCIENCES Rabat), Mesure, quantification et caractérisation des corrélations quantiques dans des systèmes d'états cohérents multipartites 2016.

[8] H. Ollivier and W. H. Zurek,Quantum Discord : A Measure of the Quantumness of Correlations , Phys. Rev. Lett.88 (2001) 017901.

[9] B. Dakic, V. Vedral et C. Brukner, Phys. Rev. Lett 105 (2010) 190502.

[10] Mazhar Ali, A. R. P. Rau and , G. Alber,Quantum discord for two-qubit X states,PHYSICAL REVIEW A 81, 042105 (2010).

[11] B. Dakic, V. Vedral et C. Brukner, Phys. Rev. Lett 105 (2010) 190502.

[12] M. Daoud et R. Ahl Laamara, Phys. Lett. A 376 (2012) 2361.

[13] S. Luo, Phys. Rev. A 77, 042303 (2008).

P50

Majorana bound states characterization and study in an antiferromagnetic skyrmions background

Esteban Iroulart [1,2], **Héctor Diego Rosales** [1,3]

[1] *Instituto de Física de Líquidos y Sistemas Biológicos, La Plata, Buenos Aires*
[2] *Departamento de Física, Facultad de Ciencias Exactas, UNLP*
[3] *Departamento de Ciencias Básicas, Facultad de Ingeniería, UNLP*

Magnetic skyrmions hold great promises for next-generation spintronics applications[1]. In parallel, the interplay of magnetism, superconductivity and spin-orbit coupling has proved to be a versatile platform for engineering topological superconductivity predicted to host non-abelian excitations, Majorana bound states (MBS), which are known for their non-Abelian statistics controlled usage in fault-tolerant topological quantum computing[2,3,4]. In this work, we study the coupling of superconducting electrons to a topological texture of antiferromagnetic skyrmions with the purpose of stabilizing MBSs. For this, different configurations were used, varying the magnetic field applied to the sample, the chemical potential and the Hund coupling, using different geometries of lattice.

[1] Gao, S., Rosales, H., Gómez Albarracín, F. A., Tsurkan, V., Kaur, G., Fennell, T., ... & Zaharko, O. (2020). *Nature*, ***586***(7827), 37-41.
[2] Nayak, C., Simon, S. H., Stern, A., Freedman, M. & Das Sarma, S. Rev. Mod. Phys. 80, **1083**–**1159** (2008)
[3] Díaz, S. A., Klinovaja, J., Loss, D., & Hoffman, S. *Physical Review B*, ***104***(21), 214501(2021).
[4] Garnier, M., Mesaros, A., & Simon, P. *Communications Physics*, ***2***(1), 1-8 (2019).

P51

Effective-mass tensor of the two-body bound states and the quantum-metric tensor of the underlying Bloch states in multiband lattices

The so-called quantum geometric tensor is one of the basic components of the geometric quantum mechanics, i.e., a complex valued matrix whose real and imaginary parts are known, respectively, as the Fubini-Study or the quantum metric tensor and Berry curvature. As the naming suggests, the quantum metric is a measure of the distance between two nearby quantum states, characterized by the local geometry of the complex quantum space. In contrast, the Berry curvature corresponds to the emergent gauge field in the quantum space, the total flux of which is related to the global topology of the quantum states, e.g. the Chern number. In striking contrast to the physical importance of the Berry curvature and quantum topology that has been put forward in the past two decades or so, there is relatively much slower progress in showing the possible connection between a physical system and its quantum metric and quantum geometry. In this poster I will present an exact relation between the inverse of the effective-mass tensor of the lowest bound states and the quantum-metric tensor of the underlying Bloch states in a multiband Hubbard model, and discuss its possible ramifications in flat-band superluids and superconductors.

P52

Electric Field Induced Spin-orbit Coupling in Graphene-based Moiré Heterostructures

Two sheets of atomically thin materials twisted by a small angle form a moiré super lattice, the electronic properties of which may be significantly different from those of a single crystal [1]. Since the discovery of superconductivity in twisted bilayer graphene [2] research on twisted materials has grown into a new field of science called twistronics. Among many intriguing phenomena realized via interface interactions in twisted materials, spin-orbit interaction is particularly attractive because of possible utilization in spintronic/topological devices. Recent theoretical and experimental studies revealed that twisted bilayer graphene proximitized by monolayer transition metal dichalcogenide and sandwiched between hexagonal boron nitride can acquire enhanced intrinsic and Rasha spin-orbit coupling, which strongly modifies flat bands near the Fermi level and affects superconducting properties [3,4]. Realistic modeling of such effects is crucial for better understanding of strongly correlated effects in such systems, as well as topological properties, for example, the quantum anomalous Hall effect [5,6]. In the following work, twisted bilayer graphene/WSe2 heterostructure will be studied theoretically from the point of view of the electronic structure and topological proper- ties. The effects of the intrinsic spin-orbit interaction induced by WSe2 will be analyzed based on sp3d5 tight-binding model. In the next step, simulation of a realistic electric field applied to the system by a self-consistent solution of the Poisson equation will be performed. Then, we analyze local effects contributing to the Rashba spin-orbit coupling. We conclude with a discussion of how proximity effects modify the low-energy physics of finite size moiré Hubbard simulator. [1] E. Y. Andrei, A. H. MacDonald, Nat. Mater. 19, 1265–1275 (2020). [2] Y. Cao, V. Fatemi, and P. Jarillo-Herrero, Nature 556, 43–50 (2018). [3] J. X. Lin, Y. H. Zhang, and J. I. A. Li, Science 375, (6579) (2022). [4] M. Gmitra, J. Fabian, Phys. Rev. Lett. 119, 146401 (2017). [5] J. Shi, J. Zhu, and A. H. MacDonald, Phys. Rev. B 103, 075122 (2021). [6] M. Serlin, C. L. Tschirhart, and A. F. Young, Science 367, 900 (2020).

P53

Spontaneous orbital magnetization of the Wigner Crystal phase in Bernal bilayer graphene

Sandeep Joy[1], **Zhiyu Dong** [2], **Leonid Levitov**[2] **and Brian Skinner** [1]

[1]*Department of Physics, The Ohio State University, Columbus, Ohio 43202, USA*
[2]*Department of Physics, Massachusetts Institute of Technology, Cambridge, MA 02139, USA*

At low density and low temperature, long-ranged Coulomb interactions in a two-dimensional electron gas cause the electrons to crystallize into a solid-like phase called a Wigner crystal (WC). In Bernal bilayer graphene, a perpendicular displacement field facilitates the formation of a WC by effectively flattening the bottom of the conduction band and thereby reducing the electrons' kinetic energy. Crucially, at large displacement field the conduction band adopts a "Mexican-hat" shape, and this shape permits localized electrons to have finite angular momentum states that are nearly degenerate in energy with the ground state. Here we show that, when the displacement field is larger than a certain critical value, Berry curvature drives the WC phase to be an orbital magnet with one unit of orbital angular momentum per electron. We calculate the corresponding phase diagram of the WC state, and we estimate its melting temperature and compressibility.

P54

Tuning the Oxygen Vacancies, Strain Engineering, and Tungsten Doping Synergistic Interactions to Control the Metal-Insulator Transition Properties of VO2 Thin Films

Murat Kabataş[1*], Shrouk E. Zaki[1], Yasin Ramzan Eker[2]

[1] Department of Nanotechnology and Advanced Materials, Graduate School of Natural and Applied Sciences, Selçuk University, Konya, Turkey
[2]Department of Metallurgy and Material Engineering, Faculty of Engineering and Architecture, Necmettin Erbakan University, Konya, Turkey
**Corresponding author: m.a.basyooni@gmail.com*

As a Peierls-Mott insulator with a metal-insulator transition (MIT) at Tc = 68° C, vanadium oxide (VO2) is known. VO_2 exhibits potential as a component for infrared switching and sensing devices because it undergoes an abrupt metal-insulator transition (MIT) at temperatures close to ambient, where the electrical resistivity varies by orders of magnitude [1]. To use VO_2 in thermoelectric, electrochromic, or thermochromic applications, the MIT parameters must be tuned. This study tunes the MIT with a low phase transition of 20 °C in the air without capsulation by combining the effects of oxygen deficiencies, strain engineering, and metal tungsten doping. We study multilayer VO_2, WO_3, $Mo0.2W_{0.8}O3$, and/or MoO_3 oxide thin film narrow hysteresis phase transition devices made by high vacuum sputtering. Characterization of the deposited films includes structural, chemical, electrical, and optical evaluation. Different conductivity patterns were seen, with $VO_{1.75}$ on FTO glass having the lowest value and VO1.75 at VO1.75/WO2.94. A single-phase transition and a small hysteresis curve were visible in VO1.75/WO2.94. The MIT temperature dropped to 35 °C as a result of the presence of oxygen vacancies, whereas $Mo0.2W0.8O3/VO_2/MoO_3$ structure achieved the lowest temperature (Tc = 20 °C). $Mo0.2W0.8O_3$ was used for the first time as an anti-reflective and anti-oxidative layer in this previous sample. This work is applied to fast phase transition devices[2].

Keywords: thin films; vanadium oxide; thermochromic; phase transition device; metal–insulator transition

[1]. M. A. Basyooni, M. Al-Dossari, S. E. Zaki, Y. R. Eker, M. Yilmaz, and M. Shaban, Nanomater. 2022, Vol. 12, Page 1470 **12**, 1470 (2022).
[2]. M. Basyooni, S. Zaki, M. Shaban, Y. E.-S. reports, and undefined 2020, Nature.Com (n.d.).

P55

Electron liquid state in the spin-1/2 anisotropic Kondo lattice

In the framework of the mean field approach, we provide analytical and numerical solution of the spin-1/2 anisotropic Kondo lattice for arbitrary dimension at half filling. Nontrivial solution for the amplitude of the field opens a gap in the fermion spectrum of an electron liquid in which local moments on the lattice sites are realized. The ground state in the insulator state is determined by a static Z2 field of local moments, which forms the lattice with a double cell. Due to hybridization between electron states a large Fermi surface is formed in the Kondo lattice. A gap in the quasi-particle spectrum is calculated depending on the magnitudes of exchange integrals for the simple lattices with different dimension. It is shown that band electrons move in a static Z2 field of local moments, the uniform configuration of the Z2 field corresponds to ground state of electron liquid and leads to formation of a lattice with a double cell. In the insulator state the fermion spectrum is electron-hole symmetric as it takes place for the Majorana spectrum. The gapped state is formed at finite values of the exchange integrals. The results of calculations are valid in the case a weak anisotropy of the exchange interaction, that alow to made conclusion that the behavior of electron liquid in an isotropic Kondo lattice is similar.

P56

An integrated probe for the transport properties of Fe-based quaternary Heusler Compound

Navdeep Kaur [1], Vipul Srivastava[1], and Ramesh Sharma[2]

[1]Department of Physics, School of Chemical Engineering and Physical Sciences, Lovely Professional University, Phagwara-144411, Punjab, India

[2]Department of Applied Science, Feroze Gandhi Institute of Engineering and Technology, Raebareli, Uttar Pradesh, India

Nowadays, an imperative need of converting waste heat into a useful source of energy or electricity, which is the main principle of thermoelectric applications, gave a hike to the research of relevant materials. In the way of which the magnificent properties of Heusler compounds escorted researchers to look them up as a significant compounds. In such context, we investigated the Fe-based quaternary Heusler compound through the density functional theory (DFT) [1]. This was initiated by the structural optimization and was done by considering the possible types of quaternary Heusler compounds, named type-I, type-II, and type-III. By means of this, further investigation, including electronic, elastic, mechanical, thermodynamic, and thermoelectric studies was led by the stable type-I structure. This followed the spin-polarized calculations that inferred the ferromagnetic phase of a compound. Further, the combined electron transfer properties through generalized gradient approximation (GGA) [2] and modified-Becke Johnson (mBJ) [3] potentials assisted in evaluating the electronic and magnetic properties. Our calculations conferred the half-metallic character of the compound with a high spin polarization in its ground state. We also gave insight into the elastically and mechanically stable nature of the compound that illustrated strengthen and toughen behavior of the compound against compression and tensile strain. Further, the quasi-harmonic model outlined the thermodynamical stability of the compound under the effect of temperature and pressure. In addition to this, the BoltzTrap code assisted in understanding the thermoelectrical efficiency of the compound and therefore the efficient value of the Seebeck coefficient and figure of merit signifies the compound as a promising material for thermoelectric applications and gave directions to the experimental study.

[1] M.C. Payne, M.P. Teter, D.C. Allan, T.A. Arias, A.J. Joannopoulos, Rev. Mod. Phys. **64**, 1045 (1992).

[2] J.P. Perdew, K. Burke, M. Ernzerhof, Phys. Rev. Lett. **77**, 3865 (1996).

[3] A.D. Becke, E.R. Johnson, J. Chem. Phys. **124**, 221101 (2006).

P57

Biaxial strain-induced band gap engineering in monolayer MoS_2 using DFT

Mayur Khan[1], and Ambuj Tripathi[3]

[1]*Materials science group, Inter -University Accelerator Centre, New Delhi -110067, India*

Corresponding author email: khanmayur253@gmail.com

2D TMDs such as MoS_2 are important due to their critical electrical and optical characteristics which tune by several methods like layer reduction, straining and etc. Since the MoS_2 is a promising material for creating the upcoming generation of electrical and optoelectronic devices because of its acceptable bandgap (1.2 eV bulk and 1.8 eV 1L) and the possibility of band gap modification by strain. The DFT computation is being used in this study to analyze the electronic band structures and band gap fluctuation of monolayer MoS_2 under biaxial strain. The DFT approach yielded a 1.78 eV band gap value for monolayer MoS_2. When the biaxial tensile strain was applied, significant changes in the electronic structures were seen. According to DFT simulations, biaxial tensile strain causes the band gap Eg to drop linearly. At 10 % applied biaxial tensile strain, 1L-MoS_2 begins to exhibit metallic behavior. Between 1.78 eV and 1.74 eV, with 0 % to 0.3 % applied biaxial strain, the band gap is adjusted under biaxial strain. The 1L-MoS_2 has a straight band gap. The direct nature of bandgap tuning may be exploited to create photodetector and solar cells based on MoS_2.

P58

Metal-insulator transitions in doped La-based superconductors with small-radius dopants

Z.S. Khudayberdiev , S. Dzhumanov , and U.T. Kurbanov

Institute of Nuclear Physics AS RUz, 100214, Tashkent, Uzbekistan

In this work, we study the possibility of realizing two distinct mechanisms of metal-insulator transitions in hole-doped cuprates induced by the localization of charge carriers near the small-radius impurities and in a deformable lattice (i.e. in the absence of impurities). The purpose of this research is to determine the criteria (i.e. conditions) for the existence of the localized states of hole carriers and solve the problem of metal-insulator transitions in La-based cuprates. The advantage of La-based cuprate versus other types of cuprates is that two distinct metal-insulator transitions in La-based cuprates driven by the strong carrier-impurity-phonon and carrier-phonon interactions occur simultaneously in a wider doping range from the lightly doped to heavily doping regime. We show that at very low doping, the separate levels of hole carriers localized near impurities and in a deformable lattice are formed in the charge-transfer gap of the cuprates. As the doping level increases towards underdoped region, the energy levels of such charge carriers start to form energy bands which gradually broaden with increasing doping. We propose a new two-carrier cuprate superconductor model for studying two distinct metal-insulator transitions occurring simultaneously in hole-doped La-based cuprate compounds. We demonstrate that when hole carriers reside in impurity and polaron bands, these metal-insulator transitions in Labased superconductors with small-radius dopants occur accordingly in a wide doping range and relatively lower doping levels.

P59

Ab initio investigation of the structural, optical, mechanical, elastic, and thermophysical performance of Ce-based oxide Perovskite for energy applications

Preeti Kumari [1], Vipul Srivastava [2], and Ramesh Sharma[3]

[1]Research Scholar, Department of Physics, Lovely Professional University, Phagwara, Jalandhar-144411, Punjab, India

[2] Professor, Department of Physics, Lovely Professional University, Phagwara, Jalandhar-14441, Punjab, India

[3]Department of Applied Science, Feroze Gandhi Institute of Engineering and Technology, Raebareli, Uttar Pradesh, India

Continuous technological advancements demand new materials with extraordinary behaviors in order to make human life more convenient and comfortable. Novel materials with their astounding properties can be served as a source of energy. In this context, Perovskite compounds are appropriate because of their well-known class and utility. This paper presents the structural, optical, elastic, mechanical, thermodynamic, and thermoelectric properties of Ce-based perovskite. The structure is optimized with FPLAPW [1] and followed a Generalised gradient potential (GGA) approach as incorporated in WIEN2K [2]. Thermoelectric properties are investigated with the classic Boltzmann transport phenomenon which is embedded in BoltzTrap code [3]. The compound study is carried out with different exchange-correlation (Xc) potential Local density approximation (LDA), WC-Cohen [4], PBE-GGA [5], and PBE-sol [6]. In addition to the above-mentioned Xcs, modified Becke Johnson (mBJ) [7] and mBJ-SOC [8] are also used for bandgap calculations. The thermoelectric performance has been analyzed by estimating the thermopower and figure of merit (temperature range 50- 1200 K). Further, thermodynamical behavior has also been discussed under pressure and temperature. Furthermore, the mechanical stability of the compound has been confirmed by using the criteria of elastic constants and shear modulus. Consequently, mechanical parameters such as shear modulus, Young's modulus, bulk modulus, anisotropy, and Poison ratio are estimated through elastic coefficients. The optical behavior of the perovskite is concluded with parameters dielectric constant, absorption coefficient (α (ω)), optical conductance (σ (ω)), reflectivity (R (ω)), electron energy loss spectra EELS (L (ω)), refractive index (n (ω)) as well as extinction coefficient (k (ω)) in the range (0-12eV) energy spectrum.

[1] P. Blaha, K. Schwarz, P. Sorantin, S.B. Trickey, Comput. Phys. Commun. **59(2)**, 399–415 (1990)
[2] P. Blaha, K. Schwarz, F. Tran, R. Laskowski, G.K.H. Madsen, L.D. Marks, J.Chem. Phys. **152(7)**, 074101 (2020).
[3] G. K. H. Madsen, D. J. Singh, Comput Phys Commun. **175(1)**, 67-71 (2006).
[4] Z. Wu and R. E. Cohen, Phys. Rev. B. **73**, 235116 (2006).
[5] J. P. Perdew, K. Burke and M Ernzerhof, Phys. Rev. Lett. **77**, 3865 (1996).
[6] Csonka, Gábor I., A. Ruzsinszky, J. P. Perdew, and S. Grimme, Journal of chemical theory and computation. **4(6),** 888-891 (2008).
[7] Becke, Axel D., Erin R. Johnson, Journal of Chemical Physics. **124(22)**, 221101 (2006).
[8] W. E. P. A. H. MacDonald and D. D. Koelling, J. Phys.C. **13**, 2675 (1980).

P60

Abstract

Shreya Kumbhakar

May 2022

The Mott metal-insulator transition remains one of the most scrutinized concepts in condensed matter physics. However, the kinetics of the charge carriers at the transition, involving both orbital and spin degrees of freedom, still remains poorly understood. A perfect platform to distinguish between the role of such competing interactions is strongly correlated oxides offering rich phase diagrams, which we use here to address the electron kinetics at the transition. We show a critical slowing down of electron kinetics at the the first order metal to Mott insulator transition in the Ruddlesden Popper oxide $Ca_3(Ru_{0.9}Ti_{0.1})_2O_7$ using low-frequency noise in resistance fluctuations. Critical slowing down of the electron kinetics is manifested as an enhancement of noise by an order of magnitude at the transition with a large shift of the spectral weight to lower frequencies. The second spectrum of noise is frequency dependent, indicating the presence of correlated fluctuations which gets suppressed under the application of a magnetic field. Our experiments provide compelling evidence of the formation of a spin-glass phase at the transition in these systems.

P61

Abstract for "Theory of phonon instabilities in Weyl semimetals at high magnetic fields"

Sarbajaya Kundu [1,2] **, Claude Bourbonnais**[2] **, and Ion Garate** [2]

[1](*Presenting author underlined) Department of Physics, University of Florida, Gainesville, Florida 32611, USA*

[2] *Département de Physique, Institut Quantique and Regroupement Québécois Sur les Matériaux de Pointe, Université de Sherbrooke, Sherbrooke, Québec J1K 2R1, Canada*

In recent times, electronic instabilities in Dirac/Weyl semimetals at high magnetic fields have attracted much attention, but the role of electron-phonon interactions therein has been largely neglected. In this context, we have recently studied possible lattice and electronic instabilities in a minimal model of a Weyl semimetal (WSM), emerging from chiral and non-chiral Landau levels, considering the interplay of electron-electron and electron-phonon interactions using a Kadanoff-Wilson renormalization group approach. We consider both the adiabatic and the nonadiabatic phonon regimes, in the presence or in the absence of improper symmetries that relate Weyl nodes of opposite chirality. We find that the Cooper channel, often neglected in recent studies, can prevent purely electronic instabilities, while enabling lattice instabilities that are not Bardeen-Cooper-Schrieffer-like. This behaviour is suppressed upon breaking the improper symmetry that relates the two Weyl nodes. Moreover, pseudoscalar phonons are found to be more prone to a Peierls instability than scalar phonons. Our study emphasizes the importance of taking electron-phonon interactions into account for a complete understanding of interacting phases of matter in Dirac and Weyl semimetals at high magnetic fields.

P62

METAL-INSULATOR TRANSITIONS IN DOPED La-BASED SUPER CONDUCTORS WITH SMALL-RADIUS DOPANTS

In this work, we study the possibility of realizing two distinct mechanisms of metal-insulator transitions in hole-doped cuprates induced by the localization of charge carriers near the small-radius impurities and in a deformable lattice (i.e. in the absence of impurities). The purpose of this research is to determine the criteria (i.e. conditions) for the existence of the localized states of hole carriers and solve the problem of metal-insulator transitions in La-based cuprates. The advantage of La-based cuprate versus other types of cuprates is that two distinct metal-insulator transitions in La-based cuprates driven by the strong carrier-impurity-phonon and carrier-phonon interactions occur simultaneously in a wider doping range from the lightly doped to heavily doping regime. We show that at very low doping, the separate levels of hole carriers localized near impurities and in a deformable lattice are formed in the charge-transfer gap of the cuprates. As the doping level increases towards underdoped region, the energy levels of such charge carriers start to form energy bands which gradually broaden with increasing doping. We propose a new two-carrier cuprate superconductor model for studying two distinct metal-insulator transitions occurring simultaneously in hole-doped La-based cuprate compounds. We demonstrate that when hole carriers reside in impurity and polaron bands, these metal-insulator transitions in La-based superconductors with small-radius dopants occur accordingly in a wide doping range and relatively lower doping levels.

P63

Non-Hertz-Millis scaling of the antiferromagnetic quantum critical metal via scalable Hybrid Monte Carlo

Peter Lunts[1,2], **Michael S. Albergo**[3], **and Michael Lindsey**[4]

[1] *Joint Quantum Institute and Department of Physics, University of Maryland, College Park, MD 20742, USA*

[2] *Center for Computational Quantum Physics, Flatiron Institute, 162 5th Avenue, New York, NY 10010, USA*

[3] *Center for Cosmology and Particle Physics, New York University, New York, NY 10003, USA*

[4] *Courant Institute of Mathematical Sciences, New York University, New York, New York 10012, USA*

We numerically study the $\mathrm{O}(3)$ spin-fermion model, a minimal model of the onset of antiferromagnetic spin-density wave (SDW) order in a two-dimensional metal. We employ a Hybrid Monte Carlo (HMC) algorithm with a novel auto-tuning procedure, which learns the optimal HMC hyperparameters in an initial warmup phase. This allows us to study unprecedentedly large systems, even at criticality. At the quantum critical point, we find a critical scaling of the dynamical spin susceptibility $\chi(\omega, \vec{q})$ that strongly violates the Hertz-Millis form, which is the first demonstrated instance of such a phenomenon in this model. The form that we do observe provides strong evidence that the universal scaling is actually governed by the fixed point near perfect hot-spot nesting of Ref. [1], even away from perfect nesting. Our work provides a concrete link between controlled calculations of SDW metallic criticality in the long-wavelength and small nesting angle limits and a microscopic finite-size model at realistic appreciable values of the nesting angle. Additionally, the HMC method we introduce is generic and can be used to study other fermionic models of quantum criticality, where there is a strong need to simulate large systems.

[1] A. Schlief, P. Lunts, and S.-S. Lee, Phys. Rev. X **7**, 021010 (2017).

P64

Multiorbital Boltzmann transport and the resistivity anisotropy of nematic FeSe

Motivated by the increasing number of crystals presenting multiple bands at low energy, we derive their electronic dc transport features by means of a linear Boltzmann equation. The interplay of random disorder, possibly having biased orbitals couplings, and symmetry is investigated in detail. Interestingly, certain types of disorder may induce anisotropic transport even in highly symmetric and isotropic systems such as a 2D Rashba gas and invalidate the relaxation time approximation[1]. The theory is able to describe almost quantitatively the resistivity anisotropy of nematic FeSe, measured in a recent experiment[2], whose microscopic description is still under debate[3]. [1] M. Marciani and L. Benfatto, Phys. Rev. B 104, 235143 (2021) [2] M. A. Tanatar et al., Phys. Rev. Lett. 117, 127001 (2016). [3] M. Marciani and L. Benfatto, arXiv:2202.12070 (accepted in PRB).

P65

Detrimental effect of disorder on two dimensional time-reversal invariant topological superconductor

The robustness against local perturbations, as long as the symmetry of the system is preserved, is a distinctive feature of topological quantum states. Magnetic impurities and defects break time-reversal invariance (TRI) and consequently, TRI topological superconductors (TSC) are fragile against this type of disorder. Non-magnetic impurities, however, preserve TRI, and one naively expects a TRI TSC to be robust against non-magnetic impurities. In this work, we study the effect of non-magnetic disorder on a TRI TSC with extended s-wave pairing, which can be engineered at the interface of a Fe-based SC and a strongly spin-orbit coupled Rashba layer. For disorder, we model two different types of non-magnetic random disorder, and we calculate the density of states for many independent impurity configurations. Contrary to naive expectation, we find that the disorder affects the topological phase strongly by closing the gap while the trivial extended s-wave and conventional s-wave SC phases remain stable. This gives a modified phase diagram where we see the expansion of the nodal phase by increasing disorder amplitude and the decay of Majorana Kramers pairs in the presence of disorder. Our finding improves our understanding of the nontrivial effect of impurities and disorder on the TRI topological phases and may help explaining the difficulty of experimental observation of TRI TSCs.

P66

Photovoltaic, Electronic and Optical properties of Cesium bromate oxygen perovskite: First-principles investigation

R. Masrour

Laboratory of Solid Physics, Faculty of Science, Sidi Mohammed Ben Abdellah University,

Dhar Mahraz, BP 1796, Fez, Morocco

* Corresponding author:rachidmasrour@hotmail.com

Abstract

The electronic and optical properties of Cesium bromate oxygen perovskite by using the full potential augmented plane wave method were performed to study. The density of States is obtained and are discussed. The Cesium bromate oxygen perovskite have semiconductor character with a wide direct gap with the gap energy 4.24 eV. The quantum efficiency, the short-circuit current and Open Circuit Voltage are investigated from ab-initio calculations.

P67

One-dimensional topological insulators and superconductors with chiral symmetry

We construct microscopical models of one-dimensional chiral topological superconductors (TSs) and insulators (TIs) and study their topological properties. As the minimal models that represent topological classes with chiral symmetry and capture the essential physical properties of the classes, we consider one-dimensional coupled chains. In case of Tis we use coupled Su-Schrieffer-Heeger models and for TSs we couple Kitaev chains. We demonstrate, that there are several ways to couple the chains, they correspond to inequivalent choices of chiral symmetry operators. We find that weak perturbations that preserve chiral symmetry of the model belonging to a certain topological class, but break other symmetries of the class, do not change its topological properties. Moreover, we analytically compute the topological invariants of the models depending on the type of coupling, and demonstrate how to generalise our results to the case of multiple coupled chains. Our findings allow to construct a system with a given winding number, by choosing a proper coupling scheme. We discuss the role of interactions on the topological properties of the constructed one-dimensional models.

P68

Thermal conductivity in TRS-breaking Weyl-semimetals in the hydrodynamic regime

Yonatan Messica [1] , **Dmitri Gutman** [1]

[1] *Department of Physics, Bar Ilan University, Ramat Gan 52900, Israel*

The hydrodynamic regime, characterized by collective motion of electrons, is recently drawing a lot of interest. This regime is especially interesting in Weyl-semimetals, as in the vicinity of the Weyl nodes, electrons and holes coexist, allowing for decoupling between charge and energy transport. We investigate the thermal conductivity for a TRS-breaking Weyl-semimetal . Near the Weyl node, e-e interactions strongly suppress the electric conductivity, but not the thermal conductivity. The anomalous Hall conductivity modifies both the longitudinal and transverse thermal conductivities, as it produces a transverse electric field in response to a particle current. This enables the thermal conductivity to remain high even for chemical potential set away from the Weyl nodes.

P69

Two-loop mass anomalous dimension in reduced quantum electrodynamics and application to dynamical fermion mass generation

We consider reduced quantum electrodynamics (RQEDdγ,de) a model describing fermions in a de-dimensional space-time and interacting via the exchange of massless bosons in dγ-dimensions (de ≤ dγ). We compute the two-loop (parity even) mass anomalous dimension, γm, in general RQED4,de with applications to RQED4,3 (graphene at its IR fixed point) and QED4. We then proceed on studying dynamical (parity even) fermion mass generation in RQED4,de by constructing a fully gauge-invariant gap equation for RQED4,de with γm as the only input. This equation allows for a straightforward analytic computation of the gauge-invariant critical coupling constant, α_c , which is such that a dynamical mass is generated for $\alpha_r > \alpha_c$, where α_r is the renormalized coupling constant, as well as the gauge-invariant critical number of fermion flavours, N_c , which is such that $\alpha_c \to \infty$ and a dynamical mass is generated for $N < N_c$.

P70

UNIVERSITY OF KENT

DIVISION of NATURAL SCIENCES

AUTHORISATION to TRAVEL FORM

When completed by the Traveller and Supervisor/PI/Line Manager, please return a signed & dated copy to the Divisional Finance Team (NATStravel@kent.ac.uk).

This form must be returned with completed Risk Assessment and Health Assessment forms.

Please read the University Travel Policy

Traveller Name:	Dr Gunnar Möller
Job Title:	Royal Society University Research Fellow
Trip Destination(s):	International Centre for Theoretical Physics (ICTP) Trieste, Italy
Departure Date:	approx. 24/8/2022
Return Date:	approx. 1/9/2022
Purpose of the Travel:	Participation in ICTP conference on "Strongly Correlated Matter: From Quantum Criticality to Flat Bands" (SMR3732)

NATURE OF TRAVEL (*Please provide full details of the trip including destination, duration, means of travel, full details why this trip is absolutely essential and unavoidable) Refer to sections 2.3, 2.7 of the policy.*

Travel to ICTP by air for participation in the ICTP conference on "Strongly Correlated Matter: From Quantum Criticality to Flat Bands" (SMR3732), which brings together leading experts from across analytical, numerical and experimental studies of strongly correlated matter. In particular, the speakers include top experts on diagrammatic Monte-Carlo approaches, and provide opportunity for discussions and collaboration.

JUSTIFICATION OF TRAVEL (*Travel should still only occur where there is budget available, where it is safe to do so, and where necessary. If you can achieve the same results by attending online, or by not travelling, you should not travel.)*

I have read and understood sections 2.3 and 2.7 of the policy and the travel remains essential ✓

COST of TRAVEL, INCLUDING INFORMATION ON THE BUDGET TO COVER IT *(Please provide full details)*

Airport transfers to London £80, Flight ca. £200, accommodation at institute (subsidised rates), subsistence (subsidised at institute). Travel funds available under Royal Society URF, project 22729.

I have completed and attached a Risk Assessment ✓ I have completed and attached a Health Assessment ✓

I confirm I will have completed the online travel insurance (where the outbound and return flight bookings are not made on a single travel itinerary with the TMC) **Section 7.1 of the policy.** ✓

Important - Please note that failure to make accurate declarations may result in disciplinary action.

Traveller Declaration

Signed ..... G. Möller ..... Dated 25/7/22

Supervisor / Principle Investigator (PI) / Line Manager Approval

Signed …….....…… Dated

Print Name:

- You also need to complete a Risk Assessment: https://www.kent.ac.uk/safety/hs/pages/travel-work-overseas/travel-work-overseas.html
- You also need to complete a Health Assessment: https://www.kent.ac.uk/safety/oh/Travel/Travel%20Health%20Assessments.html
- All travel and accommodation should be booked with our Travel Provider.
- Travel not booked with Key Travel **or** is not an outbound and return flight booking made on a single travel itinerary with the TMC needs to be registered for the University's travel insurance coverage here: https://www.kent.ac.uk/finance-staff/services/insurance/travelstaff/index.html
- Return this form with the Risk Assessment, Health Assessment, and any other supporting documentation to NATStravel@kent.ac.uk

FINANCE OFFICE USE ONLY Division Director/Nominated Authoriser's Approval

Signed …….....…… Dated

Print Name:

P71

Electron-phonon interaction in TixOy using first-principles calculations

The electronic, phonon, and electron-phonon interactions of titanium suboxide structures including TiO, Ti2O3, Ti3O5, Ti4O7, and Ti5O9 were investigated in the framework of density-functional theory. The mechanism of superconductivity in these materials seems to be phonon mediated, probably with participation of paramagnetic spin fluctuations. The influence of pressure on the superconducting transition temperature (TC) of cubic TiO and Ti4O7 could be explained by this mechanism. Our calculations predict a low TC of ~3.5 K for Ti5O9. It implies that Ti5O9 would be a superconductor lying in the weak coupling regime.

P72

The electronic structure of the conventional hydride superconductors

C. Mohammed-Krarroubi [1], N. Benayad [1], M. Djermouni [1] and A. Zaoui [1]

[1] *Laboratoire de Physique Computationnelle des Matériaux (LPCM), Université Djilali Liabès de Sidi Bel-Abbès*

Motivated by theoretical predictions of critical high temperature (TC) in many hydride (SC) superconductors, experiments have been carried out to confirm that the compressed sulphur hydride H3S where TC of 203 K at pressures around 150 GPa. Therefore, the objective of this work, on the one hand, is to know the microscopic mechanism of superconducting hydride materials and, on the other hand, to contribute to the exploration of new high-pressure SC hydrides. And in order to achieve our goals, we will use a first principle method based on the DFT theory. This theory helps us to predict the electronic, chemical, and phononic properties of hydride materials.

P73

Study of magnetic properties of Gd*TM*Si (*TM* = Mn, Ru) intermetallic compounds accounting for strong electron correlations

R.D. Mukhachev[1], A.V. Lukoyanov[1,2]

[1]*M.N. Mikheev Institute of Metal Physics of Ural Branch of Russian Academy of Sciences, Yekaterinburg, Russia*

[2]*Ural Federal University, Yekaterinburg, Russia*

The ternary intermetallic compounds GdTMSi (TM = Mn, Ru) attract the attention of researchers because of variability of physical and chemical properties and potential for practical use. They crystallize in the CeFeSi-type tetragonal structure P4/nmm. A remarkable increase of Curie temperature was found in the doped GdFeSi compound [1]. In this work, the calculations of the electronic structure were performed in Quantum ESPRESSO package [2]. The GGA+U method was used to account for strong electron correlations. For Gd ions, the values of the calculated total magnetic moment is 7.2 μ_B per Gd ion. The Ru and Si ions are non-magnetic, while the magnetic moment of the Mn ions is 2-3 μ_B, which reduces the total magnetic moment in the compositions with Mn. In the calculations for GdMnSi, the value of the total magnetic moment per formula unit was equal to 4.8 μ_B due to the magnetic moment of Mn [3]. Compound GdRuSi compared to the previously studied intermetallic compounds Gd(V, Cr, Mn, Fe,)Si has the highest value of the total density of electronic states at the Fermi level. The calculations shown that the GdTMSi compounds have differences not only in the magnetic properties, but also in the electronic structure. The electronic states near the Fermi level are determined primarily by the 3d states of the TM ions. When half of the Mn ions were replaced by Ru ions, the densities of electron states were redistributed at the Fermi level, which led to the closure of a pseudo-gap that was present in one of the spin projections in GdMnSi. Also, the magnetic moment of Mn in this case changed by more than 0.5 μ_B, which reduced the total magnetic moment in $GdMn_{0.5}Ru_{0.5}Si$ to 6 μ_B. Thus, in the studied intermetallics, we found that they are very different depending on the TM ion type, which indicates a difference in transport properties, and makes the GdTMSi intermetallics promising for use in microelectronic and magnetocaloric applications. The work was supported by RSF grant No 18-72-10098.

[1] A. G. Kuchin, S. P. Platonov, A. V. Lukoyanov, A. S. Volegov, V. S. Gaviko, R. D. Mukhachev, M. Yu. Yakovleva, Intermetallics **133**, 107183 (2021).
[2] P. Giannozzi, S. Baroni, N. Bonini, M. Calandra, et al., J. Phys.: Condens. Matter. **21**, 395502 (2009).
[3] R. D. Mukhachev, A. V. Lukoyanov, Metals **11**, 1296 (2021).

P74

Electron-vortex interaction and fermion pairing

Shantonu Mukherjee[1] **, and Amitabha Lahiri**[2]

[1, 2] *S. N. Bose National Centre for Basic Sciences, West Bengal, India, 700106*

We consider a system containing charged bosons and fermions coupled minimally to electromagnetic field where topological vortices can appear in the scalar matter. In presence of vortices, we dualize the phase of the bosonic field in terms of anti-symmetric 2-form field. The dual lagrangian contains terms that suggest an interaction between a non-local fermion current, termed spin current, and vorticity. Such an interaction was previously shown to give rise to a linear confining potential which leads to fermion pairs. To achieve such a linear potential within our theory we try to map the lagrangian of dual strings to a corresponding string field theory. Within such a string field theory there can be a phase where a linearly rising potential appears between two nonrelativistic fermions. This Linear attractive interaction between non-relativistic fermions lead to formation of pairs and hence can lead to novel phases of matter like unconvensional superconductivity etc. It can also be used in toy model of quark confinement.

[1] S. Mukherjee, A. Lahiri, *Annals Phys.* 418 (2020) 168167

[2] S. Mukherjee, A. Lahiri, *JHEP* 02 (2022) 068

P75

A stability bound on the T-linear resistivity of conventional metals

Chaitanya Murthy[1], **Akshat Pandey**[1], **Ilya Esterlis**[2], **and Steven A. Kivelson**[1]

[1]*Department of Physics, Stanford University, Stanford, CA 93405, USA*
[2]*Department of Physics, Harvard University, Cambridge MA 02138, USA*

The electrical resistivity of conventional metals varies linearly with temperature T in the regime $T > \omega_0$, where ω_0 is a characteristic phonon frequency. The corresponding transport scattering rate is $1/\tau_{\rm tr} = 2\pi\lambda T$, where λ is a dimensionless strength of the electron-phonon coupling. The fact that measured values satisfy $\lambda \lesssim 1$ has been noted in the context of a possible "Planckian" bound on transport. However, since the electron-phonon scattering is quasi-elastic in this regime, it is unlikely that Planckian considerations are relevant. We present results on the Holstein model which show that a different sort of bound is at play: a "stability" bound on λ consistent with metallic transport. We conjecture that a qualitatively similar bound on the strength of residual interactions may apply to metals more generally.

[1] C. Murthy, A. Pandey, I. Esterlis, S. A. Kivelson, "A stability bound on the T-linear resistivity of conventional metals" arXiv preprint arXiv:2112.06966 (2021).

P76

A Comparative Study on thermodynamics properties of Se-Te- Zn and Se-Te-Ag Ternary Chalcogenide Glasses

This paper presents the comparison of the influence of additives Zn and Ag on the thermodynamics properties of Se 80-x Te 20 M x (M=Ag, Zn), (0≤x≤10) glasses using Differential Scanning Calorimetry (DSC) under non-isothermal condition at different heating rates. Different theoretical models have been employed to study the activation energy of glass transition (E t) and crystallization (E C), Entropy, Enthalpy and Gibbs free energy for the best understanding of thermal stability. These parameters are found to be highly composition dependent. This also indicates that the glass network of the binary alloy is influenced significantly due to addition of the modifiers (Ag, Zn) used in the present study. Furthermore, investigated outcomes illustrate that the incorporation of fixed amount of Te with increasing Ag and Zn concentration affects the kinetic energies and glass forming abilities of the as formed glasses. However, when Zn compared with Ag glasses, it is found that they show almost the same kinetic parameters.

P77

Dynamics of exciton polaron in microtubule

In this paper, we study the dynamical properties of the exciton-polaron in the microtubule. The study was carried out using a unitary transformation and an approximate diagonalization technique. Analytically, the modeling of exciton-polaron dynamics in microtubules is presented. From this modeling, the ground state energy, mobility, and entropy of the exciton-polaron are derived as a function of the parameters characterizing the microtubule geometry. Numerical results show that, depending on the three vibrational modes (protofilament, helix, antihelix) in MTs, exciton-polaron energy is anisotropic and is more present on the protofilament than the helix and absent on the antihelix. The quasiparticles move only on the protofilaments and helix and when we take into account the variation of the protofilament vibrations by fixing the helix vibrations, the quasi-particles move between the 1st and 2nd protofilaments. When we take into account the variation of the two vibrations the quasi-particles move between the 1st and 15th protofilament. This result confirms the importance of helix vibrations on the dynamics of quasiparticles. The exchange of information between the exciton-polaron and its environment is similar to its mobility. Confirming that the quasiparticles move in the protofilament faster than the helix, the electrical field produced by the vibrations of the MT lattice may be anisotropic depending on the modes of vibration.

P78

Superconductivity and localization near a two-dimensional ferromagnetic quantum critical point

P.A. Nosov[1], **I.S. Burmistrov** [2,3], **and S. Raghu**[1,4]

[1]*Stanford Institute for Theoretical Physics, Stanford University, Stanford, CA 94305, USA*
[2]*L.D. Landau Institute for Theoretical Physics, acad. Semenova av.1-a, 142432, Chernogolovka, Russia*
[3]*Laboratory for Condensed Matter Physics, National Research University Higher School of Economics, 101000 Moscow, Russia*
[4] *Stanford Institute for Materials and Energy Sciences, SLAC National Accelerator Laboratory, Menlo Park, CA 94025, USA*

We consider a two-dimensional disordered Fermi liquid weakly coupled to the soft fluctuations associated with proximity to an Ising-ferromagnetic quantum critical point. By performing a two-loop calculation of the effective action in the modified non-linear sigma model framework [1], we derive interaction-induced corrections to the Usadel equation governing the superconducting gap function. We analyze a linearized version of this equation and show that diffusion and localization effects drastically change the interplay between fermionic incoherence and strong pairing interactions. In particular, we demonstrate that: (i) diffusive particle-particle modes (so-called 'Cooperons') acquire new dynamical scaling $z = 4$; (ii) there is an intermediate range of disorder strength where superconductivity is enhanced, eventually followed by a tendency towards the superconductor-insulator transition at stronger disorder; (iii) dephasing of particle-particle excitations leads to an additional contribution to the thermal self-energy and increases pair-breaking effects. In addition, we determine the temperature dependence of the resistivity and the phase diagram.

[1] P.A. Nosov, I.S. Burmistrov, and S. Raghu, Phys. Rev. Lett. **125**, 256604 (2020).

P79

Resistivity due to acoustic phonons scattering with chiral carriers in impure Bilayer Graphene

M. Obaidurrahman and S S Z Ashraf

Department of Physics, Faculty of Science, Aligarh Muslim University Aligarh-202002, India
* E-mail; khanobaid12@gmail.com

Abstract

In the present work, we studied the temperature, and disorder-dependent resistivity due to acoustic phonon screened and unscreened deformation potential scattering with chiral carriers in impure bilayer graphene in the Bloch Gruneisen temperature regime. We performed the analytical and numerical calculations applying Keldysh Green's function method within the impure limit, $ql<<1$ and compared the obtained results with the pure limit result. The obtained resistivity results show an enhanced temperature dependence on disorder and screening. In the disorder limit, the resistivity is proportional to T/l for the unscreened DP, which is different from the T^2 temperature dependency of the unscreened DP in the pure limit at the Fermi surface. We also compare the bilayer results with single-layer graphene so as to provide a comparative study with single-layer graphene. The temperature and disorder dependency in bilayer graphene shows the same power law as that of single-layer graphene but exhibits a difference in magnitude due to different chirality factors in the two systems.

Keywords: Bilayer graphene, deformation potential, Keldysh technique

Reference

[1] M. Obaidurrahman and S. S. Z. Ashraf, Phys. Scr. **95,** 105703, (2020).

[2] J. C. W. Song, M. Y. Reizer, and L. S. Levitov, Phys. Rev. Lett. 109, 106602, (2012).

[3] J. K. Viljas and T. T. Heikkila, Phys. Rev. B **81**, 245404, (2010).

P80

Quantum thermodynamics of strongly correlated systems

Vladimir Ohanesjan,[1] **Yevheniia Cheipesh**,[2] **Nikolay V. Gnezdilov**,[3] **Andrei I. Pavlov**,[4] and **Koenraad Schalm**[2]

[1] *Instituut-Lorentz, Δ-ITP, Universiteit Leiden, 2300 RA Leiden, The Netherlands*

[2] *Instituut-Lorentz, Δ-ITP, Universiteit Leiden, P.O. Box 9506, 2300 RA Leiden, The Netherlands*

[3] *Department of Physics, University of Florida, Gainesville, FL 32611, USA*

[4] *The Abdus Salam International Centre for Theoretical Physics (ICTP) Strada Costiera 11, I-34151 Trieste, Italy*

Abstract

We study tunneling quenches when a hot-many body quantum system is brought into an instantaneous contact with a cold many-body quantum system. The dynamics of such systems can be understood as a combination of early time von Neumann entropy gain and late time energy relaxation. We show that at the shortest timescales there is an energy increase in each system linked to the entropy gain and supported by the collective binding energy between the systems. Counterintuitively to the classical expectation, this implies that also the hotter of the two subsystems generically experiences an initial energy increase when brought into contact with a colder system. We explain this early time energy gain with a quantum thermodynamical relation that holds even for systems out of equilibrium and, in the limit where the energy relaxation overwhelms the quantum correlation build-up, reduces to a classical behavior. We use both, strongly correlated SYK systems and mixed field Ising chains with a tunneling quench to exhibit these characteristics, and study the contribution of quantum correlations to the von Neumann entropy. Interestingly, we discover that the energy dynamics of an Ising model around the quantum critical point has a similar qualitative behaviour to a strongly interacting SYK system.

P81

Intrinsic, robust, and isolated flat bands present at half-filling in the minimal model of the superconducting metal-organic framework, Cu-BHT

P82

Multiorbital SYK model: Nematicity, non-Fermi liquid, and Elastotransport

We propose and study a two-orbital lattice extension of the Sachdev-Ye-Kitaev model in the large-N limit. The phase diagram of this model features a high temperature isotropic strange metal which undergoes a first-order thermal transition into a nematic insulator or a continuous thermal transition into nematic metal phase, separated by a tunable tricritical point. These phases arise from spontaneous partial orbital polarization of the multiorbital non-Fermi liquid. We explore the spectral and transport properties of this model, including the d.c. elastoresistivity, which exhibits a peak near the nematic transition, as well as the nonzero frequency elastoconductivity. Our work offers a useful perspective on nematic phases and transport in correlated multiorbital systems.

P83

Twists and Turns of pairing from repulsive dynamical interactions

Dimitri Pimenov [1] , **Andrey V. Chubukov** [1]

[1] *FTPI, University of Minnesota*

Superconductivity requires attraction in some angular momentum channel – or does it? One way around this basic fact is to have a repulsive "dynamical" interaction which depends on the energy transfer. A physical realization of this scenario is possible in low-density materials such as SrTiO_3. In this presentation, I will explore the properties of the resulting superconductor [1], which features dynamical vortices and the elusive "odd-frequency" pairing [2]. Further, I will discuss the paradoxical disappearance of superconductivity once the repulsion gets too strong.

[1] D. Pimenov and A. V. Chubukov, NPJ Quantum Materials **7**, 45 (2022).
[2] D. Pimenov and A. V. Chubukov, arXiv:2206.01783 (2022).

P84

Transverse flow velocity and differntial Temperature in high energy nucleus nucleus collision

Transverse flow velocity and differntial Temperature in high energy nucleus nucleus collision

P85

The Reduction of the Thermal Decoherence using Hybrid Structure Toroidal Whispering Gallery Modes Resonator

In this paper, we demonstrate numerical and finite element method simulation of Thermorefractive in hybrid structure Toroidal Whispering Gallery Modes Resonator. Stochastic behavior of temperature can result in Thermorefractive noise that can excess decoherence at frequency noise lower than 10MHz Fourier frequencies. To be able to cancel Thermorefractive, a hybrid structure Toroidal Whispering Gallery Modes Resonator is simulated. We show that Thermorefractive cancelation is possible at room temperature. the thermorefractive noise is expected to decrease by > 26 dB at room temperature. This reduction can have a possible application in the position sensing measurement with an imprecision below the standard quantum limit (SQL) using cavity-enhanced optical near fields.

P86

Crystalline Anharmonicity in 2D Ferroelectric α-In_2Se_3 Single Crystal

Divya Rawat, Niraj Kumar Singh, Kewal Singh Rana, and Ajay Soni*

School of Basic Sciences, Indian Institute of Technology Mandi, Mandi, 175075, HP India,

**Corresponding author: ajay@iitmandi.ac.in*

Layered two-dimensional indium selenides (In_xSe_y) have complex stoichiometries such as In_4Se_3, In_2Se_3, InSe, and In_6Se_7.[1] These compounds posses strongly correlated phenomenon like Peierls transition and ferroelectric ordering because of its large tunability in the band gap and high carrier mobilities. Among different stoichiometric of In_xSe_y, In_2Se_3 is an emerging layered semiconductor, which exists in different phases (α, β, γ, and δ) such as hexagonal and rhombohedral.[2] Single-crystal of In_2Se_3 are an ideal candidates for examining the structural phase transformations and associated behaviour of the electrical properties.[3] Thin layer of α-In_2Se_3 also possess metallic, half-metallic, and semiconducting states based on the direction of ferroelectric polarization upon the application of an external electric field.[4] In this work, we synthesized single-crystal of *α*-In_2Se_3 by a solid-state route with an optimized temperature profile. The phase purity of crystalline α-In_2Se_3 has been examined by X-ray diffraction and Raman spectroscopy measurements. We will present the electrical, optical, and thermal transport properties to understand the crystal anharmonicity and its thermoelectric application.

References

1. Han, G., et al., *Indium Selenides: Structural Characteristics, Synthesis and Their Thermoelectric Performances.* Small, 2014. **10**(14): p. 2747-2765.
2. Hu, Y., et al., *Temperature-dependent growth of few layer β-InSe and α-In_2Se_3 single crystals for optoelectronic device.* Semiconductor Science and Technology, 2018. **33**(12): p. 125002.
3. Tao, X. and Y. Gu, *Crystalline–Crystalline Phase Transformation in Two-Dimensional In_2Se_3 Thin Layers.* Nano Letters, 2013. **13**(8): p. 3501-3505.
4. Zheng, C., et al., *Room temperature in-plane ferroelectricity in van der Waals In_2Se_3.* SCIENCE ADVANCES, 2018. **4**(7): p. eaar7720.

P87

High-T_c Superconductivity in FeSe by Exchange of Hidden Spin Fluctuations

Jose P. Rodriguez[1]

[1] *Department of Physics and Astronomy, California State University at Los Angeles, Los Angeles, California 90027, USA*

Unlike parent compounds to iron-pnictide superconductors, the bulk superconductor FeSe, which has a modest critical temperature of $T_c = 9$ K, shows no proximity to magnetic order[1]. Injecting electrons into FeSe, on the other hand, results in high-temperature superconductivity. We propose that proximity to hidden Néel order across the isotropic $d+ = d_{xz} + id_{yz}$ and $d- = d_{xz} - id_{yz}$ orbitals is what in fact drives superconductivity in FeSe. Such a hidden spin density wave (hSDW) results from nesting of electron-type and hole-type Fermi surfaces at the center and at the corner of the unfolded Brillouin zone[2]. At electron doping, exchange of the spin fluctuations associated with hSDW order results in a Lifshitz transition to strong electron-type Fermi surface pockets and weak hole-type Fermi surface pockets at the corner of the folded Brillouin zone[3]. Eliashberg theory predicts an instability to s-wave Cooper pairs that alternate in sign between the electron-type and hole-type Fermi surface pockets. At half filling, the underlying extended Hubbard model predicts an hSDW Mott insulator state due to magnetic frustration. A calculation of the dynamical spin susceptibility within the random phase approximations (RPA) finds a ring of low-energy spin excitations around the Néel wavevector[2] (π, π), in agreement with inelastic neutron scattering (INS) spectroscopy on organic-molecule intercalated FeSe[4].

[1] J.P. Rodriguez, D.S. Inosov, and J. Zhao, "Editorial: High-Tc Superconductivity in Electron-Doped Iron Selenide and Related Compounds", Front. Phys. **10**, 885420 (2022). https://www.frontiersin.org/articles/10.3389/fphy.2022.885420/full

[2] J.P. Rodriguez, "Spin Resonances in Iron Selenide High-Tc Superconductors by Proximity to a Hidden Spin Density Wave", Phys. Rev. B **102**, 024521 (2020). https://journals.aps.org/prb/abstract/10.1103/PhysRevB.102.024521

[3] J.P. Rodriguez, "Superconductivity by Hidden Spin Fluctuations in Electron-Doped Iron Selenide", Phys. Rev. B **103**, 184513 (2021). https://journals.aps.org/prb/abstract/10.1103/PhysRevB.103.184513

[4] B. Pan, Y. Shen, D. Hu, Y. Feng, J.T. Park, A.D. Christianson, Q. Wang, Y. Hao, H. Wo, Z. Yin, T.A. Maier and J. Zhao, "Structure of Spin Excitations in Heavily Electron-Doped $Li_{0.8}Fe_{0.2}$ODFeSe Superconductors", Nat. Commun. **8**,123 (2017). https://www.nature.com/articles/s41467-017-00162-x

P88

Abstract template for Schwinger-Boson mean-field study of spin-1/2 J_1-J_2-J_χ model in honeycomb lattice: thermal Hall signature

Rohit Mukherjee, Ritajit Kundu, Avinash Singh and Arijit Kundu

Department of Physics, Indian Institute of Technology Kanpur, Kanpur 208 016, India

We theoretically investigate, within the Schwinger-Boson mean-field theory, the transition from a gapped Z_2 quantum spin-liquid, in a J_1-J_2 Heisenberg spin-1/2 system in a honeycomb lattice, to a chiral Z_2 spin liquid phase under the presence of time-reversal symmetry breaking scalar chiral interaction (with amplitude J_χ). We numerically obtain a phase diagram of such J_1-J_2-J_χ system, where different ground-states are distinguished based on the gap and the nature of excitation spectrum, topological invariant of the excitations, the nature of spin-spin correlation and the symmetries of the mean-field parameters. The chiral Z_2 state is characterized by non-trivial Chern number of the excitation bands and lack of long-range magnetic order, which leads to large thermal Hall coefficient.

[1] R. Mukherjee, R. Kundu, A. Singh and A. Kundu, https://arxiv.org/abs/2108.08801.

P89

Spin Orbit Coupling driven Novel Quantum Magnetism in Iridate Double Perovskites.

Double Perovskites has been an area of interest owing to the rich physics it promises. 3d-5d based Double Perovskites are ideal to understand the interplay of Spin Orbit Coupling (SOC) with other intrinsic energy scales of the system. With this motivation, electronic structure calculation using state of the art density functional theory was performed on a series of compounds with the general formula (SrxCa1-x)2FeIrO6 with x ranging from 0 to 1. The idea was to look for the modification of the magnetic properties due to doping at the non-magnetic sites through the influence of the structural distortion. The emergence of novel insulating phases was studied from the perspective of the influence of SOC in transition metal oxides. Sr2FeIrO6 and Ca2FeIrO6 are iso-electronic and iso-valent, yet a major difference in the transition temperature was reported for them. We addressed this from the point of view of magnetic exchange interactions which was further visualized with the aid of Wannier functions. SOC plays a crucial role in obtaining the antiferromagnetic ordering for these compounds. In spite of SOC being an atomistic property, it affects Sr2FeIrO6 and Ca2FeIrO6 in dissimilar manner. The effective strength and impact of SOC is very different on them due to its delicate balance with other energy scales of the system. The enhanced structural distortion in Ca2FeIrO6, as compared to Sr2FeIrO6, diminishes the SOC strength in the former which is evident from the magnetisation density of the systems. We also show the non-monotonic behaviour of spin and orbital magnetic moment as a function of doping and SOC strength. Our investigations reveal the non trivial role played by SOC in establishing the ground state magnetic properties of the Ir based double-perovskite compounds.

P90

Fine structure of excitons in TMD type-II heterostructures

K. Sadecka [1,2] , M. Bieniek [3,1,2] , A. Wójs [1], and P. Hawrylak [2]

[1] *Department of Theoretical Physics, Wrocław University of Science and Technology, Wybrzeże Wyspiańskiego 27, 50-370 Wrocław, Poland*

[2] *Department of Physics, University of Ottawa, Ottawa, Ontario, Canada K1N 6N5*

[3] *Institut für Theoretische Physik und Astrophysik, Universität Würzburg, 97074 Würzburg, Germany*

We describe the electronic and optical properties of $MoSe_2/WSe_2$ type-II heterostructure using *ab initio* based tight-binding (TB) approximation and Bethe-Salpeter equation (BSE) [1,3]. We start with determining the electronic structure of $MoSe_2/WSe_2$ from first principles. We obtain type-II band alignment and conduction band minima at Q points. Then we perform analysis of Kohn-Sham wavefunctions allowing to detect leading layer and spin contributions. Next, we construct minimal TB model for $MoSe_2/WSe_2$ heterostructure, which allow us to understand orbital contributions to Bloch states and study wavefunctions effect on excitonic spectrum. We accurately solve BSE and determine the exciton fine structure due to type-II spin-split band arrangement [2,3] and topological moments, considering both A/B, spin bright/dark and intra-/interlayer exciton series using simplified Rytova-Keldysh non-local screening theory. In next step we analyse effect of moiré potential and compare it with fully tight-binding approach to excitons in twisted heterostructures.

[1] M. Bieniek, L. Szulakowska, and P. Hawrylak, Physical Review B **101**, 125423 (2020).
[2] K. Sadecka, Acta Physica Polonica A **141**, 2 (2022).
[3] M. Bieniek, K. Sadecka, L. Szulakowska, P. Hawrylak, Nanomaterials **1582**, 12 (2022)

P91

Quantum spin liquids in dipolar-octupolar pyrochlore magnets

Krushna C. Sahu[1], **Sambuddha Sanyal**[1]

[1]*Indian Institute of Science Education and Research, Tirupati*

We study quantum spin liquid (QSL) with low-energy fermionic quasi-particles for pyrochlore magnets with dipolar-octupolar symmetry. We classify the possible U(1) and Z_2 fermionic QSLs in such a system and compare their characteristics. Our study provides a possible way to understand the possible signatures of fermionic quasiparticles in a recent experiment on Ising pyrochlore magnet Nd_2ScNbO_7. We further calculate the dynamic spin structure factor and thermal characteristics to understand the nature of these fermionic quasiparticles through neutron scattering and linear response experiments.

P92

Unpredictable Condensate-Depletion Dynamics in one-dimensional Power-Law Traps

The dynamic depletion of a trapped one-dimensional Bose-Einstein condensate (BEC) that is driven by laser stirring is numerically explored using beyond mean-field methods. For this purpose, the multi-configurational time-dependent Hartree method for bosons (MCTDHB) [Alon et al., Phys. Rev. A 77, 033613 (2008)] is applied. In order to induce the depletion, the BEC is excited by a negative Gaussian potential (dimple) whose depth is modulated with time. The BEC is examined in various trapping geometries, with different interactions, and the condensate depletion is recorded as a function of time. A general power-law trap is considered that can be experimentally generated and shaped by the holographic methods of Bruce et al. [Bruce et al., Phys. Rev. A 84, 053410 (2011)]. The chief goal is to explore the interplay between trapping geometry and interactions in defining the depletion dynamics. It is chiefly found, that the details of these depletion dynamics are unpredictable and determined by a combination of the principle dimple depth, trap, and interactions. One significant feature of this work is that quite a number of plateaus is reached in the aforementioned dynamics.

P93

Unpredictable Condensate Depletion Dynamics in one-dimensional Power-Law Traps

The dynamic depletion of a trapped one-dimensional Bose-Einstein condensate (BEC) that is driven by laser stirring is numerically explored using beyond mean-field methods. For this purpose, the multi-configurational time-dependent Hartree method for bosons (MCTDHB) [Alon et al., Phys.Rev. A 77, 033613 (2008)] is applied. In order to induce the depletion, the BEC is excited by a negative Gaussian potential (dimple) whose depth is modulated with time. The BEC is examined in various trapping geometries, with different interactions, and the condensate depletion is recorded as a function of time. A general power-law trap is considered that can be experimentally generated and shaped by the holographic methods of Bruce et al. [Bruce et al., Phys. Rev. A 84, 053410 (2011)]. The chief goal is to explore the interplay between trapping geometry and interactions in defining the depletion dynamics. It is chiefly found, that the details of these depletion dynamics are unpredictable and determined by a combination of the principle dimple depth, trap, and interactions. One significant feature of this work is that quite a number of plateaus is reached in the aforementioned dynamics.

P94

Engineering holographic flat bands

In electronic systems with flat bands, such as twisted bilayer graphene, interaction effects govern the structure of the phase diagram. We show that a strongly interacting system featuring fermionic flat bands can be engineered using the holographic AdS/CFT duality. In particular, we find that in the holographic nematic phase, two bulk Dirac cones separated in momentum space at low temperature, approach each other as the temperature increases. They eventually collide at a critical temperature yielding a flattened band with a quadratic dispersion. On the other hand, in the symmetric (Lifshitz) phase, this quadratic dispersion relation holds for any finite temperature. We therefore obtain a first holographic, strong-coupling realization of a topological phase transition where two Berry monopoles of charge one merge into a single one with charge two.

P95

Broken Sublattice Symmetry Effects and Phase Transitions in Triangular Artificial Graphene Quantum Dots

Yasser Saleem[1], Amintor Dusko[1], Moritz Cygorek[1], Marek Korkusinski[2], and Pawel Hawrylak[1]

[1] *Department of Physics, University of Ottawa, Ottawa, Canada*
[2]*National Research Council of Canada, Ottawa, Canada*

We describe here the effects of broken sublattice symmetry, and the emergence of a phase transition in triangular artificial graphene quantum dots with zigzag edges[1]. The system consists of a structured lateral gate confining two dimensional electrons in a quantum well into artificial minima arranged in a hexagonal lattice. The sublattice symmetry breaking is generated by forming an artificial triangular graphene quantum dot with zigzag edges. The resulting Hamiltonian generates a tunable ratio of tunneling to strength of electron-electron interactions and a degree of sublattice symmetry with control over shape. Using a combination of tight binding, Hartree-Fock and configurations interaction methods we show that the ground state transitions from a metallic to an antiferromagnetic insulating phase by changing the distance between sites or depth of the confining potential. At the single particle level these triangular dots contain a macroscopically degenerate shell at the Fermi level. The shell persists at the mean-field, Hartree Fock level for weak interactions in the metallic phase but disappears for strong interactions and antiferromagnetic insulating phase. We determine the effects of electron-electron interactions on the ground state, the total spin, and the excitation spectrum as a function of filling of the system away from half-filling. We find that the half-filled charge neutral system leads to a fully spin polarized state in both metallic and antiferromagnetic regimes in accordance with Lieb's theorem. In both regimes a relatively large gap separates the spin polarized ground state to the first excited many-body state at half-filling of the degenerate shell, but by adding or removing an electron, this gap drops dramatically, and alternate total spin states emerges with energies nearly degenerate to a spin polarized ground state.

[1] Saleem, Y., Dusko, A., Cygorek, M., Korkusinski, M., & Hawrylak, P. (2022). Quantum simulator of extended bipartite Hubbard model with broken sublattice symmetry: Magnetism, correlations, and phase transitions. *Phys. Rev. B, 105*(20), 205105. https://doi.org/10.1103/PhysRevB.105.205105

P96

Andreev Transfer Torque on the Surface of three dimensional Topological Insulators

Morteza Salehi
[1] *Department of Physics, Bu-Ali Sina University, Hamadan,65178, Iran.*

In-plane magnetization on the surface of three-dimensional topological insulators (3D TIs) relocates the Dirac cone's location in the k-space [1]. We theoretically demonstrate that a ferromagnetic/superconductor junction on the surface of 3D TIs has anomalous Andreev reflection. In contrast to metallic or Graphene junction[2,3], this Andreev reflection is neither specular nor retro-reflection. Electron and hole cones separate in the presence of in-plane magnetization according to the magnitude of magnetization. For incoming Dirac fermions from the ferromagnetic side of the junction, there is a probability of being reflected as a hole due to the Andreev mechanism. In the ballistic regime, the parallel component of the wave vector is conserved during the scattering processes. Because of this condition, the reflected holes find different propagation directions. This imbalance causes a torque on the surface of the junction, which we called it *Andreev transfer torque*.

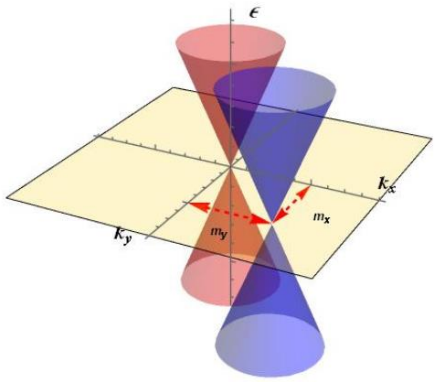

Figure 1: The dispersion relation of Dirac fermions in the k-space. The red cone located at the origin of k-space whereas the blue on tuned according to the value of in-place magnetization {-m_y, m_x}.

*This work was supported by the Program Committee.
[1] R. Beiranvand and M. Salehi, J. Phys. Condens. Matter **33**, 325401 (2020).
[2] C. W. J. Beenakker, Phys. Rev. Lett. **97** (6), 067007 (2006).
[3] M. de Jong and C. W. J. Beenakker, Phys. Rev. Lett. **74** , 1657 (1995).

P97

Quantum order-by-disorder induced phase transition in Rydberg ladders with staggered detuning

Madhumita Sarkar, Mainak Pal, Arnab Sen and Krishnendu Sengupta

School of Physical Sciences, Indian Association for the Cultivation of Science, Kolkata 700032, India

$^{87}\mathrm{Rb}$ atoms are known to have long-lived Rydberg excited states with controllable excitation amplitude (detuning) and strong repulsive van der Waals interaction $V_{\mathbf{r}\mathbf{r}'}$ between excited atoms at sites $\mathbf{r}$ and $\mathbf{r}'$. We study such atoms in a two-leg ladder geometry in the presence of both staggered and uniform detuning with amplitudes Δ and λ respectively. We show that when $V_{\mathbf{r}\mathbf{r}'} \gg (\ll)\Delta, \lambda$ for $|\mathbf{r} - \mathbf{r}'| = 1(> 1)$, these ladders host a plateau for a wide range of λ/Δ where the ground states are selected by a quantum order-by-disorder mechanism from a macroscopically degenerate manifold of Fock states with fixed Rydberg excitation density $1/4$. Our study further unravels the presence of an emergent Ising transition stabilized via the order-by-disorder mechanism inside the plateau. We identify the competing terms responsible for the transition and estimate a critical detuning $\lambda_c/\Delta = 1/3$ which agrees well with exact-diagonalization based numerical studies. We also study the fate of this transition for a realistic interaction potential $V_{\mathbf{r}\mathbf{r}'} = V_0/|\mathbf{r} - \mathbf{r}'|^6$ and demonstrate that it survives for a wide range of V_0, and provide analytic estimate of λ_c as a function of V_0. This allows for the possibility of a direct verification of this transition in standard experiments which we discuss.

Degenerate versus non-degenerate Josephson parametric amplifiers' gains and application in quantum two-mode squeezed radar

Seyed Mohammad Hosseiny[1], Milad Norouzi[2], Jamileh Seyed-Yazdi[2], Fatemeh Irannezhad[2]

[1]*Department of Physics, Faculty of Science, Urmia University, Iran.*

[2]*Department of Physics, Faculty of Science, Vali-e-Asr University of Rafsanjan, Iran.*

Abstract

Since the gain of Josephson parametric amplifier (JPA) plays a key role in the amplifier performance and improvement of a quantum radar performance, in this work we evaluate the difference between the gains of a degenerate versus non-degenerate Josephson parametric amplifier (D-JPA and ND-JPA respectively) and its application in a two-mode squeezed (QTMS) radar. The ND-JPA power gain shows a better behavior, which leads to improved signal-to-noise (SNR) ratio in quantum radar and, consequently, improved QTMS radar operation. There is also an increase in the quality factor of the non-degenerate case, which leads to a reduction in energy loss.

Introduction

Amplification is an important element in quantum sensing and quantum information processing. For example, rereading superconducting qubits requires a microwave amplification that adds, as low noise as possible, to the signal [1-4]. Parametric amplifiers, operated by nonlinearity of Josephson junctions, are regularly used in superconducting quantum information experiments [5-14]. One of the important aspects to evaluate the performance of a practical parametric amplifier is the high saturation power, for example, the ability to maintain the desired gain for a large input signal power [15-28].

QTMS radar, as shown in Figure 1, uses a JPA that includes superconducting quantum interference device (SQUID) to generate a stream of entangled photons (signal/idler) and send signal to the target. The echo measures the reflection of the target with the idler we previously sent to the detector, and finally inferred the presence or absence of the target [29].

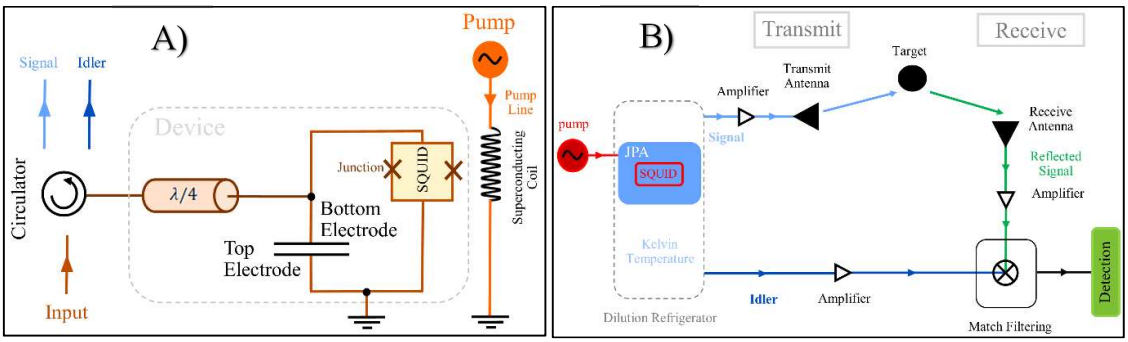

Fig. 1. A) JPA's circuit. B) block diagram of QTMS radar.

Discussion and Results

There are two types of JPAs based on pumping [30-31]: (1) Degenerate JPA (D-JPA). The signal and idler have the same frequency. (2) Non-degenerate JPA (ND-JPA). The signal and idler have not the same frequency.

In this study, we compared the difference between power gain of D-JPA and ND-JPA as shown in Fig. 2. In this figure, we see that, the power gain of signal of ND-JPA is lower than maximum power gain of D-JPA. Hence, as we can see in Fig. 3, the SNR in quantum radar is improved for the ND-JPA case compared to the D-JPA case. Therefore, the performance of our quantum radar will be better when we use ND-JPA. In Fig. 4, there is an increase in the quality factor of the non-degenerate case, which leads to a reduction in energy loss.

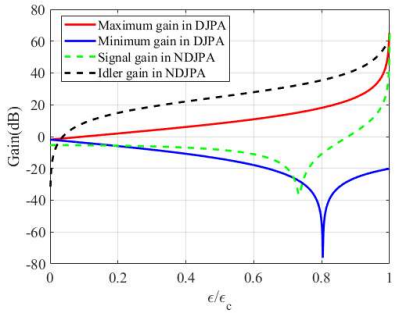

Fig. 2. The comparison of power gain of D-JPA and ND-JPA versus normalization modulation amplitude when Q_{int}=2200, Qext=240.

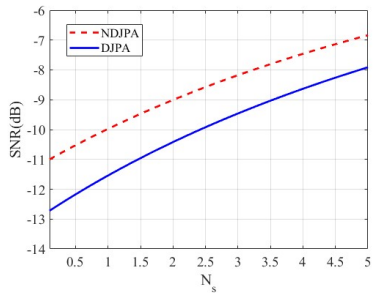

Fig. 3. The comparison of SNR in ND-JPA and JPA in the same condition.

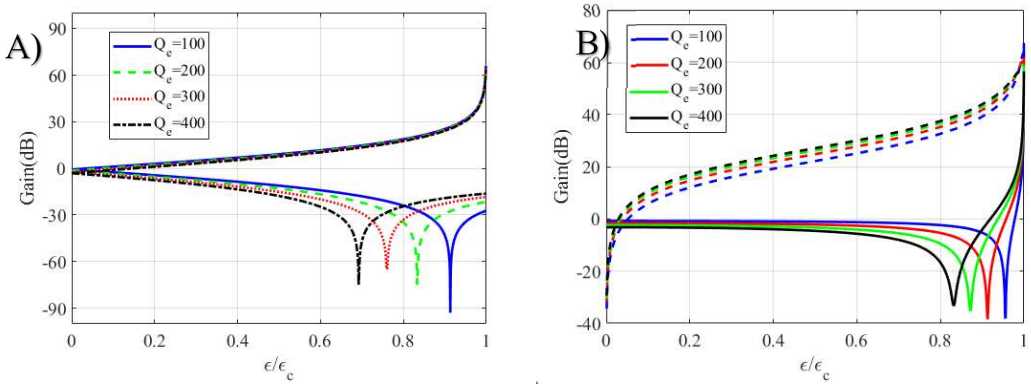

Fig. 4. The power gain of D-JPA (A) and ND-JPA (B) versus normalization modulation amplitude increasing quality factor when $Q_{int} = 2200$.

Conclusion

Since it was observed that the signal and idler power gain of ND-JPA show a better performance, so it has a performance improvement in the SNR ratio in QTMS, which in turn improves the performance of the quantum radar. It was also observed that a ND-JPA can have a higher quality factor and consequently less energy loss than the degenerate case. Therefore, it is suggested to use a ND-JPA in a QTMS to improve the performance.

References

[1] A. A. Clerk, M. H. Devoret, S. M. Girvin, F. Marquardt, and R. J. Schoelkopf, Introduction to quantum noise, measurement, and amplification, Rev. Mod. Phys. **82**, 1155 (2010).

[2] W. H. A. Yariv, and A. E. Siegman, Quantum fluctuations and noise in parametric processes. I. Phys. Rev. **124**, 1646 (1961).
[3] J. P. Gordon, W. H. Louisell, and L. R. Walker, Quantum fluctuations and noise in parametric processes. II, Phys. Rev. **129**, 481 (1963).
[4] C.M. Caves, Quantum limits on noise in linear amplifiers, Phys. Rev. D **26**, 1817 (1982).
[5] M. A. Castellanos-Beltran and K. W. Lehnert, Widely tunable parametric amplifier based on a superconducting quantum interference device array resonator, Appl. Phys. Lett. **91**, 083509 (2007).
[6] M. A. Castellanos-Beltran, K. D. Irwin, G. C. Hilton, L. R. Vale, and K. W. Lehnert, Amplification and squeezing of quantum noise with a tunable josephson metamaterial, Nat. Phys. **4**, 929 (2008).
[7] T. Yamamoto, K. Inomata, M. Watanabe, K. Matsuba, T. Miyazaki, W. D. Oliver, Y. Nakamura, and J. S. Tsai, Fluxdriven Josephson parametric amplifier, Appl. Phys. Lett. **93**, 042510 (2008).
[8] N. Bergeal, F. Schackert, M. Metcalfe, R. Vijay, V. E. Manucharyan, L. Frunzio, D. E. Prober, R. J. Schoelkopf, S. M. Girvin, and M. H. Devoret, Phase-preserving amplification near the quantum limit with a Josephson ring modulator, Nature (London) **465**, 64 (2010).
[9] N. Bergeal, R. Vijay, V. E. Manucharyan, I. Siddiqi, R. J. Schoelkopf, S. M. Girvin, and M. H. Devoret, Analog information processing at the quantum limit with a Josephson ring modulator, Nat. Phys. **6**, 296 (2010).
[10] M. Hatridge, R. Vijay, D. H. Slichter, J. Clarke, and I. Siddiqi, Dispersive magnetometry with a quantum limited squid parametric amplifier, Phys. Rev. B **83**, 134501 (2011).
[11] N. Roch, E. Flurin, F. Nguyen, P. Morfin, P. Campagne-Ibarcq, M. H. Devoret, and B. Huard, Widely Tunable, Nondegenerate Three-Wave Mixing Microwave Device Operating Near the Quantum Limit, Phys. Rev. Lett. **108**, 147701 (2012).
[12] R. Vijay, D. H. Slichter, and I. Siddiqi, Observation of Quantum Jumps in a Superconducting Artificial Atom, Phys. Rev. Lett. **106**, 110502 (2011).
[13] J. E. Johnson, C. Macklin, D. H. Slichter, R. Vijay, E. B. Weingarten, J. Clarke, and I. Siddiqi, Heralded State Preparation in a Superconducting Qubit, Phys. Rev. Lett. **109**, 050506 (2012).
[14] C. Eichler, D. Bozyigit, and A. Wallraff, Characterizing quantum microwave radiation and its entanglement with superconducting qubits using linear detectors, Phys. Rev. A **86**, 032106 (2012).
[15] A. Metelmann and A. A. Clerk, Quantum-Limited Amplification Via Reservoir Engineering, Phys. Rev. Lett. **112**, 133904 (2014).
[16] L. Spietz, K. Irwin, and J. Aumentado, Superconducting quantum interference device amplifiers with over 27 GHz of gainbandwidth product operated in the 4–8 GHz frequency range, Appl. Phys. Lett. **95**, 092505 (2009).
[17] T. C. Chien, O. Lanes, C. Liu, X. Cao, P. Lu, S. Motz, G. Liu, D. Pekker, and M. Hatridge, Multiparametric amplification and qubit measurement with a Kerr-free Josephson ring modulator, arXiv:1903.02102 [Phys. Rev. A (to be published)].
[18] A. Metelmann and A. A. Clerk, Nonreciprocal Photon Transmission and Amplification Via Reservoir Engineering, Phys. Rev. X **5**, 021025 (2015).
[19] Q. Zhong, S. K. Ozdemir, A. Eisfeld, A. Metelmann, and R. El-Ganainy, Exceptional Points-Based Optical Amplifiers, Phys. Rev. Appl. **13**, 014070 (2020).
[20] A. Kamal, A. Marblestone, and M. Devoret, Signal-topump back action and self-oscillation in double-pump Josephson parametric amplifier, Phys. Rev. B **79**, 184301 (2009).
[21] B. Abdo, A. Kamal, and M. Devoret, Nondegenerate three-wave mixing with the Josephson ring modulator, Phys. Rev. B **87**, 014508 (2013).
[22] C. Eichler and A. Wallraff, Controlling the dynamic range of a Josephson parametric amplifier, EPJ Quantum Tech. **1**, 2 (2014).
[23] B. A. Kochetov and A. Fedorov, Higher-order nonlinear effects in a Josephson parametric amplifier, Phys. Rev. B **92**, 224304 (2015).
[24] G. Liu, T.-C. Chien, X. Cao, O. Lanes, E. Alpern, D. Pekker, and M. Hatridge, Josephson parametric converter saturation and higher order effects, Appl. Phys. Lett. **111**, 202603 (2017).
[25] N. E. Frattini, V. V. Sivak, A. Lingenfelter, S. Shankar, and M. H. Devoret, Optimizing the Nonlinearity and Dissipation of a SNAIL Parametric Amplifier for Dynamic Range, Phys. Rev. Appl. **10**, 054020 (2018).
[26] A. Roy and M. Devoret, Quantum-limited parametric amplification with Josephson circuits in the regime of pump depletion, Phys. Rev. B **98**, 045405 (2018).
[27] D. M. Pozar, *Microwave Engineering*, 4th ed. (Wiley, New York, 2011).
[28] L. Chenxu, T. Chien, M. Hatridge, and D. Pekker, Optimizing Josephson-ring-modulator-based Josephson parametric amplifiers via full Hamiltonian control, Phys. Rev. A **101**, 042323 (2020).
[29] D. Luong, CW Sandbo Chang, A. M. Vadiraj, A. Damini, C. M. Wilson, and B. Balaji, Receiver operating characteristics for a prototype quantum two-mode squeezing radar. *IEEE Trans. Aerosp. Electron. Syst.* **56**, 2041-2060 (2019).
[30] A. Blais, R.-S. Huang, A. Wallraff, S. M. Girvin, and R. J. Schoelkopf, Cavity quantum electrodynamics for superconducting electrical circuits: An architecture for quantum computation, *Phys. Rev. A* ***69***, 062320 (2004).
[32] Pogorzalek, Stefan, Kirill G. Fedorov, Ling Zhong, Jan Goetz, Friedrich Wulschner, Michael Fischer, Peter Eder et al. "Flux-driven Josephson parametric amplifiers: Hysteretic flux response and nondegenerate gain measurements." *arXiv preprint arXiv:1609.09041* (2016).
[33] Krüger, Philipp, and Kirill G. Fedorov. "*Fortgeschrittenenpraktikum: The Josephson Parametric Amplifier*." 2021.

P98

Tunneling conductance in surface states of a topological insulator and Single Weyl node

Milad Norouzi[1], Jamileh Seyedyazdi[1], Fatemeh Irannezhad[1], Seyed Mohammad Hosseiny[2]

[1]Department of Physics, Faculty of Science, Vali-e-Asr University of Rafsanjan, Iran.
[2]Department of Physics, Faculty of Science, Urmia University, Urmia, Iran

In this study, we demonstrate that it is possible to form a junction of non-homogeneous metallic states of topological insulators and spin-singlet Weyl s-wave superconductors. The conductivity due to quantum tunneling by Blonder-Tinkham-Klapwijk (BTK) method can be adjusted via the chemical potential on both sides of the junction and the effect of Burstein shift due to the applied voltage.

P99

Theory of spin-lattice interaction in Tb2Ti2O7

We develop a theory for the spin-lattice coupling through magneto-elastic interaction in Tb2Ti2O7. First, we study the coupling of single ion ground doublet to both inversion even and inversion odd optical phonons. We show that neither the dynamic John-Teller (JT)(linear spin-lattice coupling to even inversion phonons), nor the dynamic Renner-Teller (RT) coupling (quadratic coupling to inversion odd phonons) are able to split the ground doublet. We nd that the even parity non- dispersive optical mode splits into two branches as the result of RT coupling. We also include the effect of coupling between the ground and excited crystal eld doublets as the result of spin-lattice interaction and nd that such a coupling is also unable to remove the degeneracy of both ground and excited doublets nevertheless give rise to the renormalization of the excitation gap.

P100

Photo-induced quantum phase transitions in moiré superlattices

Currently, so-called strongly correlated many-body systems constitute one of the richest playgrounds in condensed matter physics. Moir´e systems provide a rich platform for studies of strong correlation physics. Motivated by the experimental developments, we discuss photo-induced quantum phase transitions in TMDs moiré superlattices. We will identify the metal-insulator phase transition by constructing a phase diagram for the bilayer TMDs.

P101

Significant improvement of critical current density in (Bi1.6Pb0.4)Sr2Ca2Cu3-yCoyO10 superconductors

Bi1.6Pb0.4Sr2Ca2Cu3-yCOyO10+δ were prepared by solid state method. Structural phase identifications have been done using X-ray analysis which proves the coexistence of Bi-2223 and Bi-2212 phases confirmed by Raman and magnetic measurements. The critical transition temperature Tc and critical current density Jc values were measured using superconducting quantum interference device magnetometer (SQUID) and by the magneto-optical technique. A remarkable rapid decrease to the diamagnetic signal in the magnetization versus temperature M(T) at 110K and higher Jc around 3.5x108 A/m2 was achieved for Co-doped samples.

P102

Kondo effect in magic angle twisted bilayer graphene

A.S. Shankar[1], **D.O.Oriekhov**[1], **A.K. Mitchell** [2], **L. Fritz** [3]

[1]*Instituut-Lorentz for Theoretical Physics, Universiteit Leiden, P.O. Box 9506, 2300 RA Leiden, The Netherlands*

[2]*School of Physics, University College Dublin, Belfield, Dublin 4, Ireland and Centre for Quantum Engineering, Science, and Technology, University College Dublin, Belfield, Dublin 4, Ireland*

[3]*Institute for Theoretical Physics, Utrecht University, 3584 CE Utrecht, The Netherlands*

Higher order van-Hove singularities (vHS) with a power law density of states have been proposed recently in [1]. We investigate the creation of a higher order vHS from a collision of two ordinary logarithmic vHS in twisted bilayer graphene across the magic angle $\theta = 1.05^\circ$ through means of the Kondo effect. Higher order saddle points are calculated precisely by diagonalizing the Bistritzer-MacDonald model. We predict a large elevation of the Kondo temperature, which could be relevant as an experimental probe of the higher order vHS.

[1] Yuan,N.F.Q. , Isobe,H. & Fu.L. , Nat.Commun. **10**, 5769 (2019).

P103

Microwave response of a chiral Majorana interferometer

We consider an interferometer based on artificially induced topological superconductivity and chiral one-dimensional (1D) Majorana fermions. The (nontopological) superconducting island inducing the superconducting correlations in the topological substrate is assumed to be floating. This allows probing the physics of interfering Majorana modes via microwave response, i.e., the frequency-dependent impedance between the island and the earth. Namely, the charging and discharging of the island are controlled by the time-delayed interference of chiral Majorana excitations in both normal and Andreev channels. We argue that microwave measurements provide a direct way to observe the physics of 1D chiral Majorana modes. In our approach, we use the Keldysh action technique to derive the impedance of the island relative to the ground (source and drain), which is due to the currents in the edge modes.

P104

Electronic Studies of Transition Metal Doped Bi_2Se_3 and Bi_2Te_3 Topological Insulators

Shailja Sharma [1] , **C.S. Yadav** [1]

[1] *School of Basic Sciences, Indian Institute of Technology Mandi, Mandi (H.P.) India-175075*

Bi_2Se_3 and Bi_2Te_3 are the most explored and promising three-dimensional topological insulators (TIs) for studying exotic physical phenomena such as topological superconductivity. The fundamental property that underpins the TIs is spin-orbit coupling (SOC) and time reversal symmetry. SOC is large in materials with high Z elements as their constituents such as bismuth in Bi_2Se_3 and Bi_2Te_3.[1] Comparative magnetotransport studies of transition metal (Fe, Nb, Ag, Au, Pt, and Pd) doped Bi_2Se_3 and Bi_2Te_3 single crystals, synthesised by the melt-grown method have been explored. Magnetoresistance in Fe-intercalated Bi_2Se_3 show quadratic dependence upon applied magnetic fields and follows Kohler's scaling rule.[2] Unconventional superconductivity emerges in the Nb-doped Bi_2Se_3, which is studied for the Seebeck and Nernst effect, and anisotropic upper critical field.[3] Noble metals (Pd, Pt, and Au) are characterized by presence of topologically derived surface states, which have long been known as Shockley surface states in Au.[4] As these are high Z elements, thus doping Bi_2Se_3 with noble metals may enhance their electronic properties. The presence of topological surface states have been confirmed by angle dependence of Shubnikov-de Haas (SdH) oscillations and weak antilocalization effects.[6] Pd-doped Bi_2Te_3 showed a cross-over from *n*-type to *p*-type behaviour with increasing Pd content, which has been observed in Hall and angle-resolved photoemission spectroscopy (ARPES) results. Comparison of different physical parameters obtained in SdH oscillations and ARPES are analysed.[7]

References:

[1] M.Z. Hasan and C.L. Kane, *Colloquium: Topological Insulators,* Rev. Mod. Phys. **82**, 3045-3067 (2010).

[2] S. Sharma, C.S. Yadav, *Structural and magnetotransport studies of Iron-intercalated Bi_2Se_3 single crystals,* Phys. Status Solidi B 2000086 (2020)

[3] S. Sharma, C.S. Yadav, *Anisotropic upper critical field, Seebeck and Nernst coefficient of Topological superconductor: $Nb_{0.20}Bi_2Se_3$* (under review) (arXiv: 2107.00432)

[4] B. Yan, B. Stadtmüller, N. Haag, S. Jakobs, J. Seidel, D. Jungkenn, S. Mathias, M. Cinchetti, M. Aeschlimann and C. Felser, *Topological states on the gold surface.* Nat. Commun. **6**, 10167 (2015).

[5] S. Sharma, S. Kumar, K. Shimada, C.S. Yadav. *Quantum Oscillations and ARPES studies on Pt, Pd and Au doped Bi_2Se_3 Topological Insulators.* (Under preparation)

[6] S. Sharma, S. Kumar, G. C. Tewari, G. Sharma, E. F. Schwier, K. Shimada, A. Taraphder, and C.S. Yadav, *Magnetotransport and high-resolution angle-resolved photoemission spectroscopy studies of palladium-doped Bi_2Te_3* , Phys. Rev. B **105**, 115120 (2022)

P105

Bipolaronic high-temperature superconductivity

Electron-lattice interactions play a prominent role in quantum materials, making a deeper understanding of direct routes to phonon-mediated high-transition-temperature (Tc) superconductivity desirable. However, it has been known for decades that weak electron-phonon coupling gives rise to low values of Tc, while strong electron-phonon coupling leads to lattice instability or formation of bipolarons, generally assumed to be detrimental to superconductivity. Thus, the route to high-Tc materials from phonon-mediated mechanisms has heretofore appeared to be limited to raising the phonon frequency as in the hydrogen sulfides. Here we present a simple model for phonon-mediated high-Tc superconductivity based on superfluidity of light bipolarons. In contrast to the greatly simplified Holstein model where lattice distortions modulate the electron's potential energy, we investigate the situation where lattice distortions modulate the electron hopping. This physics gives rise to small-size, yet light bipolarons, which we study using a sign-problem-free quantum Monte Carlo approach, demonstrating a new route to phonon-mediated high-Tc superconductivity. We find that Tc in our model generically and significantly exceeds typical upper bounds based on Migdal-Eliashberg theory or superfluidity of Holstein bipolarons. Our work establishes principles towards the design of high-Tc superconductors via functional material engineering.

P106

Effective Field Theories for Fracton Phases of Matter

Huan Souza[1], **Heitor Casasola**[2], **and Pedro R. S. Gomes**[2]

[1]*Faculdade de Física, Universidade Federal do Pará, 66075-110, Belém, Pará, Brazil.*
[2]*Departamento de Física, Universidade Estadual de Londrina, 86057-970, Londrina, PR, Brazil*

In recent years a new phase of matter named fractons has been discovered [1, 2]. This is a topological phase with very exotic physical properties. One imprint is the presence of excitations with severe restrictions of mobility: isolated quasiparticles are completely immobile, whereas certain bound states can eventually be mobile [3]. This kind of excitation first arose in the context of spin liquids [1] and now is known to appear also in different contexts like elasticity theory and linearized gravity [3]. One approach to studying this unusual state is to use field theoretical models exhibiting generalized symmetries that can lead to conservation laws in agreement with fracton physics. In certain situations these generalized symmetries are so-called higher-form symmetries, namely, symmetries that imply conservation of charges that are n-forms (n is bigger than zero, which would be the usual case). Field theories with generalized symmetries exhibit many interesting properties. One can also construct a gauge theory that exhibits this exotic phenomenology [4, 5]. This can be done by using a tensor gauge theory that ultimately describes gapless fracton phases. Such gauge theories have a close connection with gravitational physics and this is a subject of great interest since its discovery. In this work, we present a field theoretical description of generalized symmetries to describe this new state of matter.

[1] Claudio Chamon, Phys. Rev. Lett. 94, 040402 (2005).
[2] Jeongwan Haah, Phys. Rev. A 83, 042330 (2011).
[3] M. Pretko, Xie Chen and Yizhi You, International Journal of Modern Physics A, Vol. 35, No. 06, 2030003 (2020)
[4] M. Pretko, Phys. Rev. D 96, no.2, 024051 (2017)
[5] Y. H. Du, U. Mehta, D. X. Nguyen and D. T. Son, SciPost Phys. 12, 050 (2022)

P107

Correlation Factor Taking into Account Spherical Harmonics Through Hypergeometric Functions to Calculate Energies of Lithium-Like Ions

Malick SOW [1*], Ahmadou WAGUE[1], Boubacar SOW[1]

[1] Atoms Lasers Laboratory, Department of Physics, Faculty of Sciences and Technologies, University Cheikh Anta Diop, Dakar, Senegal
*malick711.sow@ucad.edu.sn

Calculations of the energy levels of atoms and ions with Z ≤ 10 are carried out in this paper. We used a new trial wave function [1] including spherical harmonics through hypergeometric functions to calculate via a new variational procedure the correlation factor, total energy, kinetic energy, Coulomb interaction between the atomic nucleus and the three electrons and the Coulomb interaction between electrons for the $(1s^2 2s)\ ^2S^e$, $(1sns^2)\ ^2S^e$, $(2sns)\ ^2S^e$ and $(2snp)\ ^2P^¤$ states. The present results are compared to other experimental and theoretical values [2]. The accurate data presented in this work may be a useful guideline for future experimental and other theoretical studies for electron correlation effects in doubly excited three- electron states.

[1] Boubacar Sow, Malick Sow, Ahmadou Zague, Int. J. of Applied Mathematics and Theoretical Physics. **6(2)**, 26-34 (2020).
[2] Youssou Gning, Malick Sow et al.. Rad. Phys. and Chem. **106**, 1– 6 (2015).

P108

Quantum critical point in the high-pressure structure of $CeSb_2$

Oliver P. Squire, Stephen A. Hodgson, Jiasheng Chen, Christian K. de Podesta, Patricia L. Alireza and F. Malte Grosche

Cavendish Laboratory, University of Cambridge, Cambridge CB3 0HE, UK

Ce-based heavy fermion compounds exhibit a variety of exotic states brought about by strong electronic correlations. Their properties are often susceptible to pressure-tuning, which can stabilise new phases and push materials through quantum phase transitions.

$CeSb_2$ at ambient pressure displays a series of complex magnetic phases and is thought to adopt a ferromagnetic ground state, a rare case in Ce systems which invites further study [1]. Magnetic transitions have been known to depend only weakly on applied pressure up to about 20 kbar, where material properties change abruptly [2]. Using high-pressure powder X-ray diffraction, we have recently demonstrated that this abrupt change can be attributed to a structural transition, and we have resolved the high pressure crystal structure [3]. Here, we focus on the low-temperature properties in the new high-pressure structure.

We have accessed the high-pressure structure of $CeSb_2$ using both piston-cylinder and anvil pressure cells at mK temperatures. Our resistivity and AC heat capacity data reveal two new phase transition anomalies which move to lower temperatures with increasing pressure. The temperature dependence of the resistivity above the ordering temperature is unusually steep, suggesting a low coherence temperature and very high effective masses. In the pressure region where the transitions extrapolate to zero temperature, we observe non-Fermi liquid behaviour, suggesting the presence of a quantum critical point. We will show data on the temperature-, field- and pressure-dependence of the resistivity in the vicinity of the quantum critical point, and we will discuss our findings in the context of recent experimental and theoretical results in other heavy fermion compounds.

[1] S. L. Bud'ko, P. C. Canfield, C. H. Mielke, and A. H. Lacerda, Phys. Rev. B **57**, 13624 (1998).
[2] T. Kagayama, Y. Uwatoko, S. L. Bud'ko, and P. C. Canfield, Physica B: Condensed Matter **359–361**, 320 (2005).
[3] C. K. de Podesta *et al.*, to be published (2022).

P109

Driven Hubbard model on a triangular lattice: tunable Heisenberg antiferromagnet with chiral three-spin term

Samudra Sur[1], **Adithi Udupa**[1], **and Diptiman Sen**[1,2]

[1]*Center for High Energy Physics, Indian Institute of Science, Bengaluru 560012, India*
[2]*Department of Physics, Indian Institute of Science, Bengaluru 560012, India*

We study the effects of a periodically varying electric field on the Hubbard model at half-filling on a triangular lattice. The electric field is incorporated through the phase of the nearest-neighbor hopping amplitude via the Peierls prescription. When the on-site interaction U is much larger than the hopping, the effective Hamiltonian H_{eff} describing the spin sector can be found using a Floquet perturbation theory. To third order in the hopping, H_{eff} is found to have the form of a Heisenberg antiferromagnet with three different nearest-neighbor couplings $(J_\alpha, J_\beta, J_\gamma)$ on bonds lying along the different directions. Remarkably, when the periodic driving does not have time-reversal symmetry, H_{eff} can also have a chiral three-spin interaction in each triangle, with the coefficient C of the interaction having opposite signs on up- and down-pointing triangles. Thus periodic driving which breaks time-reversal symmetry can simulate the effect of a perpendicular magnetic flux which is known to generate such a chiral term in the spin sector, even though our model does not have a magnetic flux. The four parameters $(J_\alpha, J_\beta, J_\gamma, C)$ depend on the amplitude, frequency and direction of the oscillating electric field. We then study the spin model as a function of these parameters using exact diagonalization and find a rich phase diagram of the ground state with seven different phases consisting of two kinds of ordered phases (collinear and coplanar) and disordered phases. Thus periodic driving of the Hubbard model on the triangular lattice can lead to an effective spin model whose couplings can be tuned over a range of values thereby producing a variety of interesting phases.

P110

Microscopic origin of Strongly Correlated ACrO3

P111

Carbon Nanotube Tunneling Field-Effect Transistor as a Radiation Sensor: A quantum Simulation Study

In today's world, the radiation dosimetry is an important operation in several sensitive domains, and this extends to the medicine, defense, security, and nuclear industry. Therefore, the development of high-performance dosimeters is in dire need. Herein, a new radiation sensitive field-effect nanotransistor (RADFET) is proposed using quantum mechanical simulation. The dosimeter is based on a gate-all-around p-i-n CNT tunnel field-effect nanotransistor that employs the radiation-induced electrostatic modulation as a radiation sensing principle. The used quantum simulation is based on the non-equilibrium Green's function (NEGF) formalism, which is coupled self-consistently with a Poisson equation for the cylindrical device geometry. The physics, quantum mechanical transport, and sensitivity behavior of the proposed nanoscale dosimeter were thoroughly investigated including the electron potential distribution, energy-position-resolved current spectrum, charge density, and drain current. The computational investigations have revealed that the proposed nanoscale tunnel FET-based dosimeter is effective in radiation sensing over a wide range of absorbed radiation dose. In addition, the most sensitive region in the transfer characteristic has been identified, where an ultra-high sensitivity has been recorded. The encouraging results recorded in this computational study empower the proposed TFET-based dosimeter to be a promising radiation sensor for high-performance security and defense applications.

P112

Topological chiral currents in the Gross-Neveu model extension

We unveil an interesting connection of Lorentz-violating quantum field theories, studied in the context of the standard model extension, and Hubbard-type models of topological crystalline phases. These models can be interpreted as a regularisation of the former and, as hereby discussed, explored with current quantum simulators based on ultra-cold atoms in optical Raman lattices. In particular, we present a complete analysis of the CreutzHubbard ladder under a generic magnetic flux, which regularises a Gross-Neveu model extension, and presents a characteristic circulating chiral current whose non-zero value arises from a specific violation of Lorentz invariance. We present a complete phase diagram with trivial insulators, ferromagnetic and anti-ferromagnetic phases, and current-carrying topological crystalline phases. These predictions are benchmarked using tools from condensed matter and quantum-information science, showing that self-consistent Hartree-Fock and strong-coupling Dzyaloshinskii-Moriya methods capture the essence of the phase diagram in different regimes, which is further explored using extensive numerical simulations based on matrix-product states.

P113

Emerging exotic phases in magnetic spin systems due to RKKY interaction

The competition between exchange and RKKY interactions may lead to effective frustrated systems. The origin of the RKKY term is due to interaction of magnetic moments with itinerant electrons; it is, in principle, long-ranged, and depends on the Fermi momentum of the electrons and a global coupling constant. In this work, we propose to study a simple model for Ising spins in the square lattice, considering both ferromagnetic and antiferromagnetic exchange couplings and competing RKKY interactions. We analyze what values of the coupling constants and the Fermi momentum lead to systems with stronger magnetic frustration, focusing around the parameters where the effective nearest neighbor coupling is suppressed. We explore the low temperature phases numerically, using the Monte Carlo Metropolis algorithm. We find that competing interactions in combination with an external magnetic field give rise to a plethora of exotic plateaux. This is a first step towards exploring the effect of RKKY interactions in more complex systems.

P114

Quantum Chaos, Superconductivity, and Information Scrambling in Disordered Magic-Angle Twisted Bilayer Graphene

Chenan Wei[1] **and Tigran A Sedrakyan**[1]

[1]*(Presenting author underlined) Department of Physics, University of Massachusetts, Amherst, Massachusetts 01003, USA*

We numerically and analytically study the properties of the twisted bilayer graphene (TBG) on Coulomb disordered substrate. We show that the strongly disordered TBG with the chemical potential in the flatband can be understood as a system of weakly coupled Sachdev-Ye-Kitaev (SYK) clusters, each being maximally chaotic. The thermodynamic entropy of such strongly disordered TBG and the specific heat capacity is calculated and shown to be consistent with coupled SYK model, that describes the strange metal phase. With strong disorder, the Gaussian orthogonal ensemble dominates disordered TBG's long-time chaotic dynamics, whereas quantum scrambling appears in the short-time dynamics. Namely, At low temperatures, the associated Lyapunov exponent shows a linear dependency on the temperature, and the slope is 56% of the proposed upper bound. These results show that the strongly disordered TBG is a quantum chaotic strange metal exhibiting non-Fermi liquid behavior. Moreover, the weakly disorder TBG supports exponential decay in the out-of-time-ordered correlator, which is in agreement with the Larkin-Ovchinnikov result for superconductors.

P115

Magneto-topological-induced transitions in multi-component superconductors

Multi-component spin-singlet superconductors with competing 0- and π-pairing couplings, as in s_{++} and $s_{\pm}$ phases, are close to instabilities with a spontaneous breaking of time-reversal symmetry. We demonstrate that the modification of the kinetic energy of superconducting electrons in doubly connected superconducting cylinder, determined by the applied flux, generally drives transitions from chiral superconducting states to configurations that are time-reversal symmetric. This magneto-topological-induced changeover is investigated by means of a Ginzburg-Landau approach for a two-band superconductor with interband interactions and impurity scattering. We find that the application of a magnetic flux can convert a chiral $s_{\pm}+is_{++}$ state into a $s_{\pm}$ configuration and vice versa or tune the energy splitting of chiral states having inequivalent pairing amplitudes. We discuss signatures for the detection of these phases and of the corresponding transitions in mesoscopic superconducting loops.

P116

Triangular lattice Hubbard Model

To investigate the effect of geometric frustration on the Fermi-Hubbard model the simplest lattice structure is the triangular one. Theoretical research on this subject predicts a rich, yet controversial, phase diagram with strange metals, unconventional superconductivity and spin liquids. Variational Monte Carlo (VMC) and Density Matrix Renormalization Group (DMRG) simulations fails to agree weather the spin liquid is gaped or if it breaks time-reversal symmetry. DMRG results could be biased by the quasi one dimensional lattices that they are restricted to, which also prevents true long-range order due to the Mermin-Wagner theorem. We aim to reduce the bias from the VMC ansatz by performing imaginary-projection with Auxiliary Field Quantum Monte Carlo (AFQMC). Unfortunately, to handle the sign problem, a constrained path approximation have to be applied. Also, we intend to perform a much needed investigation of the doped system where strange metallic behavior has been reported by DMRG and unconventional superconductivity could occur.

P117

New diluted magnetic semiconductors: DFT prediction

N. Zeggai [1], N. Benayad [1], M. Djermouni [1] and A. Zaoui [1]

[1] *Laboratoire de Physique Computationnelle des Matériaux (LPCM), Université Djilali Liabès de Sidi Bel-Abbès*

In all III-V and II-VI prototype magnetic semiconductor materials (DMS), such as GaAs or ZnO doped in Mn, the maximum Curie Temperature (T_C) remains limited to 180-200 K. So far, the magnetic mechanism is not fully understood. These difficulties could be overcome in the family of semiconductors (SC) I-II-V and I-III-IV recently discovered. In these families of SCs, the handling of charge and spin is independent.

On the other hand, the record of the T_C value reported for ferromagnetic semiconductors III-V doped in Iron (Ga, Fe) Sb, reached 340 K, restoring hope in the DMS projects. These materials have certain advantages over those doped in Mn. In addition, the similarity between the SC III-V GaSb and the semiconductors I-II-V (NaZnAs) and I-III-IV (NaGaSi) gives us the idea of looking for an iron-based DMS that can be characteristically easy with a relatively high critical temperature. To achieve this goal, we used the DFT theory to describe the electronic structure of the proposed DMS.

P118

Quantifying entanglement in non-Gaussian systems using the Wigner function

Mustapha ZIANE [1], Morad EL BAZ [1,]

[1](Mohammed 5th University of Rabat)

In this work, we address the issue of entanglement identifying in continuous variables systems providing a new approach to quantify the entanglement amount. We introduce and develop a geometric measure of entanglement for the class of non-Gaussian states based on the negativity property of the Wigner function. We prove that this quantity satisfies the natural properties expected from a good entanglement monotone.
We evaluate and analyse this entanglement measure for some relevant bipartite systems, and investigate the relevancy of this approach to visualize and quantify the different kinds of entanglement in the case of multipartite systems. We show qualitatively that our quantity can serve as a direct measure of genuine entanglement in tripartite states, independently of bipartite constructions [1].

[1] Ziane, M., & El Baz, M. Direct measure of genuine tripartite entanglement independent from bipartite constructions. Quantum Information Processing, 17(8), 1-11 (2018).

P119

Superconductivity in flat-band semimetals

Alexander A. Zyuzin [1] and A. Yu. Zyuzin [2]

[1] *Department of Applied Physics, Aalto University, FI-00076 AALTO, Finland*
[2] *Ioffe Physical-Technical Institute, St Petersburg 194214, Russia*

It is believed that the flat-band stimulated superconductivity may have relatively large values of the superconducting transition temperature [1, 2]. Several materials were proposed to host nearly flat bands such as, for example, multilayer graphene with rhombohedral stacking [3], twisted bilayer graphene [4], and semimetals with high pseudo-spin quasiparticles [5]. The recently discovered superconductivity in twisted bilayer graphene provides a unique platform for the flat band stimulated Cooper pairing [6].

Although, the effect of the flat band on superconductivity can be twofold [7]. Despite favoring Cooper pair formation, its nearly dispersionless nature can be a serious impediment to pair condensation. The Cooper pairs formation and their condensation may occur at different temperatures.

The conditions for the emergence of the preformed Cooper pairs in materials hosting flat bands will be presented. As a particular example, a semimetal with a pair of three-band crossing points at which a flat band intersects with a Dirac cone will be considered. It will be shown that the flat band promotes local Cooper pair formation so that the system may be modeled as an array of superconducting grains. The delocalized states give rise to the phase-coherent superconductivity at low temperatures.

*This work was supported by the Academy of Finland.

[1] V. Khodel' and V. Shaginyan, JETP Lett. 51, 553 (1990).
[2] G. Volovik, JETP Lett. 107, 516 (2018).
[3] T. Heikkila, N. Kopnin, and G. Volovik, JETP Lett. 94, 233 (2011).
[4] E. Andrei and A. MacDonald, Nature Material 19, 1265 (2021).
[5] B. Lv *et al.*, Rev. Mod. Phys. 93, 025002 (2021).
[6] Y. Cao *et al.*, Nature 556, 43 (2018).
[7] A. A. Zyuzin, A. Yu. Zyuzin, arxiv: 2109.07520.